2021-12-20

Experimental and Numerical Analysis of Convective Heat Transfer of Nanofluids

Saleamlak, Mulu Asfaw

BAHIR DAR UNIVERSITY

BAHIR DAR INSTITUTE OF TECHNOLOGY

SCHOOL OF POSTGRADUATE STUDIES

FACULTY OF MECHANICAL AND INDUSTRIAL ENGINEERING

Experimental and Numerical Analysis of Convective Heat Transfer of Nanofluids

Saleamlak Mulu Asfaw

Advisor: Prof. Kathiravan Raja

Co-Advisor: Mr. Million Asfaw

BAHIR DAR, ETHIOPIA

December 20, 2021

DECLARATION

I, the undersigned, declare that the thesis comprises my own work. In compliance with internationally accepted practices, I have acknowledged and refereed all materials used in this work. I understand that non-adherence to the principles of academic honesty and integrity, misrepresentation/ fabrication of any idea/data/fact/source will constitute sufficient ground for disciplinary action by the University and can also evoke penal action from the sources which have not been properly cited or acknowledged.

Saleamlak Mulu Asfaw		28/09/2021
Name of the student	Signature	Date

This thesis has been submitted for examination with my approval as a university advisor.

Prof. Kathiravan Raja		28/09/2021
Advisor Name	Signature	Date

BAHIR DAR UNIVERSITY
BAHIR DAR INSTITUTE OF TECHNOLOGY
SCHOOL OF GRADUATE STUDIES
FACULTY OF MECHANICAL AND INDUSTRIAL ENGINEERING

Approval of thesis for defense result

I hereby confirm that the changes required by the examiners have been carried out and incorporated in the final thesis.

Name of Student: **Saleamlak Mulu Asfaw** Signature _____ Date 16/12/2021

As members of the board of examiners, we examined this thesis entitled **"Experimental and Numerical Analysis of Convective Heat Transfer of Nanofluids"** by **Saleamlak Mulu Asfaw**. We hereby certify that the thesis is accepted for fulfilling the requirements for the award of the degree of Masters of science in **"Thermal Engineering"**.

Board of Examiners

Dr RAJA KADHIRAYAN		16/12/2021
Advisor name	Signature	Date
Abdulkadir Aman (PhD)		26/11/21
External Examiner	Signature	Date
Bimrew Tamrat (PhD)		16/12/21
Internal Examiner	Signature	Date
Dessie Tarekegn		16/12/21
Chair Person	Signature	Date
Temesgen Assefa		16/12/21
Chair Holder	Signature	Date
Eyhiru Z.		16/12/2021
Faculty Dean	Signature	Date

ABSTRACT

A nanofluid is a new heat transfer fluid produced by mixing a base fluid and solid nano sized particles. It has been reported this fluid has great potential in heat transfer applications, because of its increased thermal conductivity and even increased Nusselt number due to higher thermal conductivity, Brownian motion of nanoparticles, and other various effects on heat transfer phenomenon. But its potential in heat transfer applications has not been confirmed yet due to lack of conclusive information to predict the performance in heat transfer equipments. The aim of this thesis work is to predict convective heat transfer of copper in ethylene glycol nanofluids both experimentally and numerically. A locally fabricated convective heat transfer set up and a computational fluid dynamics (CFD) code in ANSYS Fluent 2021 R2 was used to obtain results in a circular pipe with constant wall heat flux boundary conditions in a turbulent flow.

The forced convective heat transfer was studied with horizontal circular smooth stainless-steel tube with Reynolds numbers varying in the range of 4000-10000 and volume concentration of 0.1%, 0.5%,1%. In this thesis work, the effect of several parameters such as Reynolds number, volume fraction and inlet temperature on heat transfer and flow characteristics were investigated. Both the experimental and numerical results, in a good agreement to each other ($\pm$5.7 % average deviation), show that the nanofluid with all values of particle concentrations achieved higher Nusselt number than pure ethylene glycol where the nanofluid with the highest particle concentration achieved the highest Nusselt number. For all the cases Nusselt number increased with the increase of Reynolds number and distance along the tube. On average scale, for Reynolds number of 10000 and inlet temperature of 303.15K, Nusselt number increases to 1.1 times for nanofluids of 1% particle concentration compared to the base fluid. Friction factor increases with increasing volume fraction and inlet temperature for both the numerical and experimental analyses.

Keywords: Copper-ethylene glycol nanofluids, Constant heat flux, Turbulent flow, Circular pipe, Computational Fluid Dynamics (CFD), Heat transfer enhancement

CONTENTS

NOMENCLATURE

C	specific heat at constant pressure
D	diameter of the test section
d_f	equivalent diameter of a base fluid molecule
d_p	nanoparticle diameter
k	thermal conductivity
k_b	Boltzmann constant = 1.38066×10^{23} J/K
h	average heat transfer coefficient in test section
h_x	local heat transfer coefficient
L	length of the test section
$\dot{m}$	mass flow rate
M	molecular weight of the base fluid
N	Avogadro number = 6.022×10^{23} mol^{-1}
Nu	Nusselt number
Nu_x	local Nusselt number
Pr	Prandtl number
Re	Reynolds number
Re_{np}	nanoparticle Reynolds number
T	temperature
T_m	bulk temperature
V	velocity
P	pressure

Greek symbols

α	thermal diffusivity
ε	turbulent kinetic energy dissipation rate
κ	turbulent kinetic energy
μ	dynamic viscosity
ρ	mass density
$\bar{\bar{\tau}}$	stress tensor
ϕ	nanoparticle volume fraction

Subscripts

avg	average
eff	effective, relative to the nanofluid
f	base fluid
fr	freezing point of the base liquid
in	inlet of the test section
out	outlet of the test section
p	nanoparticle
r	radial
t	turbulent
w	tube wall
x	axial

LIST OF FIGURES

LIST OF TABLES

CHAPTER ONE

1. INTRODUCTION

Under this chapter a thorough background information and rationale behind this thesis work is presented under different subsections. The scientific recent status and importance of nanofluids is highlighted first under background subsection. The problem that this research work aimed to solve is stated clearly and the main objectives planned to be achieved are outlined subsequently. Lately, the expected significance of this research and the extent to which it will stretched under the imposed limitations is clearly defined.

1.1. Background

Heat transfer technology, in its all-application areas with ever-increasing heat flux brought by the unbelievably increasing demand of heat current, is standing at a critical juncture. For instance, the exponential growth in electronics, communication, and computing technologies and their devices through miniaturization and an enhanced rate of operation and storage of data with ever-increasing thermal loads (as shown in the Fig 1.1)has brought about serious challenges in the thermal management of these devices[1]. In another important area, the field of optical devices like Lasers, high-power x-rays, and optical fibers being integral parts of today's computation, scientific measurement, material processing, medicine, material synthesis and communication devices, their increasing power with decreasing size also calls for innovative cooling technology. Besides the inherent need for improvement limited floorspace in industrial applications and weight limitations in space applications also calls for smaller size heat transfer devices to transfer a considerable amount of heat flux over a large distance[2]. Continuous efforts have been made to augment heat transfer and thereby increase energy and fuel efficiencies by reducing heat transfer time (enhancing heat transfer rate) and minimizing size of heat transfer equipments applying both active and passive techniques.

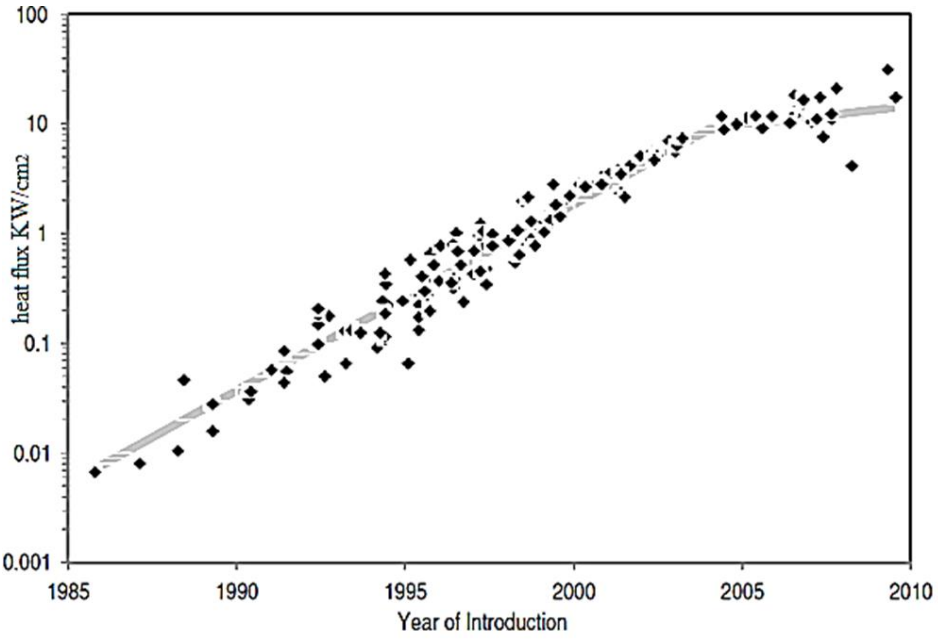

Figure 1-1: Heat flux vs. year of cooling technology development[3]

The former technique includes the vibration of the heated surface and fluid, the injection or suction of fluid, etc. which requires an external power input. On the other hand, the latter one requires no direct application of external power but by means such as the use of extended surfaces, introducing swirl flow devices, and additives for liquids and gases[4]. When metered with the same objective of any heat transfer technique, to strive for improved thermal contact (enhanced heat transfer coefficient) and reduced pumping power (improved thermohydraulic efficiency), the success of all these efforts is limited to the thermophysical properties of the working fluid most of the time to thermal conductivity, heat capacity, viscosity etc. So, improving the thermophysical properties of the working fluid is the overriding technique which will also pave the way for effectiveness of other augmentation techniques[5].

More than just a century ago the idea of the suspending solid particles into the conventional heat transfer fluid came to Maxwell's mind as a means to enhance the thermal conductivity of the fluids given that the thermal conductivity of solids is much higher than that of fluids[6]. Since then, milli and micro sized solid particles have been suspended to wide range of conventional heat transfer fluids, and a satisfactory enhancement in thermal conductivity has been achieved. But this improvement comes

with a handful of problems like rapid particle settling, channel erosion, clogging etc. which are mainly associated with the large size of particles[7]. The advancement of Nano technology (since 1959 by Richard Feynman) enables the reduction of the size of particles into nano-scale. Nano particles being suspended in conventional fluids can avoid the aforementioned difficulties of micro and macro size particles. In fact it awards us with anomalous enhancements mainly due to its innovative properties like higher specific surface area, higher stability and uniformity of the colloidal suspension, lower pumping power required to achieve the equivalent heat transfer, reduced particle clogging and higher level of control of the thermodynamics and transport properties by varying the particle material, concentration, size, and shape[8].

Since 1990s a drastically increasing number of investigations is being done (as shown in the Fig 1.2) in an effort to shed light on the possibility of the application of those suspensions (called nanofluids as coined by Choi in 1995) in heat transfer equipments. Even though the number of articles being published on this subject has increased dramatically, the data required to design a nanofluid flown heat transfer equipment is not yet abundant enough. It is not even conclusive to claim the possibility of replacing conventional heat transfer fluids by nanofluids is good idea. This is because for one hand the results of the investigations are contradictory to each other which is not yet reconciled and heat transfer characteristics of nanofluids is dependent on a wide range of non-traditional variables, such as particle size, shape, and surface treatment whose relationships has not yet well understood.

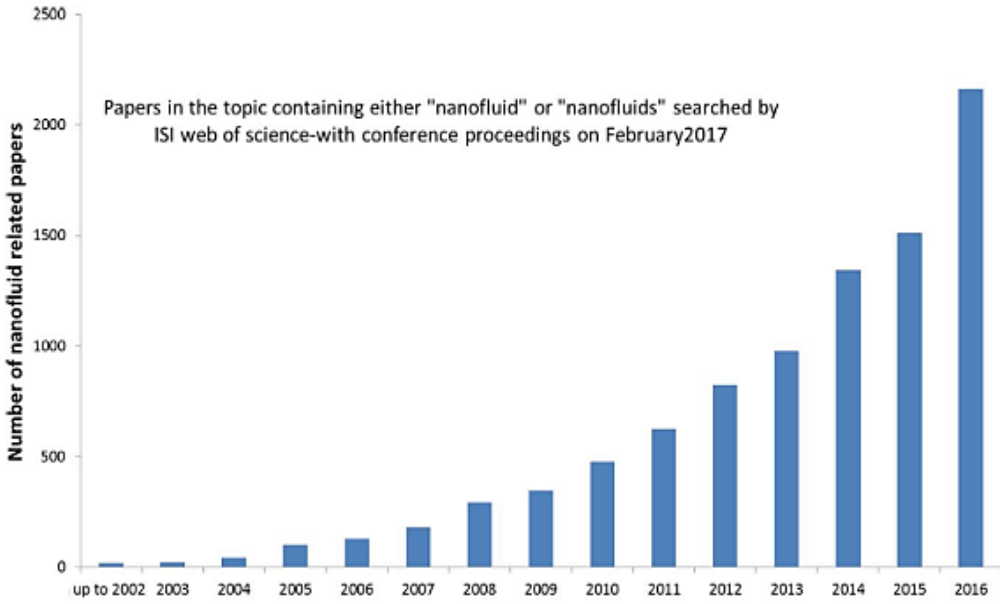

Figure 1-2 Number of publications containing the term nanofluid in literature[9]

Both numerical and experimental approaches have to be used in combination to unravel the real mechanisms behind the enhancing effect of nano particles added interplaying among the molecular scale, microscale, mesoscale and macroscale. These all reasons make all the research struggles to be directed towards is quarter a century old challenge.

1.1.1 Preparation of nanofluids

Nanofluids are not just mixtures of base fluid and nanoparticles. Rather they are uniform, stable, durable, colloidal suspensions with minimal accumulation of particles and no chemical alteration of base fluid. Their preparation is not just mixing rather a thorough step by step process. Researchers have developed a number of methods (generally categorized as single step or two step method) to prepare Cu-ethylene glycol nanofluid for their experiments[10]. The two-step method is to prepare nanoparticles in a separate step first and to suspend it into the base fluid later. The decisive step is the production of the Cu nanoparticles. Various methods for the synthesis of copper nanoparticles employing chemical, physical and biological techniques considering bottom-up and top-down methods synthesis have been investigated. The top-down approach where a bulk piece of a required material is reduced to nanosized dimensions using cutting, grinding and etching techniques (i.e., nanomaterials are prepared from larger entities without atomic-level

control) requires highly vacuumed systems and costly equipments. Hence the bottom up approach where the structure of nanoparticles is constructed from atoms, molecules or clusters is preferred[10].

Of all the recommended bottom-up methods chemical reduction method is typically preferable. On one hand it is easy, cost effective and efficient, on the other hand optimizing the experimental factors (like the molar ratio of the precursor salt with the reducing agent) is possible to improve size and dispersion. In addition, it only requires normal environmental conditions[11]. The size of nanoparticles is actually dependent on time of the reaction, the type and concentration of the reducing agent, the concentration of the Cu ions, the P^H the temperature[12]. The size of nanoparticles gets more smaller and smaller as the concentration of the reducing agent increases.

1.1.2 Characterization of nanofluids

The nano particles after being prepared, its size and morphology(composition) have to be analyzed, collectively called characterization. By characterization, it is to mean the through measurement of the thermophysical properties of the nanofluid including the particle size, density, viscosity, specific heat capacity, thermal conductivity etc. with the research graded procedures and equipments. There are two ways of characterizing nanoparticles. The first one is to experimentally measure the size and the size distribution of the nanoparticles prepared with the aid of optical instruments like energy dispersive X-ray spectroscopy (EDS), dynamic light scattering (DLS), transmission electron microscopy (TEM). The other way is to prepare the nanoparticle with controlled concentrations, temperature, time and other reaction variables to achieve the required size and distribution of the nanoparticles with previously established procedure which has been proved to produce the same size and morphology of the nanoparticle. The former way of characterization is accurate but expensive.

1.2. Problem statement

It has been a few decades ago since researchers report the anomalously enhanced heat transfer capability of nanofluids than conventional fluids. But, the amount of experimental data which can be reproduced so that it will assure that nanofluids shall be used as potential heat transfer fluid is still limited. There is also an ongoing debate about the magnitudes of these enhancements that exists between those of who agreed in the anomaly of the enhancements. To the best of the authors knowledge, the specific design (selection) of the nanofluid was not good enough to represent all the changes the suspension brought about to the base fluid in favor of exposing effects. Besides, no theory has been able to provide a solid and well-established explanation for the physical basis of the possible anomalous heat transfer enhancement of nanofluids. So, in designing the nanofluid a kind of a tradeoff has to be done between thermal conductivity increasing factors and viscosity decreasing factors like particle concentration and particle size.

1.3. Objective of the study

1.1.1. General objective

The general objective of this thesis is to investigate forced convective heat transfer of Copper/ethylene glycol (Cu/EG) nanofluid in turbulent flow both experimentally and numerically.

1.1.2. Specific objectives

The list of the tasks to be accomplished to complete this thesis work are

1. To prepare and characterize the nano fluids of Cu nanoparticle of different concentration suspended in ethylene glycol as a base fluid.
2. To experimentally investigate the convective heat transfer of the prepared nanofluid with varying Reynolds number, particle loading and inlet temperature.
3. To numerically investigate the convective heat transfer of the prepared nanofluid with both single phase and two-phase model in fluent code.
4. To validate the experimental and numerical results with each other and with theoretical correlations from the relevant literatures.

1.4. Scope and limitations of the study

This thesis work primarily focused on the forced convective heat transfer of Cu-EG nanofluid in a turbulent horizontal circular tube. The investigation will be accomplished by two approaches, experimental and numerical which finally be subjected to comparison to each other. In both cases the effect of particle concentration, Reynolds number, inlet temperature on forced convective heat transfer and pressure drop will be the main subject of interest. The preparation and characterization of the nanofluid for the experimental work is also the concern of this masters undertaking. In addition, the experimental setup for the sake of measuring the heat transfer coefficient is to be manufactured locally.

Thermophysical properties are only calculated from empirical correlations from the literature. Due to the limitation of the small rating of the pump used to supply pressure, higher Reynolds number turbulent flow could not be achieved for when the nanofluid was passed through the tube. As a result, the friction factor and heat transfer results for the nanofluid was measured mostly in the lower Reynolds number turbulent region only limited to 10000. Nanoparticle concentration was only limited to 1% due to the high cost of the raw materials and low yield of nanoparticle per each round of preparation process. Besides due to lack of sufficient computing power, only 2D axisymmetric analysis was done neglecting the circumferential migration of nanoparticles.

1.5. Significance of the study

Since the subject of nanofluids is more than just two decades old challenge, every piece of effort will really be greatly appreciated. The success of this research work will contribute a lot to the realization of nanofluids to practical application in any heat transfer appliances. It is also expected to bring about critical insights towards the design of nanofluids and tradeoff between the viscosity and thermal conductivity to bring about a significant heat transfer enhancement. Given that the number of both experimental and numerical data are limited, the very reproduction of any previous effort with very minor extra achievement will be warmly welcomed. That is why this research topic is worth considered.

It is also important for our research community to cope up to the recent reaches of outside counterparts in a way that the collaborated effort will bring communal benefit. The science of nanofluid is not yet well introduced to our country. And such kind of researches will be a very nice way of familiarizing such hot heat transfer issue. Most importantly, to have this experience in this newly emerging research area is a privilege in the first place and will have a great deal of advancement in practical, experimental, numerical and theoretical knowledge of the involved researchers

1.6. Thesis organization

This thesis comprises five main chapters with appendices at the end.

Chapter 1 Introduction: One of these chapters is the present introductory chapter, which summarizes the background, aims or objectives, the research question to be addressed, the scope and limitations, significance of the thesis work.

Chapter 2 Literature review: This chapter explores the literature on the nanofluid concepts from preparation methods to thermophysical properties. Previous studies on numerical simulation and experimental work on enhancing the heat transfer employing nanofluids in various applications were critically discussed with strong arguments of the success of the results from the point of view of our objective.

Chapter 3 Materials and methods: This chapter presents the nature of the experimental and numerical setups used to study the nanofluid heat transfer. The procedure for preparation and characterization of the Cu-EG nanofluid experimental setup fabrication, the mathematical formulations of the governing equations of the flow and modelling of the thermophysical properties through the user defined functions etc. are briefly discussed.

Chapter 4 Result and discussion: Both the experimental and numerical results of the respective set ups with clear discussions are subsequently presented. Comparison of those results with each other and the existing literature is also the subject of this chapter.

Chapter 5 Conclusions and recommendations: This chapter summarizes the main findings from this research, and the recommendations for future researches.

CHAPTER TWO

2. LITERATURE REVIEW

A number of research papers from various reputed journals regarding turbulent convective heat transfer have been collected and studied. This chapter presents a comprehensive review of convective heat transfer utilizing nanofluids in forced convection flows. This review focus on the concepts behind nanofluids and their thermophysical properties, along with appropriate ways to perform mathematical and computational modelling of such nanofluids. Approaches of the synthesis of nanofluids will also be surveyed. The numerical and experimental methods used to investigate nanofluids in convective heat transfer are the focus of this chapter; the findings of these investigations will also be given.

2.1. Introduction

Heat transfer enhancement has always been a challenge mainly due to energy conservation issues, exponential growth of heat flux density due to miniaturization in electronic and heat transfer equipments, compacted design of heat transfer devices. A long list of both active and passive techniques has been the subject of investigation but their success can't satisfy the demand of enhanced heat transfer. The target of heat transfer enhancement is increasing the product of heat transfer coefficient and heat transfer area (hA) which can be achieved by assembling extended surfaces and displaced inserts, roughening surfaces, coating surfaces, swirling the flow, introducing fluid additives. The intension is increasing the heat transfer area and/or creating turbulence on the solid-fluid interface which can only come true by additional material requirement and excessive exergy payment (pressure penalty)[13].

Most of the passive techniques require modification or replacement of the existing heat transfer equipment with the new design. They are also subjected to the manufacturing limitations. Even worse these techniques have reached to the state of bottle neck since they all are subjected to the thermal conductivity of the working fluid. So, it goes without saying that enhancing the thermal conductivity of the heat transfer fluid can enhance the

heat transfer capability of existing heat transfer systems. The new design of the heat transfer equipments will also be compact and efficient[4].

The thermal conductivities of solids are orders of magnitude higher than liquids mainly due to the closeness of the solid particles to each other as shown in table 2.1. The idea of suspending solid particles into the conventional working fluid (base fluid) appears to enhance the thermal conductivity of the base fluids as proposed by Maxwell a century ago[6]. Having this concept in mind a great deal of research effort has been mobilized towards exploring the possibility of application of this novel idea ever since it has been proposed. Micro and macro sized solid particles were suspended into base fluids and their thermal performance effects have been measured. The results claim that the thermal conductivity of the fluids did really get enhanced but a number of concerns come with the application of this suspensions in heat transfer systems. Amongst them the large size of the suspended particles exposes the system for clogging and erosion of the flow channel, fouling heat transfer surface due to rapid settlement, enhanced pressure-drop. It is also expected to suspend high concentrations (>10%) of solid particles to achieve the required surface area to volume ratio which in turn makes the fluid muddy[14].

Reducing the size of the particles to nano scale which was actually possible almost a century after Maxwell proposed his idea was unifying solution to almost all of the aforementioned problems. The suspension of nano sized solid particles into the conventional heat transfer fluids called as nanofluids (as coined by Choi in 1995) have been the very hot issue of the two and half decades old heat transfer engineering challenge. Nanofluids are uniform colloidal suspensions of nanosized solid particles in a liquid. A number of researches have been done regarding the preparation, stability characterization[15]–[21], thermal conductivity[1], [6 -10] and pressure drop aspects of nanofluids so as to generate enough data to decide if and when the application of nanofluids is helpful. Conduction experiments have indicated that nanofluids tend to have substantially higher thermal conductivity than the base fluids.

Table 2-1 Thermal conductivities of some commonly used fluids and solids

Material	Thermal conductivity (W/m-K)
Metallic solids	
Silver	429
Cupper	401
Aluminum	237
Nonmetallic solids	
Silicon	148
Metallic liquids	
Sodium @ 644K	72.3
Nonmetallic liquids	
Water	0.613
Ethylene glycol	0.245

Earlier investigations were only directed towards measuring thermal conductivity enhancement which can never be a conclusive evidence for applying a nano fluids in any heat transfer equipment requiring a better performance[25]. Thermal conductivity is actually one of the fluid properties. All the required flow conditions and fluid properties should be available to decide whether the given nanofluid is applicable to given constraint or not. A manifestation of all these properties and conditions is heat transfer coefficient. So, knowing the value of heat transfer coefficient can serve as a conclusive evidence in the decision to select a nanofluid for a particular application because knowing the heat transfer coefficient can only be true if the thermal conductivity, density, viscosity specific heat capacity, Reynolds number and all other flow and fluid properties are known[14].

A number of both experimental and numerical researches has been done with this respect. Almost all the reports agrees on the very presence of the heat transfer enhancement of suspending nano particles into the base fluids which is way more higher than the thermal conductivity enhancement[2], [26]–[33]. Thermal dispersion (due to the chaotic movement of nanoparticles), boundary layer suppression, migration of nanoparticles and

the subsequent disturbance of the boundary layer, the flattened velocity profile caused by the particle migration to the centerline of pipe are some of the proposed mechanisms responsible for the enhancement[34]–[37]. But there is still a great deal of variation in the magnitude of enhancement for each solid-liquid combination at each particle loading, diameter and shape which is yet to be reconciled.

2.2. Effect of Reynolds number, nano particle type, size, concentration, inlet temperature and base fluid type on heat transfer coefficient and pressure drop of nanofluids

The real mechanisms for the measured heat transfer enhancements are not fully understood yet. It is because the very nature of nanofluid needs the molecular and microscopic approach at a time. But recently tremendous and seemingly fruitful efforts are being applied to reveal these complex happenings. Using both numerical and experimental studies, investigators strived to unravel the enhancement of convective heat transfer in nanofluids.

It has been proved that the Nusselt number or non-dimensional heat transfer coefficient of nanofluids increases with volume fraction, inlet temperature, Reynolds number[27], [30]–[33], [38]–[43] as evidenced by reduction in tube wall temperature at a constant heat flux [1,2]. Li Qiang et al. experimentally investigated Cu/water nanofluid in a straight brass tube to see the effect of particle concentration and flow velocity on the HTC and pressure drop. According to their results HTC is observed to increase with particle concentration (60% at 2% volume fraction) and flow velocity comparably coincident with HTC predicted by theoretical correlations. They articulated the thermal dispersion, boundary layer suppression and thermal conductivity augmentation as a reason for such an enhancement[46]. Abkar et al. also presented a respective enhancement of Nusselt number of 30% and 22% for water-Al_2O_3 and water-TiO_2 at 1.6% with an experiment in straight copper tube fully developed laminar flow[47].

Zamzamian et al. carried out a turbulent, forced convective heat transfer experiment on aluminum oxide and copper oxide in ethylene glycol nanofluids in double pipe and plate heat exchanger in an effort to examine the effect of inlet temperature and particle loading

on the heat transfer capability. For a 1% volume fraction of CuO in ethylene glycol a Nusselt number enhancement of 37% and 49% is achieved for double pipe and plate heat exchanger respectively. And for a 1% volume fraction of Al_2O_3 in ethylene glycol a Nusselt number enhancement of 26% and 38% is achieved for double pipe and plate heat exchanger respectively. In both cases the enhancement is even steeper at higher inlet temperatures[32]. Xuan et al. scrutinized the HTC and the friction factor of Cu-water nanofluid in turbulent tube experimental test rig at a range of Reynolds number of 10000 to 25000 and particle loading of 0.2 to 2%. Their result depicts that the HTC increases with particle loading and flow velocity with more than 39% for 2% particle loading. The pressure drop of dilute suspensions is almost the same to the base fluid[48].

Although these seemingly strong agreements, there is still a great deal of variation in the magnitude of the enhancement. Even some researchers also claimed that HTC of base fluids decreases when nanofluids are suspended into it. Pak and Cho investigate experimentally $\gamma - Al_2O_3$-water and TiO_2-water nanofluid of 13-27 nm particle size in a turbulent horizontal circular tube. Their result shows that Nusselt number increases with Reynolds number and volume fraction but for larger volume fractions it is considerably smaller than base fluid. They also recommended that clever selection of particles having higher thermal conductivity and larger size (smaller viscosity) has to be done to use nanofluids as a working medium to enhance heat transfer performance[49]. Because viscosity increases with the surface area of the suspended materials. But the effect of this is far lesser when the particle concentration is smaller[31].

Some are even against the assertion of an anomalous heat transfer enhancement. They believe that the increment can be predicted by the available theoretical correlations. they strongly argue that if the data presentation or comparison basis is pumping power rather than Reynolds number, the Nusselt number is the same as the base fluid. Comparing Nusselt number based on Reynolds number cannot be done at the same mass flow rate[41].

Jung et al. experimentally measured the convective heat transfer coefficient of Al_2O_3-water nanofluid in the fully developed region of a circular straight tube with a constant heat flux. An increment of heat transfer coefficient from 14% to 30% was observed as the

temperature of the fluid increases from 22℃ to 75℃ at 3.0% volume fraction. They proposed the decrease of kinematic viscosity of nanofluid which leads to the increased Brownian motion as a mechanism for the observed enhancement[39]

Namburu et al numerically analyzed the turbulent flow and heat transfer behavior of CuO, Al2O3, SiO2 in EG/water (60:40 by mass) nanofluids in a circular tube subjected to constant heat flux. Nusselt number of the nanofluid increases with volume fraction for a fixed particle type and size. Their results also witnessed that Nusselt number increases with thermal conductivity of the particle (particle type) at a fixed volume fraction and particle size. They also said that Nusselt number and viscosity increases as the particle size decreases at a fixed particle type and volume fraction[50]. But all these comparisons are made at constant Reynolds number which has nothing to say about the pumping power.

Saha, G. and Paul, M[51]. numerically investigated the effect of volume concentration and particle type and size of Al_2O_3 and TiO_2 nanoparticles in water flowing in a turbulent manner through horizontal circular pipe. Evidently, they concluded that heat transfer rate increases, with almost no significant extra penalty of pumping power, with Reynolds number, particle concentration rises and with particle diameter decrease. In addition, Al_2O_3-water nanofluid shows better heat transfer performance than TiO_2-water nanofluid. Delay in boundary layer growth, decrease in boundary layer thickness and enhancement of thermal conductivity or Prandtl number are among the reasons attributed for such behaviors.

Namburu et al[50]. analyzed the turbulent flow and heat transfer behavior of CuO, Al_2O_3 and SiO_2 nano particles of different particle diameter and concentration in ethylene glycol and water mixture in a circular tube under a constant heat flux boundary condition using numerical methods. For the same particle concentration of SiO_2 nano particle, they observed that smaller diameter results in higher viscosity. Using a smaller nano particle demands a greater number of particles to achieve the same particle concentration, leading to high surface area and more interaction with the surrounding and then higher viscosity. Besides, CuO nano particles yielded better heat transfer enhancement than others due its

inherent higher thermal conductivity. They agreed with other researchers on the positive effect of particle concentration and Reynolds number on Nusselt number

Moraveji and Beheshti investigated numerically nanofluids of Al_2O_3, TiO_2 and CuO in carboxy methyl cellulose aqueous solution in horizontal circular tube under constant wall temperature and turbulent flow conditions in an effort to predict the effect of particle type, size and loading on the forced convection heat transfer. Heat transfer coefficient was proved to increase with nano particle concentration and Peclet number. The simulated results and the experimental data they compared their results with agreed very well which confirms that single phase model can predict heat transfer coefficient sufficiently given that the particle size is small enough[52].

Bianco et al. used Al_2O_3/water nano fluid to understood the effect of particle loading on forced convective heat transfer in a turbulent circular tube using two different numerical approaches. They reported that the heat transfer coefficient ratio is proportional to particle loading and Reynolds number. Their comparison between their models shows that mixture model follows exactly the same behavior with single phase model but the deviation gets intense as the particle loading increases[44]. The closeness of the result would have been magnified if more accurate thermophysical property correlations have been used.

2.3. Single phase and multiphase model comparison

Still now two main approaches (single-phase model and multi-phase model) of evaluating the effect of suspension of nanoparticles into the conventional fluid have been used. The basic distinction being the assumption that nanofluids with ultrafine particles can be treated as single phase homogeneous liquid with the treatment of the nanoparticles being in thermal equilibrium without any slip with host fluid molecules (relative velocity is negligible). With accurate effective thermophysical properties provided conventional mass, momentum and energy equations can be applied to nanofluid thermal and hydraulic characteristics determination[53].

The choice of the model is open to the volume fraction, the particle size, the accuracy required, the available computational power and time. A number of papers have been

reported based in this particular model [14,15,19,20] which shows single phase model is good enough to predict the heat transfer and flow characteristics of nanofluids. The success of this model relies on the fineness of the nano particle and the degree of dilution of the suspension plus the accuracy of the models used to predict the effective thermophysical properties[50]. When the volume fraction is smaller (dilute suspension), the particle-particle interactions or interphase forces are negligible which makes the single-phase model more accurate. Especially in the turbulent flow regime a relatively small volume fraction is required to bring about sufficient movement across the boundary layer and thermal mixing which are responsible for the required enhancement. Besides single-phase model is simple and requires least computational resource at reasonable accuracy sacrifice[45].

Kumar et al. studied the flow and heat transfer characteristics of Al_2O_3/water nano fluid in a turbulent pipe at a constant wall temperature condition using CFD modeling. They observed that for low particle loading the increase in pressure drop is not as steep as the Nusselt number increase which makes low particle loading nanofluids an effective heat transfer augmentation technique. The single-phase model is again proved to predict the experimental values with reasonable accuracy for less than 1% particle loading[55]. Esfandiary et al[57]. numerically compared single-phase and Eulerian multi-phase models in predicting convective heat transfer coefficient and pressure drop of alumina-water nanofluid in a uniformly heated pipe. Compared with experimental results from the literature, they reported that single phase analysis results are more accurate than the two-phase model.

Bianco et al[50]. analyzed a turbulent forced convection flow of waterAl_2O_3 nanofluid in a circular tube under uniform heat flux boundary conditions to compare the accuracy of single-phase and multi-phase models. They reported that compared to experimental results from literature, both the models detect the same decrease in wall temperature for particle concentrations up to 1%. But after that single-phase model starts to underestimate the wall temperature and the variations increases with particle concentration. Similar behavior was also observed for bulk temperature.

2.4. Turbulent model comparison

There are no defined standard criteria for selection of turbulence models. The capabilities and limitations of the existing turbulence models is subjective to range and type of flow under study. Thus, evaluating the performance of each turbulence models which passes the screening test has always been the prior and decisive step in any numerical study of fluid flow and heat transfer problems. Not every turbulent model closely approximates nanofluid heat transfer coefficient and friction factor. Choosing the turbulence model which predicts the flow and thermal behavior of nanofluids with close precision has been the subject of investigation since the numerical exploration of the nanofluid heat transfer potential[58]. Among the several factors: the physics of flow field, the computational resource available and level of accuracy required are the most decisive to be taken in to consideration.

Bayat and Nikseresht investigated Standard k-ε, Renormalized Group (RNG) k-ε, the Realizable k-ε, the Standard k-ω, the Shear Stress Transport (SST) k-ω and the Reynolds Stress (RSM) turbulent models a circular tube with a constant heat flux condition. They chose realizable k-ε turbulent model with the near wall enhanced function for turbulence modeling. This model has been preferred over others in many other investigations [59] after being compared with experimental data and corresponding numerical predictions by several turbulence models combined with different wall functions.

Mahdavi et al[60] compared the heat transfer enhancement effect of four different nanofluids using the different ANSYS Fluent built in turbulence models with respect to the experimental results from the literature. Their result shows that all the two-equation k-ε models predict the heat transfer coefficient with a good precision except the RNG k-ε equation which (better estimates the pressure drop) over predicts the heat transfer coefficient by 12%. Whereas the RSM equation is proved to calculate the heat transfer equation with a higher precision which turned out to underestimate the pressure drop by 14 to 16 %. Boertz et al[61] compared standard k-ε, k-ω and k-ω-SST simulations in a turbulent pipe with that of empirical results of friction factor and Nusselt number from the literature. The k-ω-SST is found to deliver the lowest deviations to empirical correlations.

2.5. Concluding remarks

The controversy on the claim of the reality of the heat transfer enhancement is believed to be the abuse of the advantage increasing nanoparticles concentration due to lack of the proper design of the nanofluid. Both the thermal conductivity and viscosity increase with increasing particle concentration which have a conflicting effect on the convective heat transfer coefficient[40]. It appears there is and should be a critical or optimal value of volume fraction for maximum enhancement for a given flow setup[11 – 15].

Sahin et al. evaluates the convective heat transfer coefficient under turbulent flow in horizontal aluminum tube of a range of volume fraction of CuO- water nanofluid in an effort to predict the critical volume fraction. The result shows that heat transfer only increases up to 1% volume fraction. Any increase in volume fraction of the CuO drastically decreases the Nusselt number. The maximum enhancement is recorded at 0.05% volume fraction and 16000 Reynolds number[65].

Corcione et al. claims that the advantage of the nanofluids should only be judged in terms of the global energetic performance. They out louds that their exists an optimal particle loading for a given Reynolds number, aspect ratio of the test section and particle diameter that will result maximum rate of heat transfer at a fixed pumping power or minimum pumping power at a fixed rate if heat transfer [62].

Gosselin et al. also recommended a tradeoff to optimize the competing effect of thermal conductivity and viscosity increase with the amount of particle added so as to maximize the rate of heat transfer at a given pumping power. They also commented on the data presentation styles which prevails in most of the publications as it must not be at a fixed Reynolds number which literally means at a fixed mass flowrate but may at a different pumping requirement[63]. Some other researchers reflected the same standpoint on the data presentation style. They asserted that heat transfer enhancement must be compared against the constant global energy performance of the test section[49].

Starting from the very beginning of its history, nanofluid science is simply filled with bunch of experiments with inconclusive results and some contradictory propositions that

are supposed to be the reasons for anomalousness of the results. It lacks conclusive evidence to synthesize a nanofluid pertinent to some real word problems which optimizes all thermal transport properties. Improving one thermal property may degrade the other. For the record in almost all of the suspensions thermal conductivity increases with volume fraction but this increases the viscosity which will in turn reduce the convective heat transfer coefficient, the most important attribute for a fluid to compete for a given heat transfer application. The convective heat transfer coefficient by itself is a function of a long list of parameters besides to thermal conductivity and viscosity.

Therefore, judicious decision should be taken when selecting a nanofluid that will balance the heat transfer enhancement and the pressure drop penalty. The models and correlations proposed to predict this property are by far the longest list which pitfalls to select with. The type of the nano fluid and regime of the flow it will be experimented in must be selected in the way that will reconcile these contradictions. The fluid which will result in agreement in all extremes of these fluids have to be tested in a condition that will represent most of practical circumstances that the nanofluid is to be applied. Perhaps Cu/ethylene glycol nanofluid is the best suit.

CHAPTER THREE

3. MATERIALS AND METHODS

In this chapter the whole list of procedures followed and equipments used to solve the main and aforementioned problem were outlined. The nanofluid selection, preparation, characterization techniques were clearly discussed. The experimental and numerical approaches typically applied to this research work were presented. The experimental philosophy for measuring the effect of nanofluids on convective heat transfer and the numerical procedure for simulating the same phenomena with the methods of comparison and validation were described.

3.1. Selection of nanofluid

The right combination of nano particles and base fluids is the first and most important decision to be made to reach the roof of enhancement nanofluids can bless. Base fluid of the highest Prandtl number (for EG ranging from 47 to 150 based on temperature) and nano particles of the highest thermal conductivity (for Cu 401 W/m.℃) is believed to be the favorable choice[27]. Besides that, EG has been commonly used as the main cooling fluid and anti-freezing agent in heat exchangers and thus improving its thermal properties will be of a great importance. Thermophysical properties of dispersed nano particles must be significantly different from those of carrier fluids. The density difference between nano particles and base fluid must not be exaggerated so that settling won't be a concern. Otherwise, electrostatic repulsion forces between particle surfaces or surfactants should be applied to the dispersion. The latter method looks easy to apply but found to cause significant changes in the thermophysical properties of dispersed fluids. Metal nanoparticles have attracted considerable interest particularly because of the size dependence of physical and chemical properties and its enormous technological potential. They actually have the highest thermal conductivity since 20% of their atoms are on the surface for particles finer than 20 nm making the thermally interactive[21].

3.1.1. Particle loading and particle size selection

Particle size and particle loading are the next decisive issues to be considered in such a way that the conflicting effect of them on the heat transfer coefficient is optimized. To

achieve a fixed particle loading with smaller particles requires larger number of particles which in turn is the higher surface area to volume ratio[50]. The lower the particle size and the higher the particle loading are the higher the thermal conductivity and viscosity. Nanofluids are only worth using as a fluid medium for convective heat transfer enhancement as long as the increase in the pressure drop due to the addition of the nano particles is not significantly large to offset the heat transfer enhancement[62].

For this thesis work nanofluid of Cu nano particles in ethylene glycol was selected and prepared at an smaller particle size (nearly 20 nm) and lower particle loadings possible (up to 1%) so that the highest enhancement at a reasonable viscosity increase as outlined from the literatures can be achieved.

3.2. Preparation of the Cu-EG nanofluid

A two-step method, chemical reduction method and subsequent ultrasonication, was adopted to prepare nanofluids of required particle size and volume concentration.

3.2.1. Preparation of Cu nanoparticles

For this particular experiment, the Cu nano particles was prepared by reducing copper (II) sulfate Penta hydrate ($CuSO_4.5H_2O$, precursor) by sodium borohydride ($NaBH_4$) with adopted chemical reduction method from Khatoon et al[11]. Both the chemicals used in the present study ($CuSO_4.5H_2O$ and $NaBH_4$) were reagent grade purchased from Alpha chemical LTD. Double distilled de-ionized water was used for making the solutions. The right procedures followed with the proper proportion of all the ingredients used were described in detail and summarized in the schematic on Fig 3.1 followed by the list of equipments used to execute each procedure in Organic lab of food and chemical engineering faculty of the institute.

1. 0.02M of aqueous $CuSO_4.5H_2O$ was prepared by adding 2g of $CuSO_4.5H_2O$ to 400 ml distilled water
2. 0.02M of aqueous $NaBH_4$ was prepared by adding 0.4g of $NaBH_4$ to 500 ml distilled water
3. $NaBH_4$ solution was transferred into a 2000 ml flask using a graduated cylinder

4. $NaBH_4$ solution was stirred with a magnetic stirrer and heated for 10 minutes at 85℃ on a hot plate.
5. Then 400 ml of $CuS0_4.5H_20$ solution was added to the flask drop by drop, at a rate of 1 drop / second, using a burette.
6. The mixture was heat at 85℃ for another 5 minutes with continuous stirring.
7. Cover the flask with aluminum foil and keep the settled residue in hot air oven.

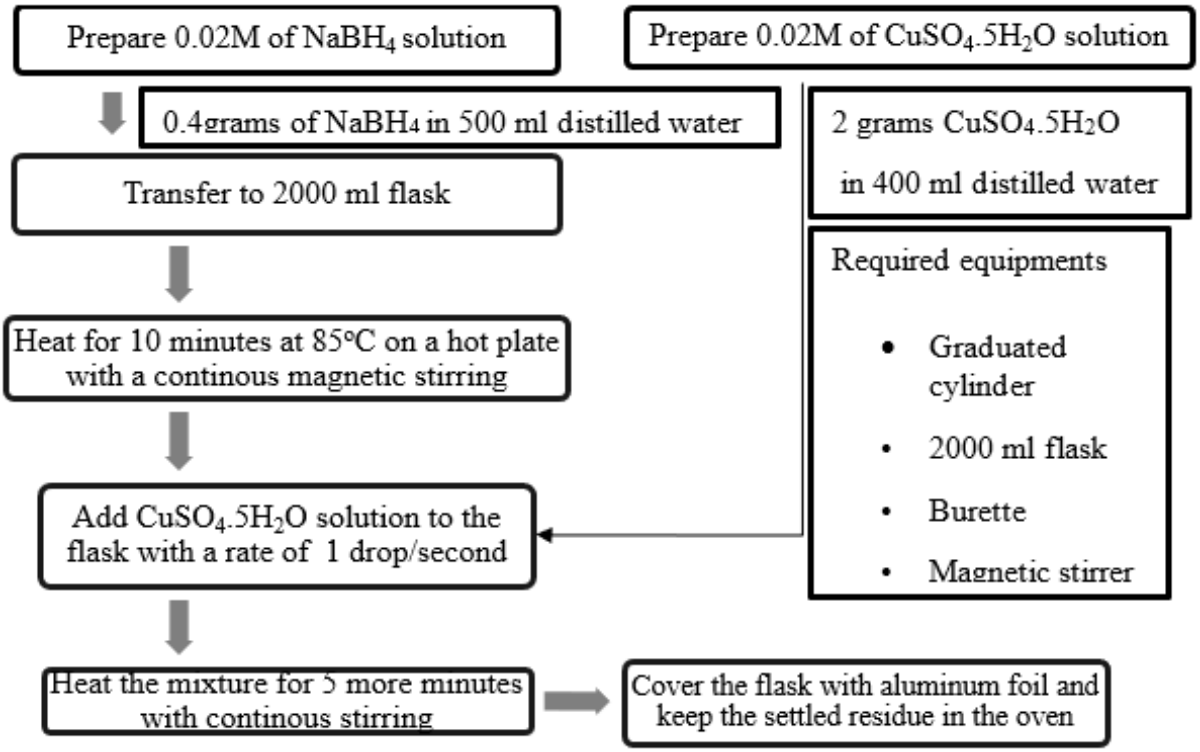

Figure 3-1 schematic diagram for the preparation procedure of Cu nanoparticle.

Figure 3-2 Reagents used and respective solutions prepared

The prepared nanofluid was mixed with ethylene glycol according to the right proportions demanded by the particle concentrations based on the calculation in apendix C and altrasonicated for uniform and sustainable suspension.

3.3. Characterization of the nanofluid

The optical properties of the synthesized CuNPs were determined by an ultraviolet visible (UV-Vis) absorption spectrophotometer available (PerkinElmer Lambda 35) in the range of 500-750 nm, in quartz tubes cleaned from dust and impurities. The sample for the UV-vis spectroscopy was made by diluting 20 mg of Cu nanoparticles in 10 ml distilled water since distilled water was used as a blanking solution.

Figure 3-3 UV-Vis absorption spectrophotometer and prepared sample in the quartz tube

The particle size distribution of the copper nanoparticles was analyzed by a DLS instrument (Malvern, Nano-ZS)

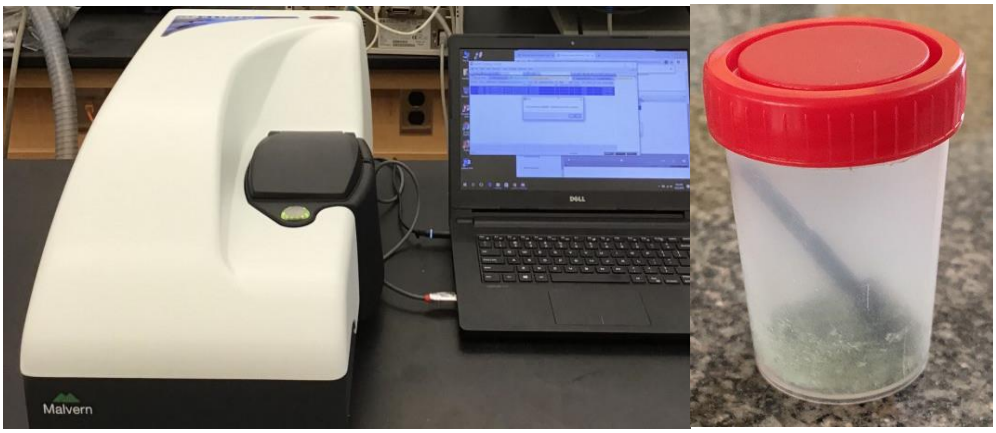

Figure 3-4 DLS instrument and nano particle sample

3.4. Design of Experiment (DOE)

An experimental set up as shown in the pictorial view in fig 3.5 was adopted from literature to carry out the forced convective experiments for the nanofluids based on the following considerations. Since a complete understanding of the enhanced heat transfer of nanofluids is aimed, geometry of the problem should be as simple as possible so that fundamental procedures can be applied and any parameter that provides heat transfer enhancement can easily be recognized. Therefore, a straight pipe, which is one of the most common configurations of any heat transfer equipments in industry, is the most proper instrument for this study. In addition, a forced single-phase internal turbulent flow through a circular tube is the most commonly encountered engineering heat transfer problem because of its key role in studying, designing, and implementing practical turbulent flow of nanofluid in application systems.

Heat transfer coefficients of prepared base and nanofluids will be measured using a locally built test rig. A schematic of heat transfer test rig is shown in Figure 3.5. The fluid flows from the a 10L reservoir through a centrifugal pump. The centrifugal pump is sized to cover a wide range of flowrates up to 35 lit/min. Based on the properties of the nanofluid, particularly viscosity, the pump can cover a Reynolds number range from 4000 to 10000.

The fluid then enters the stainless-steel test section. There are eight thermocouples two of which are placed in the fluid at both the inlet and outlet of this section the rest are on the wall of the test section arranged axially separated by a proper interval. The test section itself was formed from 20mm diameter and 1100mm length (long enough to achieve fully turbulent flow at the end) stainless- steel tubing. The entire heat exchange section was wrapped in heat tape which provides a constant heat flux to the fluid. A layer of insulation was wrapped around the heating tape to ensure low heat loses within the heat exchange section. Temperatures were monitored in real time using a data acquisition system monitored built in by Squirrel view program designed for the system.

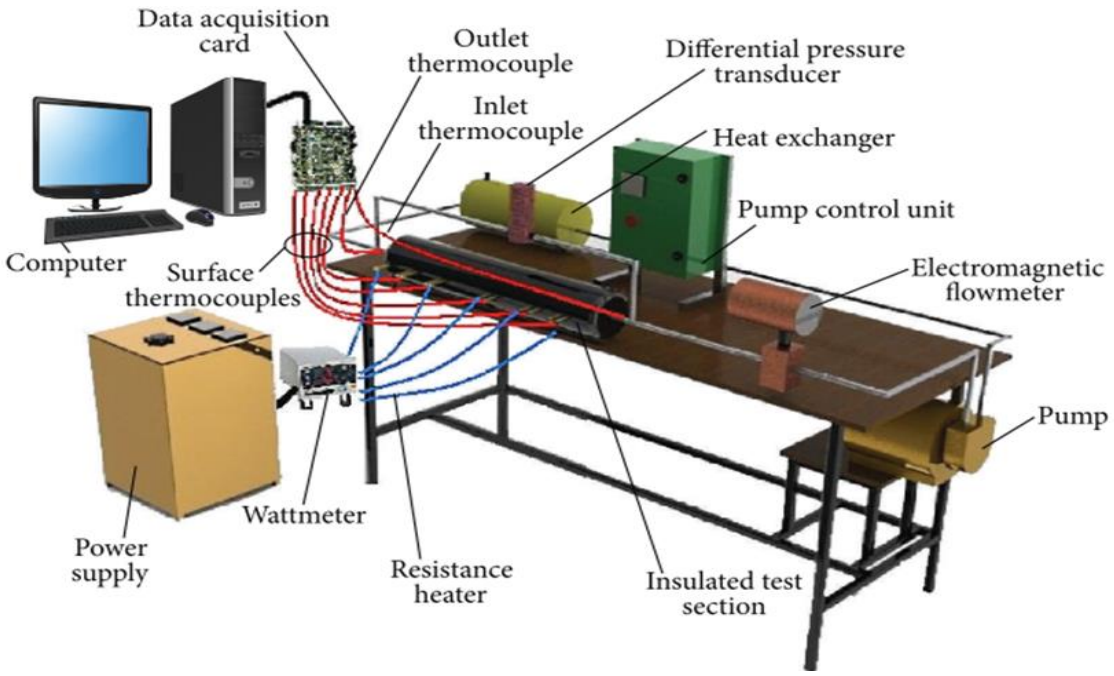

Figure 3-5 A schematic of proposed heat transfer test rig[65]

The reservoir stores the nanofluid which is circulated through the entire flow loop and then flow back to the reservoir a centrifugal pump. An air-cooled heat exchanger right after the test section removes any heat gained by the fluid when passing through the heated test section. The DC power supply unit supplies the current for heating up the test section.

3.4.1. Fabrication of the experimental setup

The experimental set up consisted of a flow loop, a test section (heating unit), a cooling unit, a flow measuring unit and a pressure drop measuring unit.

Test section

The test section made from stainless steel pipe of 20mm internal diameter with length of 1100 mm and 1 mm thickness. A 500 W heater tape was evenly rapped around all over the length of the test section which is connected with the power source controlled by the power controller for providing constant heat flux. To measure the surface temperature four K-Type 3m cable length, 100mm probe length, 6mm probe diameter and 8mm threaded thermocouples were fixed evenly spaced along the length and evenly distributed along the circumference of the stainless-steel pipe. The thermocouples were fixed to the pipe wall with a threaded holder to ensure sufficient contact between the thermocouple probe and tube surface and to avoid the damage of the probe tip and the interference of processes like welding and soldering. Two additional thermocouples of similar features were used for measuring the fluid temperature at the inlet and outlet sections.

Figure 3-6 Silicon rubber heater tape, K-type thermocouples and U-tube manometer

The test section was isolated from both upstream and downstream components both thermally and electrically by nylon bushings to avoid axial heat loss. Its outer surface was also thermally insulated with a 30mm and 25mm thick fiber glass fiberglass tube to avoid radial heat loss.

Figure 3-7 Heater tape wrapped around the stainless-steel tube

All the thermocouples were connected to a Squirrel 2020 series datalogger which in turn is connected to a computer via USB measures input signals of temperature with thermocouples. The data acquisition unit used for this experiment comprises of Squirrel 2020 series data logger connected to a computer.

Flow loop

The flow loop was made from commercial galvanized steel and stainless-steel pipe (the test section) flanged together at the two ends of the test section in such a way that the axial heat transfer is reduced to its negligible level compared to the radial conduction. All the equipments like the pump, cooler, valves, manometers and reservoir tank are fixed to the flow loop with the proper alignment. A centrifugal pump with a maximum rated speed of 1750 RPM and rated for a maximum flow of 35 LPM was used with its suction side connected to the reservoir and its discharge side is connected to a Tee dividing the flow through the closed loop and a bypass. The flow loop in return is fixed to the primarily rigid structured support made from angle iron.

Figure 3-8 Flow loop with power supply reservoir, heat exchanger and manometers fixed

A simple concentric orifice plate made from 30mm diameter thin stainless-steel sheet with a 12 mm round edged circular hole was fixed in the flow loop. A U-tube manometer was tapped one pipe diameter across the orifice plate (both upstream and downstream) to measure the pressure drop.

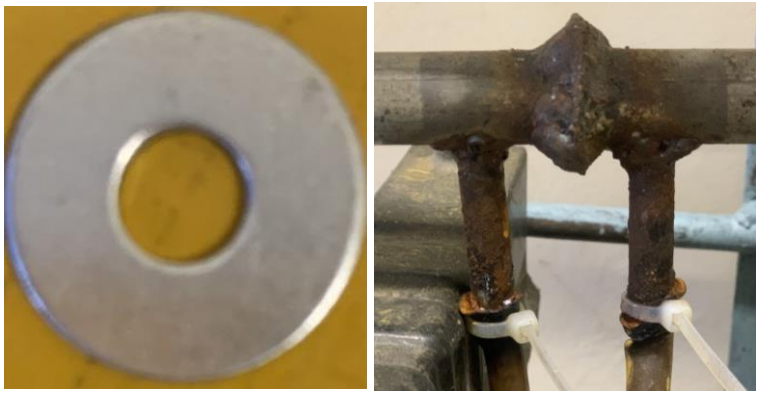

Figure 3-9 Orifice plate and orifice meter

The complete experimental setup with all the required components fixed and ready for measurement was shown in the Fig 3.10.

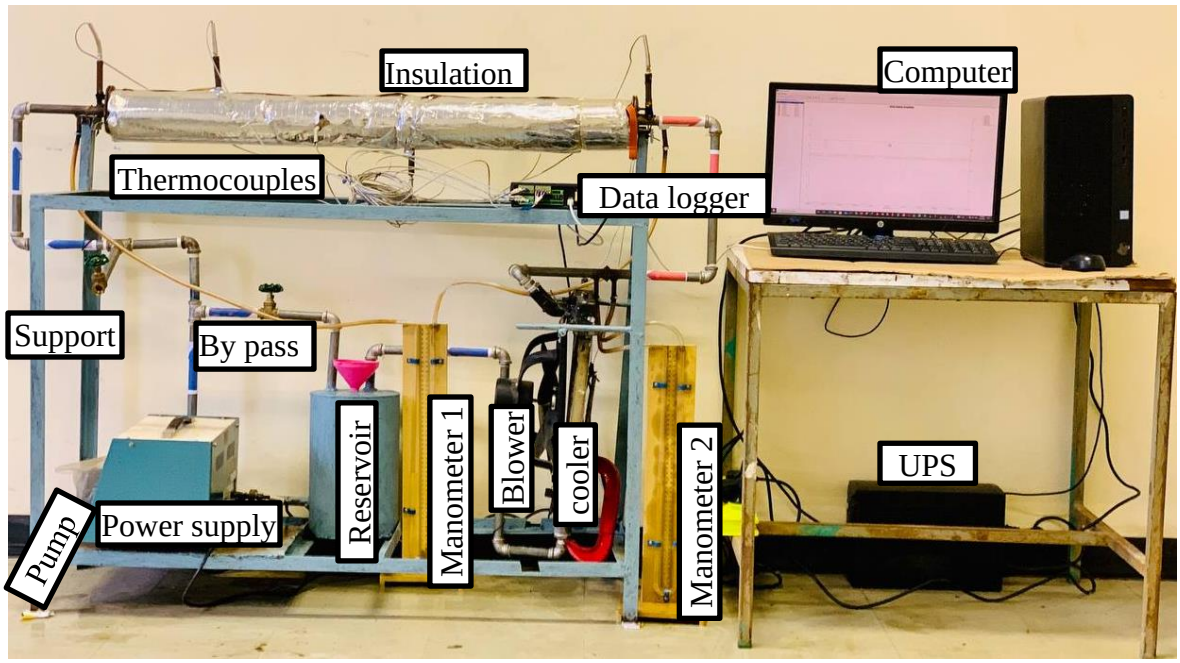

Figure 3-10 Experimental set up

3.4.2. Calibration of the experimental set up

Typical measurements for base fluids were carried out for the validation of the constructed system or check the reliability of the setup which ensures the correctness of the results, repeatability of the tests. By comparing the measured Nusselt numbers of ethylene glycol at the fully developed turbulent flow with the calculated values using one of the traditional models available in the literature. Bejan [66] recommends the equation given by Gnielinski,

$$Nu = \frac{{}^{f_n}/_2\,(Re - 10^3)Pr}{1 + 12.7\left({}^{f_n}/_2\right)^{1/2}\left(Pr^{2/3} - 1\right)}\left[1 + \left({}^{D}/_{L}\right)^{2/3}\right] \tag{3.1}$$

over the traditional Dittus–Boelter equation, because the errors are usually limited to about ±10% than ±40% for Dittus-Boelter equation.

Where, the fluid the physical properties must be evaluated at the bulk temperature T_m and the Fanning friction factor f_n defined by the so-called Fanning equation for smooth tubes can be calculated through the relation

$$f_n = 0.25(0.79lnRe - 1.64)^{-2} \quad (3.2)$$

Darcy friction factor expressed via the Blasius equation[67] was used to validate the rheology aspect of the analysis

$$f = 4C_f = 4(0.0791Re^{-0.25}) \quad (3.3)$$

The result was expressed in terms of coincidence between the two and precision of the experimental result.

3.4.3. **Experimental philosophy**

The heat transfer coefficients of the nanofluids were measured in horizontal copper tube with constant heat flux on the wall. At a given flow velocity and inlet temperature the effect of particle concentration on convective heat transfer coefficient and pressure drop is measured. Again, at a given particle concentration and flow velocity the effect of inlet temperature on convective heat transfer coefficient and pressure drop is measured. Also, at a given particle concentration and inlet temperature, the effect of flow velocity on convective heat transfer coefficient and pressure drop is measured. The characterization measurements were conducted at the same temperature ranges of the convective heat transfer measurements in order to study the stability of the fluids in the temperature range.

During the experimental runs, the tube outer wall temperatures, inlet and outlet temperatures of the nanofluid, mass flow rates and electric power inputs as well the static pressures are measured. The inner wall temperatures are calculated by applying the 1-D (radial) heat conduction equation in radial direction. The bulk fluid temperature along the axial distance in the test section is obtained through the energy balance between the point where the heat transfer coefficient is to be obtained and the entrance of the test section. From the measured values of temperatures, the local convective heat transfer coefficient and the Nusselt number of nanofluids at a given flow condition are determined. The same procedure is repeated for different, heat flux and inlet temperatures and at different operating conditions. Enough care has been taken to avoid any interference of the tape heater with the thermocouples. To control the temperature of the test fluid, a cooling section was provided after the test section so as to keep the temperature constant at the inlet conditions.

3.4.4. Test procedure

Heat transfer coefficients of prepared base and nanofluids were measured using a lab-built test rig. A constant-heat-flux boundary condition was achieved by heating the heat transfer test section electrically with a constant DC power supply. The uniform heat flux condition was ensured by checking thermocouple readings at four circumferentially different points along the test section.

The heat transfer measurement procedures are:

- set up the blower;
- Start the pump and circulate the fluid until inlet fluid temperature is stable at the bath temperature using different capacity blowers;
- Set up desired flow rate and heating tape power
- Record data after the system reaches steady state (usually in 20-30min).

3.5. Numerical set up

In this subchapter, the mathematical models and the numerical approaches employed to solve them in the present study were discussed. The governing equations of the flow and heat transfer, the numerical code and CFD solution method were presented. The geometrical modeling, the mesh generation with all the boundary zones properly labelled were also reported. The general flow chart followed while solving the aforementioned procedure using commercial ANSYS Fluent 2021R2 software was as shown in the Fig 3.11.

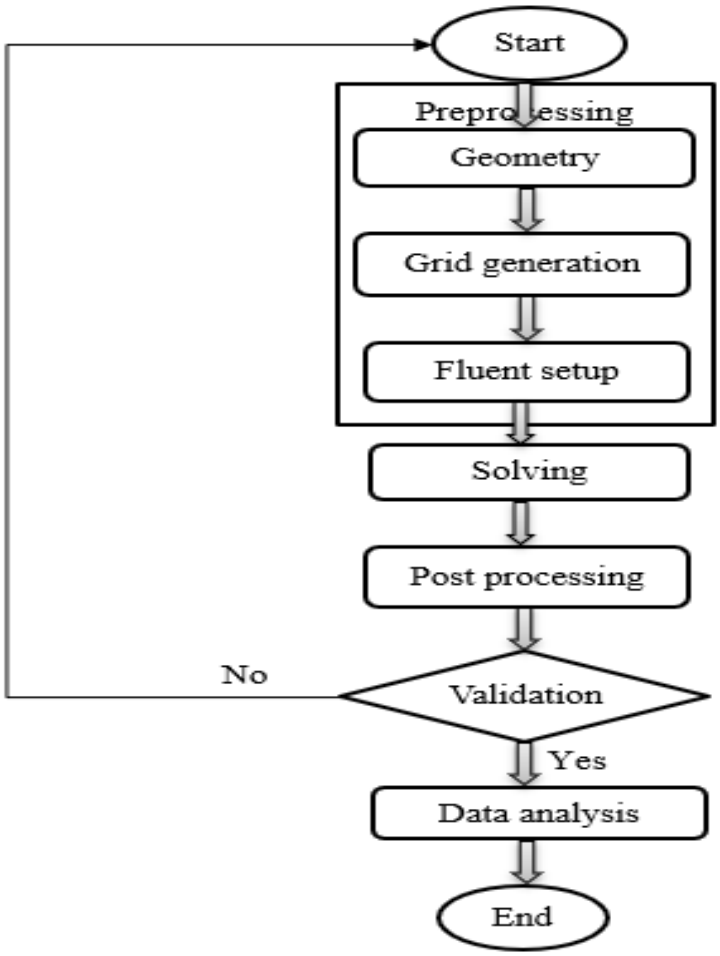

Figure 3-11 CFD flow chart

3.5.1. Geometry

The geometrical configuration investigated in the present research was created by ANSYS Design modeler 2021R2. The dimensions of the geometric model drawn were exactly the same to the dimensions of experimental set-up used to make the comparison a fair test. Two-dimensional axisymmetric configuration has been considered which reflects half the circular pipe used in the experiment so as to save computational resource. A 2D axisymmetric surface of the pipe with the internal diameter and total length of 10mm by 1100 mm was sketched respectively (considering the number of times the simulation has to be repeated). The surface body was treated as a fluid body so that the fluent data base assigns the fluid properties automatically.

Figure 3-12 Axisymmetric geometry of the circular tube

3.5.2. Grid generation

A staggered grid to evaluate velocity components at the center of control volume interfaces and scalar quantities at the center of control volume was generated by ANSYS Meshing 2021R2. A finer mesh towards the wall was generated using face meshing and edge sizing with metrics of different number of divisions along the axial and transversal direction. The uniform grid in the axial direction and non-uniform structured grid with a mesh successive ratio (bias) of 1.5 in the radial direction were considered in order to control any large deviations of flow and temperature fields near the wall regions.

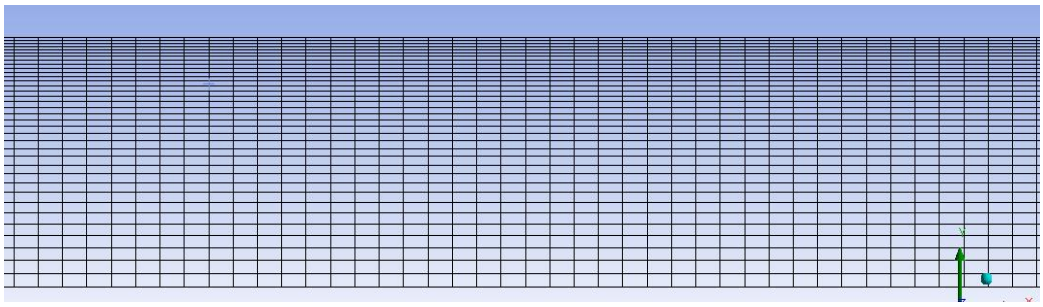

Figure 3-13 Structured non uniform grid

The cells were grouped into boundary zones where the boundary conditions are applied on them. The boundary zones such as inlet, outlet and wall zones were named selected to call while setting up boundary conditions.

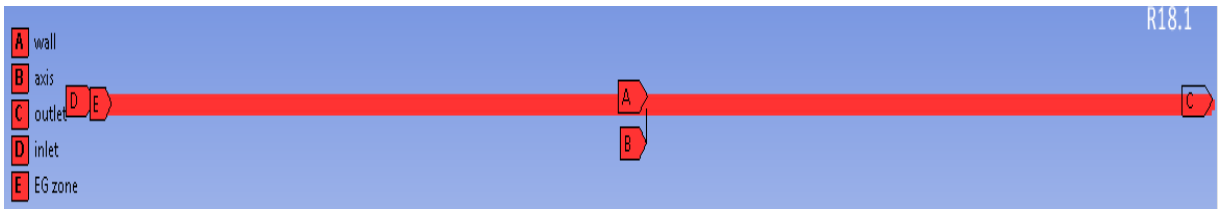

Figure 3-14 Named selected boundary zones

3.5.3. Modeling

There are commonly four popular approaches for numerically studying nanofluids: the single-phase model, the mixture multiphase model, the Eulerian-Eulerian multiphase model and the Euler-Lagrange multiphase model. Almost all of them have been applied to nanofluid heat transfer under different investigations. Euler-Lagrange multiphase model was proved to predict to the best accuracy. But for smaller particle diameter and lower particle loading nanofluids the accuracy achieved is too expensive. The single-phase model is the economical choice for the aforementioned particular case provided that the robust models are used to predict the thermophysical properties. In this model, it was assumed that the base fluid and nanoparticles are perfectly mixed and can be treated as a mixture. Any interphase forces and momentum exchange between liquid and solid particles are neglected since single phase modeling assumes base fluid and nanoparticles mix homogeneously so that there is no additional mechanism to contribute to heat transfer other than existing mechanisms for pure fluids. The assumption of treating nano fluids as conventional single phase fluids gets more realistic since the relative velocity decreases as the particle size decreases[50].

Based on the following assumptions the continuity, momentum and energy equations were written for steady, forced turbulent convection flow and heat transfer of a nanofluid flowing inside a straight tube of circular cross section.

- Fluid flow is incompressible, Newtonian and turbulent,
- The Boussinesq approximation is negligible as the pipe is placed horizontally,
- Fluid phase and nanoparticles phase are in thermal equilibrium and no-slip between them and they flow with the same local velocity
- Nanoparticles are spherical and uniform in size and shape
- Radiation effects and viscous dissipation are negligible
- The wall of the pipe was assumed to be perfectly smooth with zero roughness height

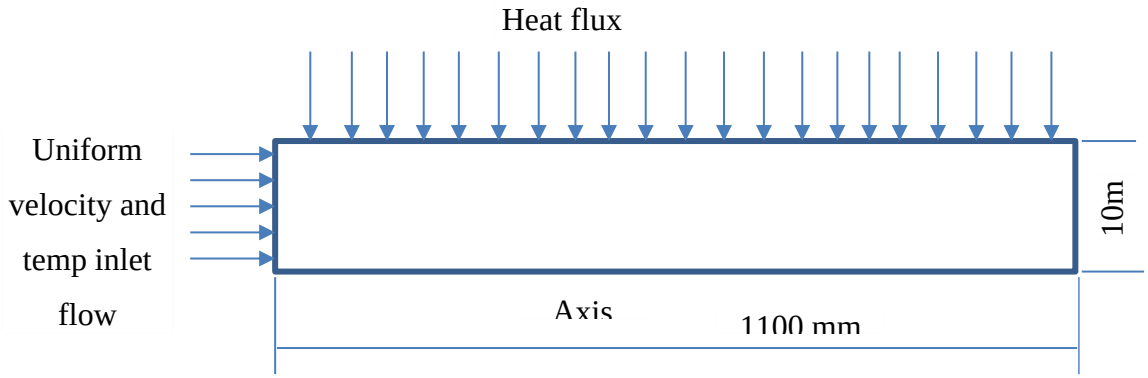

Figure 3-15 Schematic diagram of axisymmetric geometry of the circular tube with the boundary conditions

In this study, the single-phase model for numerical investigation of two dimensional symmetric steady, forced turbulence convection flow of nanofluid inside a horizontal circular tube was used. Moreover, nanofluids were assumed to be incompressible and Newtonian. Therefore, steady state conservation of mass, momentum, and energy equations were used. Under these relaxations, the classical theory of single-phase fluid can be applied to nanofluids[68]. The derivations of the equations will not be listed here assuming the reader is familiar with the field.

Continuity equation:

$$\frac{\partial \rho_{nf}}{\partial t} + \nabla \cdot (\rho_{nf} V_{nf}) = 0 \tag{3.4}$$

For incompressible flows, the first term in the above equation becomes zero, then the continuity equation will be

$$\nabla \cdot V_{nf} = 0$$

Although the actual turbulent flow is three dimensional regardless of how simple the flow boundaries due to the constant wall heat flux boundary condition, the circumferential temperature field variation is negligible. So, the simplified spherical coordinate continuity equation will be

$$\frac{\partial V_r}{\partial r} + \frac{V_r}{r} + \frac{\partial V_x}{\partial x} = 0 \tag{3.5}$$

Momentum equation:

$$\frac{\partial}{\partial t}(\rho_{nf}V_{nf}) + \nabla\cdot(\rho_{nf}V_{nf}V_{nf}) = -\nabla \mathrm{P} + \nabla\bar{\bar{\tau}} + \rho_{nf}\mathbb{g} \quad (3.6)$$

Neglecting the body and all the interphase forces and rearranging will give the radial and axial momentum equations in the spherical coordinate.

Axial momentum equation

$$\rho_{nf}\left(V_x\frac{\partial V_x}{\partial x} + V_r\frac{\partial V_x}{\partial r}\right) = -\frac{\partial P}{\partial x} + \left[\frac{1}{r}\frac{\partial}{\partial r}\left(r(\mu_{nf}+\mu_t)\frac{\partial V_x}{\partial r}\right) + \frac{\partial}{\partial x}\left((\mu_{nf}+\mu_t)\frac{\partial V_x}{\partial x}\right)\right] \quad (3.7)$$

Radial momentum equation

$$\rho_{nf}\left(V_x\frac{\partial V_r}{\partial x} + V_r\frac{\partial V_r}{\partial r}\right) = -\frac{\partial P}{\partial r} + \left[\frac{1}{r}\frac{\partial}{\partial r}\left(r(\mu_{nf}+\mu_t)\frac{\partial V_r}{\partial r}\right) + \frac{\partial}{\partial x}\left((\mu_{nf}+\mu_t)\frac{\partial V_r}{\partial x}\right) - \frac{V_r}{r^2}(\mu_{nf}+\mu_t)\right] \quad (3.8)$$

Energy equation

$$V_x\frac{\partial T}{\partial x} + V_r\frac{\partial T}{\partial r} = \left[\frac{\partial}{\partial x}\left((\alpha_{nf}+\alpha_t)\frac{\partial T}{\partial x}\right) + \frac{1}{r}\frac{\partial}{\partial r}\left(r(\alpha_{nf}+\alpha_t)\frac{\partial T}{\partial r}\right)\right] \quad (3.9)$$

Where, μ_{nf} is molecular viscosity can be calculated from the viscosity ratio formula

μ_t is eddy viscosity is to be computed from an appropriate turbulence model.

α_{nf} is molecular thermal diffusivity which can be calculated from

$$\alpha_{nf} = \frac{k_{nf}}{\rho_{nf}Cp_{nf}} \quad (3.10)$$

α_t is turbulent thermal diffusivity which can be calculated from

$$\alpha_t = \frac{k_t}{\rho_t Cp_t} \quad (3.11)$$

- **Turbulence model**

Turbulent flow is one in which the fluid particles rapidly mix as they move along due to random three-dimensional velocity fluctuations. Due to turbulence's random, three

dimensional, chaotic and stochastic nature, analytical solution for turbulent flow is not available. Hence, in the turbulent regime semi-empirical theories are used to model the flow. The k- ε model (the most economical and competent in close prediction of empirical results) introduces two new equations, one for the turbulent kinetic energy and the other for the rate of dissipation. But let express turbulent (eddy) viscosity first calculated from[69]

$$\mu_t = \rho_{nf} C_\mu \frac{k^2}{\varepsilon} \tag{3.12}$$

Turbulent kinetic energy K was calculated from

$$\Delta \cdot \left(\rho_{nf} V_K\right) = \Delta \cdot \left(\mu_{nf} + \frac{\mu_t}{\sigma_k}\right) \Delta K + G_K - \rho_{nf}{}^{\varepsilon} \tag{3.13}$$

Similarly, the steady dissipation rate ε was calculated from

$$\Delta \cdot \left(\rho_{nf} V_\varepsilon\right) = \Delta \cdot \left(\mu_{nf} + \frac{\mu_t}{\sigma_\varepsilon}\right) \Delta \varepsilon + C_{1\varepsilon} \frac{\varepsilon}{K} G_K - C_{2\varepsilon} \rho_{nf} \frac{\varepsilon^2}{K} \tag{3.14}$$

Where, $G_K = 2\mu_t[\nabla V + (\nabla V)^T]$ is the rate of turbulent kinetic energy and C_μ, $C_{1\varepsilon}$, $C_{2\varepsilon}$, σ_k and σ_ε are chosen to be empirical constants in the turbulence transport equations 0.09, 1.44, 1.92, 1.0 and 1.3 respectively[70].

- **Wall Functions**

Wall functions are used to approximate variables as turbulence, velocity and pressure in the region near a wall, called the boundary layer. To be able to resolve the fluid behavior without using some kind of assumption or simplification the mesh in this region must be very fine resulting in some cases unnecessarily long computation times. Therefore, it is of great use, in cases where the boundary layer is of less importance, to use some kind of wall function approximation. The wall functions rely on the existence of a logarithmic region in the velocity profile, in the logarithmic layer the profile is[71]

$$u^+ = \frac{\bar{v}_t}{u_\tau} = \frac{1}{\kappa} \ln(y^+) + B \tag{3.15}$$

Where, $\bar{v}_t$ is the mean velocity parallel to the wall, u_τ is the shear velocity and is calculated by $\sqrt{|\tau_w|/\rho}$ with τ_w is the shear stress at the wall. Moreover, κ is the Karman constant which is equal to 0.41, B an empirically derived constant related to the thickness of the viscous sub layer and y^+ is the dimensionless distance from the wall calculated by

$$y^+ = \frac{\rho u_\tau y}{\mu} \tag{3.16}$$

Boundary conditions

The governing equations of the fluid flow are non-linear and simplified coupled partial differential conservation equations, subjected to the following boundary conditions in addition to the assumptions mainly due to the geometrical constraints, symmetry, inlet and outlet conditions etc[72].

- Axially and circumferentially uniform wall heat flux since heat transfer analysis objective is prediction of wall temperature variation $T_w(x)$ and the design objective is to control this temperature and to keep it under an allowable limit
- The fully developed conditions prevail at the exit section because the tube was long enough (selected to be based on the length to diameter ratio) so that the flow and temperature fields are assumed fully developed which means zero normal axial gradients for all flow and heat transfer variables except pressure
- Steady, forced turbulent convection flow
- Both the flow and the thermal field are assumed to be axisymmetric with respect to the tube main axis
- On the tube wall, the usual no-slip conditions and uniform heat flux were imposed, while both turbulent kinetic energy and dissipation of turbulent kinetic energy are equal to zero.
- At the tube inlet section, uniform axial velocity specified by the Reynolds number, uniform axial temperature, turbulent intensity (estimated by $I = 0.16(\mathrm{Re})^{-1/8}$) and the hydraulic diameter (D_h) were specified for an initial guess of turbulent quantities (k and ε).

- Only half of the tube was modeled due to the symmetry as a result, a rectangular domain with dimensions of 0.01m × 1m is created. On the lower wall (axis) of the modeled domain, the axis boundary condition was applied.

Computational method

The computational fluid dynamics code Fluent was used for solving this problem. The system of governing equations was solved by control volume approach.

- Finite volume method: Control-volume technique converts the governing equations to a set of algebraic equations that can be solved numerically. The control volume approach employs the conservation statement or physical law represented by the entire governing equations over finite control volumes.
- Grid schemes used are staggered in which velocity components are evaluated at the center of control volume interfaces and all scalar quantities are evaluated in the center of control volume
- Second order upwind scheme was employed to discretize equations.
- Pressure and velocity were coupled using [coupled] algorithm to entertain speedy convergence.
- In all cases, the residual terms for all of the equations were less than 10^{-6}

3.5.4. Numerical procedure

In this numerical analysis the finite volume method employed so as to solve the partial differential equations which was accomplished with the following list of tasks,

- Division of the flow domain into discrete control volumes using a computational grid generator ANSYS meshing 2021R2
- Integration of the all-governing equations on the individual control volumes to construct nonlinear algebraic equations (called discretization) for the discrete dependent variables (“unknowns”) such as velocities, pressure, temperature, and conserved scalars using second order upwind scheme.

Second order upwind scheme is employed to achieve higher-order accuracy at the cell faces through a Taylor series expansion of the cell-centered solution about the cell

centroid. By considering the steady conservation equation for transport of a scalar quantity φ, discretization of the governing equations can be illustrated most easily by[70]

$$\oint \rho\varphi\vec{v} \cdot d\vec{A} = \oint \Gamma_{\varphi} \nabla\varphi \cdot d\vec{A} + \int_{V} S_{\varphi} dV \tag{3.17}$$

Where, ρ is density, $\vec{v}$ is velocity vector ($\vec{v} = v_r\hat{r} + v_x\hat{k}$), $\vec{A}$ is surface area vector, Γ_{φ} is diffusion coefficient for φ, $\nabla\varphi$ is gradient of φ ($\nabla\varphi = (\frac{\partial\varphi_r}{\partial r} + \frac{\varphi_r}{r})\hat{r} + \frac{\partial\varphi_x}{\partial x}\hat{k}$) and S_{φ} is the source of φ per unit volume. The integration is applied to each control volume, or cell, in the computational domain which yields

$$\sum_{f}^{N_{faces}} \rho_f \vec{v}_f \varphi_f \cdot \vec{A}_f = \sum_{f}^{N_{faces}} \Gamma_{\varphi} \nabla\varphi_f \cdot \vec{A}_f + S_{\varphi} V \tag{3.18}$$

Where, N_{faces} is number of faces enclosing the given cell, φ_f is the value of φ convected through the face f, $\rho_f \vec{v}_f \varphi_f$ is the mass flux through the face, $\vec{A}_f$ is area of the face ($\vec{A}_f = A_r\hat{r} + A_z\hat{k}$), $\nabla\varphi_f$ is gradient of φ at the face and V is the cell volume. In second-order unwinding, the face value φ_f is computed using the following expression[70]

$$\varphi_f = \varphi + \nabla\varphi . \vec{r} \tag{3.19}$$

Where, φ and $\nabla\varphi$ are the cell-centered value and its gradient in the upstream cell, and $\vec{r}$ is the displacement vector from the upstream cell centroid to the face centroid.

The gradient $\nabla\varphi$ at the cell center $c0$ is computed from Least Squares Cell-Based method which by the way is limited by standard gradient or slope limiter to prevent spurious oscillations, which would otherwise appear in the solution flow field near shocks, discontinuities, or near rapid local changes in the flow field

$$\begin{aligned} (\Delta\varphi_r)_{c0} &= \sum_{i=i}^{n} W^r\, io \cdot (\varphi_{ci} - \varphi_{c0}) \\ (\Delta\varphi_x)_{c0} &= \sum_{i=i}^{n} W^x\, io \cdot (\varphi_{ci} - \varphi_{c0}) \end{aligned} \tag{3.20}$$

- Linearization of the discretized equations and solution of the resultant linear equation system iteratively so as to obtain a converged numerical solution to yield updated values of the dependent variables with the pressure-based solver using a coupled algorithm (to couple the pressure and pressure correction equation and momentum equations) where each iteration in each cell consists of the steps illustrated in Figure 3.16 with pseudo transient under relaxation of automatic pseudo transient time step size.

The above discretized equation contains unknown scalar variable φ at the cell center and neighboring cells which makes the equation nonlinear with respect to these variables. After being linearized, it can be expressed as

$$a_p \varphi = \sum_{nb} a_{nb} \varphi_{nb} + b \tag{3.21}$$

Where, the subscript nb refers to neighbor cells, a_p and a_{nb} are the linearized coefficients for φ and φ_{nb}

Writing similar equations for all cells results in a set of algebraic equations with a sparse coefficient matrix. In the pressure-based solver, the projection method where the velocity field is obtained by solving the momentum equations, the pressure and pressure correction equation is obtained by manipulating the continuity and momentum equations and pressure field is obtained by solving pressure and the pressure correction equation. For all the simulations carried out in the present analysis, convergence criteria for the solutions were fixed for the iterative procedure to be terminated when the residuals become less than 10^{-6}. The under- relaxation factors for the sake of stability of the converged solutions are left at their default values.

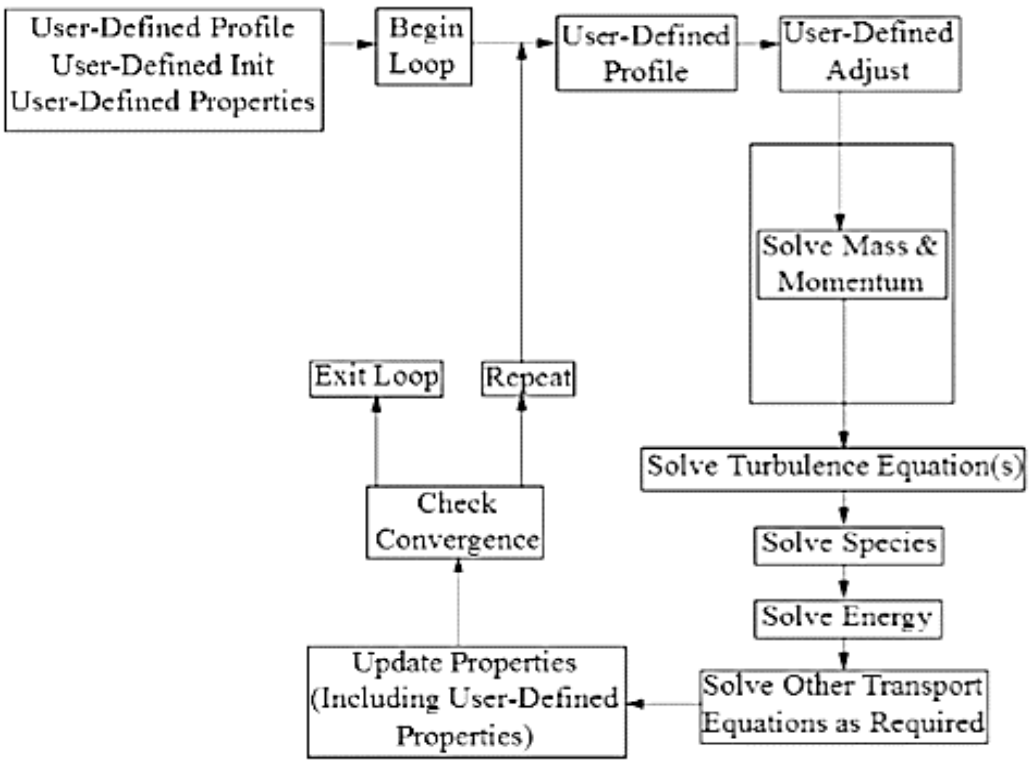

Figure 3-16 Solution procedure for pressure-based solver (reprinted from ANSYS Fluent theory guide)[70]

3.5.5. Modelling nanoparticles using a user-defined function (UDF)

Instead of defining material properties for each volume fraction and running the simulation again and again, all thermophysical properties of the nanofluids ae customized so that the software can run it at once. A user defined function, or UDF (C or C++ function that can be dynamically loaded with the ANSYS Fluent solver to enhance its embedded standard features), for each of the volume fractions is written to be fed as material database and attached as appendices. Its importance arises when enhancing existing fluent models, customizing boundary conditions, adjusting material property definition, etc. is required.

3.5.6. Thermo-physical properties of nanofluids

The thermophysical properties of nanofluids such as density, viscosity, and heat capacity were evaluated using most related theoretical and empirical correlations from literatures

based on single phase fluid assumption given that the lower concentration of nanoparticles.

Particle concentration can be expressed either in mass or volume fraction. But volume fraction is usually preferred to mass fraction because most of the forces especially the hydrodynamic forces are surface forces not body forces. Unfortunately, it is much more difficult to prepare a suspension of desired volume fraction precisely. Then a strategy of calculating a mass concentration of a desired volume fraction and preparing a suspension of a resulting mass concentration was followed. Volume concentration is the fraction of space of total suspension occupied by suspended material. Mathematically expressed as

$$\phi_v = \frac{space\ occupied\ by\ the\ suspended\ material}{space\ occupied\ by\ the\ total\ suspension} \tag{3.22}$$

$$\phi_v = \frac{1}{\left({}^{100}/_{\phi_m}\right)\left({}^{\rho_p}/_{\rho_f}\right)+1} \times 100\% \tag{3.23}$$

Density: The effective density of the nanofluid is defined as [73]

$$\rho_{eff} = (1-\phi)\rho_f + \phi\rho_p \tag{3.24}$$

Specific heat capacity: In the same fashion the specific heat capacity of the nanofluid can be expressed in terms of the volume fraction, density of both base fluid and nanoparticle and the respective specific heats[74].

$$C_{eff} = \frac{(1-\phi)(\rho C)_f + \phi(\rho C)_p}{(1-\phi)\rho_f + \phi\rho_p} \tag{3.25}$$

Thermal conductivity: Two groups of relations are available on the literatures used to predict thermal conductivity namely theoretical models and empirical correlations. The former is usually developed by taking all the mechanisms and possible reasons of enhancement. A very great deal of discrepancy has been observed between themselves and with the experimental data. The latter is proposed on the basis of a wide variety of experimental data. Here in this work, for the needed prediction of nanofluid effective thermophysical properties with adequate accuracy, the most robust empirical relation proposed by Corcione[75] with regression analysis of 1.86% standard deviation of error

was used to predict the thermal conductivity which depends on the temperature and concentration of nanofluid, diameter and thermal conductivity of nanoparticles as well as the base fluid. He based his regression on a wide range of experimental data extracted from the following resources whose details on the nanofluid type, the size of the suspended nanoparticles and the measuring method are tabulated below.

Table 3-1 Details of literatures used to model thermal conductivity and viscosity by Corcione.

Literature source	**Nanofluid type**	**Nanoparticle size**	**Measuring method**
Masuda et al	TiO_2 + water	27 nm	Transient hot-wire
Lee et al	CuO + water Al_2O_3 + water CuO+ ethylene glycol Al_2O_3 + ethylene glycol	23.6 nm 38.4 nm 23.6 nm 38.4 nm	Transient hot-wire
Eastman et al	Cu+ ethylene glycol	10 nm	Transient hot-wire
Das et al	CuO + water Al_2O_3 + water	28.6 nm 38.4 nm	Temperature oscillation
Chon et al	Al_2O_3 + water	47 nm	Transient hot-wire
Chon and Kihm	Al_2O_3 + water Al_2O_3 + water	47 nm 150 nm	Transient hot-wire
Murshed et al	Al_2O_3 + water Al_2O_3 + ethylene glycol	80 nm 80 nm	Transient hot-wire
Mintsa et al	CuO + water	29 nm	Transient hot-wire
Duangthongsuk and Wongwises	TiO_2 + water	21 nm	Transient hot-wire

The range of the experimental data covers the most commonly used base fluids (water and ethylene glycol), nano particles (TiO_2, CuO, Al_2O_3, Cu), wide range of particle size

$(10 - 150)$ and both the most commonly used methods of thermal conductivity measurement. More specifically it includes the solid-liquid combination used for the experiment which makes the correlation ideal.

$$\frac{k_{eff}}{k_f} = 1 + 4.4{Re_{np}}^{0.4} + {Pr_f}^{0.66}\left(\frac{T}{T_{fr}}\right)^{10}\left(\frac{k_p}{k_f}\right)^{0.03}\phi^{0.66} \tag{3.26}$$

Where, T is the nanofluid temperature in Kelvin degrees, T_{fr} is the freezing point of the base liquid, k_p is the thermal conductivity of the solid nanoparticles, ϕ is the nanoparticle volume fraction and Re_{np} is the nanoparticle Reynolds number expressed as

$$Re_{np} = \frac{2\rho_f k_b T}{\pi {\mu_f}^2 d_p} \tag{3.27}$$

Where, $k_b = 1.38066 \times 10^{-23}$ J/K is Boltzmann constant. From the above correlation the thermal conductivity of nanofluid depends on the temperature and concentration of nanofluid, diameter and thermal conductivity of nanoparticles as well as the base fluid.

Dynamic viscosity: From the same literatures, Corcione [75] proposed the following correlation to evaluate dynamic viscosity with 1.84% standard deviation of error.

$$\frac{\mu_{eff}}{\mu_f} = \frac{1}{1 - 34.87\left(\frac{d_p}{d_f}\right)^{-0.3}\phi^{1.03}} \tag{3.28}$$

With base fluid molecular diameter of $d_f = 0.1\left[\frac{6M}{N\pi\rho_{fo}}\right]^{1/3}$ where, M is the molar mass of the base fluid, $N = 6.022 \times 10^{23}$ is the Avogadro number and ρ_{fo} is the density of the base fluid at $T = 273.15K$

All the above properties of the base fluid and the nanoparticle varies with temperature. So, does that of the nanofluid. But comparatively the variation of those properties of the nanoparticle with respect to temperature is negligible. Therefore, only the properties of the base fluid as a function of temperature is given as correlated from the empirical data from literatures[76].

Table 3-2 Variation of base fluid properties with respect to temperature

Property	Formula	Unit
Density	$\rho_f = 1334.5 - 0.8T$	kg/m^3
Thermal conductivity	$k_f = 0.24511 + 1.755 \times 10^{-4}T - 8.52 \times 10^{-7}T^2$	W/m.℃
Specific heat	$c_f = 1076.6135 + 4.6278\mathrm{T}$	j/kg. K
Viscosity	$\mu_f = 0.0373e^{-0.0756T} + 0.0196e^{-0.0235T}$	kg/m. s

Some of the required reference thermophysical properties and other parameters of the base fluid and the nanoparticle required for the calculation of the thermophysical properties of the nanofluid are collected and summarized as follows[77].

Table 3-3 Thermophysical properties of base fluid and nanoparticles at 293 K adopted from heat transfer Databook

Property	Unit	Cu Nanoparticle		Ethylene glycol	
		Symbol	Value	Symbol	Value
Density	kg/m^3	ρ_p	8933	ρ_f	1109
Density of base fluid at room temperature	kg/m^3	ρ_{fo}			1097
Thermal conductivity	W m^{-1} K^{-1}	k_p	401	k_f	0.256
heat capacity	kJ/kg · K	C_p	0.39	C_f	2.84
Dynamic viscosity	N s/m^2	μ_f			0.0162
Molar mass	g/mol	M			62.07
Avogadro number		N			6.022×10^{23}
Boltzmann constant	J/K	k_b			1.38066×10^{-23}
Freezing point of the base liquid	K	T_{fr}			260.2

3.5.7. Validation procedure for the numerical model

Before the application of the numerical set up to the case of nanofluid heat transfer, it was verified by considering the flow of pure EG inside the flow configuration described and compared with the previously published traditional correlations to demonstrate the validity and precision of the model. The resulting Nusselt number was plotted against Reynolds number and compared with the Gnielinski equation (equation 3.1) which was plotted on the same coordinate. Darcy friction factor expressed via the Blasius equation (equation 3.3) was used to validate the rheology aspect of the analysis.

3.6. Grid independence test

The mesh has a significant impact on the accuracy of the solution as well as the rate of convergence. The CPU time is also directly affected by the quality of the mesh. Grid independence study was required to be carried out to find out the optimum grid size without compromising the accuracy of results. All the solutions obtained in this research was tested by the so-called grid independency test so that the solution should not be mesh dependent. In this test, the number of cells is increased to the level where any extra refinement does not affect the solution accuracy. Different mesh sizes were tested in order to examine the effect of number of cell volumes on the Nusselt number (to check the grid sensitivity) by varying the total number of grid distributions in both the axial and the radial directions.

Confirming that the computational model is generating grid insensitive results, nanofluids with varying concentrations were analyzed at various Reynolds numbers with applied constant heat flux q'' on the upper wall. A heat flux of 7580 W/m^2 was selected in our simulations because comparing numerical results with the experimental one was required.

3.7. Data reduction methods

The raw data recorded has to be analyzed and some meaningful parameters have to be calculated from the measured independent variables. Usually dimensionless heat transfer coefficient (Nusselt number) is used instead of just heat transfer coefficient

3.7.1. Nusselt number calculation

Heat transfer coefficient is the proportionality constant between the heat flux and the thermodynamic driving force for the flow of heat and shows how effectively heat can be transferred within a system. The local heat transfer coefficient can be calculated from the formula [43]

$$h(x) = \frac{q}{T_{w,in}(x) - T_f(x)} \tag{3.29}$$

where,x is the axial location

q is the heat flux which can be calculated from an energy balance.

$$q = \frac{\rho C_p \dot{Q}}{\pi D L}\left(T_{f,out} - T_{f,in}\right) = \frac{\rho C_p \dot{Q}}{\pi D L}\Delta T_f \tag{3.30}$$

where D is the inner diameter of the test section, L is the length of the test section, ρ, C_p and $\dot{Q}$ the fluid density, heat capacity and volumetric flow rate, respectively. Both temperatures $T_{f,in}$ at $x = 0$ and $T_{f,out}$ at $x = L$ can be measured with the immersed thermocouples placed at both ends of the test section.

$T_f(x)$, the fluid local temperature, can be determined from a linear relation between test section inlet and outlet temperatures ($T_{f,in}$ and $T_{f,out}$)

$$T_f(x) = \frac{x}{L}\, T_{f,out} + (1 - \frac{x}{L})T_{f,in} \tag{3.31}$$

$T_{w,in}(x)$, The inner wall temperature, can be determined from a radial heat conduction calculation by using outer wall temperature, ($T_{w,out}(x)$, measured by the thermocouples placed in the outer wall of the test section and the local heat generated in the test section wall per unit length $\acute{q}$(x)

$$T_{w,in}(x) = T_{w,out}(x) + \frac{\acute{q}(\mathrm{x})}{4\pi k_{tube}}(\frac{1 + \ln(R_d) - (R_d)}{1 - (R_d)}) \tag{3.32}$$

where, k_{tube} is the thermal conductivity of the test section

$$R_d = (\frac{D}{D_{exit}})^2$$

The axial heat flux is neglected in the $h(x)$ calculation since experimental measurements show that it is, at least, 20 times smaller than the radial heat flux contribution. The local Reynolds and Prandtl numbers were calculated with the thermophysical properties based on local mean bulk temperature. The Nusselt number in the thermally fully developed region was determined by averaging local Nusselt numbers over the heat transfer test section.

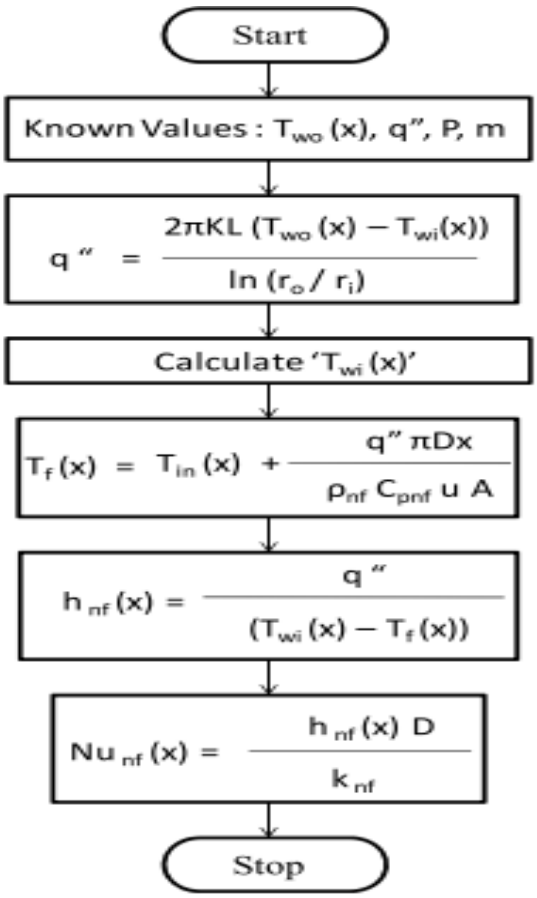

Figure 3-17 Flow chart for calculating Nusselt number[55]

3.7.2. Friction coefficient calculation

Using the pressure head directly recorded from the manometers, pressure drop was calculated as

$$P_{inlet} - P_{outlet} = \rho h \tag{3.33}$$

The pressure drop was used to calculate the friction factor as [67]

$$f = \frac{(P_{inlet} - P_{outlet})2D}{\rho L V^2} \tag{3.34}$$

3.7.3. Flow rate calculation

From orifice meter the flowrate of the fluid flow was calculated as

$$\dot{Q} = \frac{A_2}{\sqrt{\left[1 - \left({}^{A_2}/_{A_1}\right)^2\right]}} \left[\sqrt{\frac{2g(P_{inlet} - P_{outlet})}{\rho}}\right] \tag{3.35}$$

The overall procedure followed to address this research problem was summarized in the Fig 3.18.

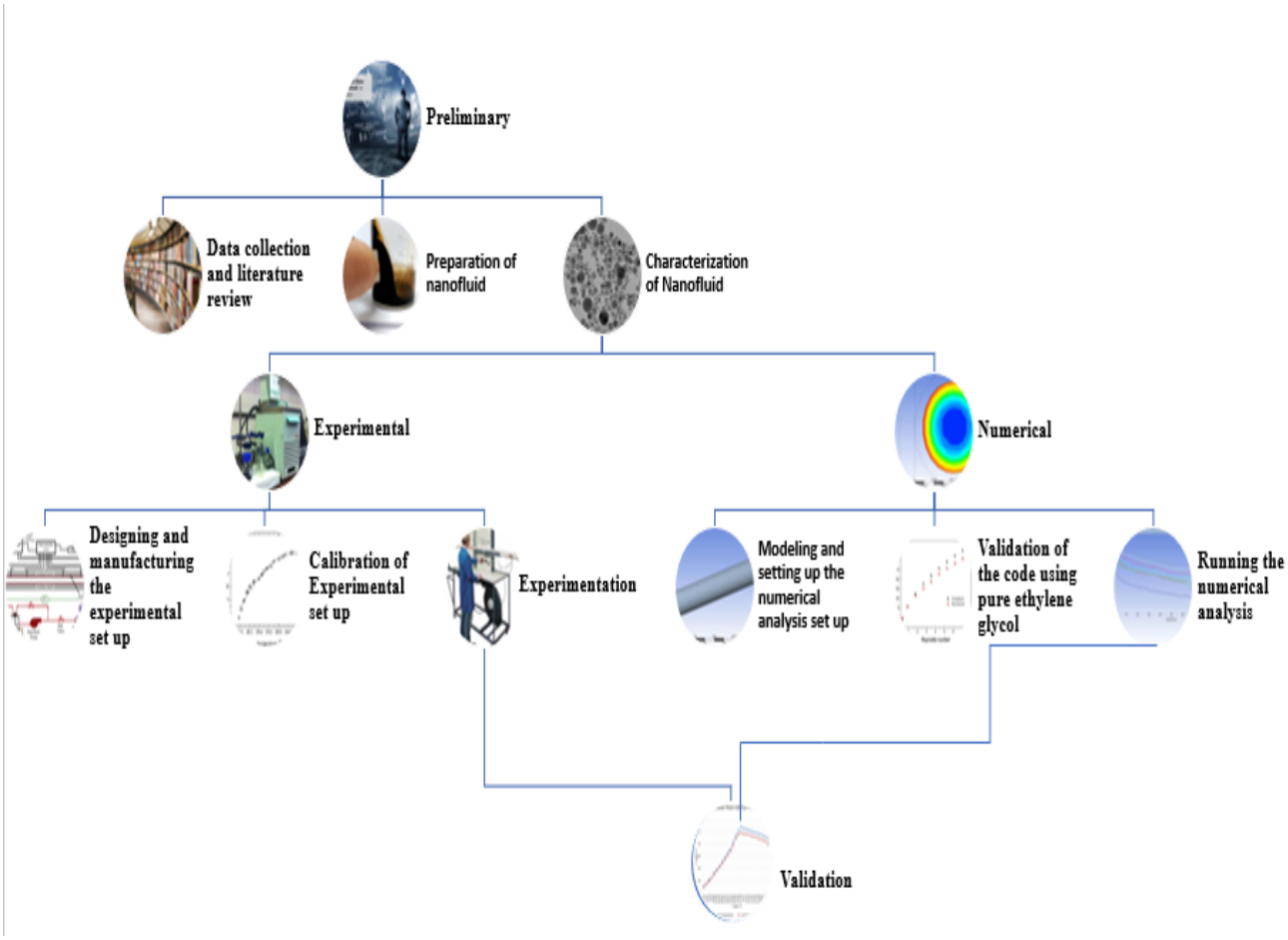

Figure 3-18 Overall procedure of the thesis

CHAPTER FOUR

4. RESULTS AND DISCUSSION

This chapter focuses on the presentation and discussion of both the experimental and numerical findings. Both the experimental and numerical data for all the test sets of different parameters was analyzed and compared to each other and with relevant correlations.

4.1. Nanoparticle preparation result

Based on the track record of color change of the synthesis pathway, the reaction is completed and the coper nanoparticles are produced. The color less $NaBH_4$ solution was changed to dark brown immediately after the first drop of the precursor solution which signals the start of the reduction reaction. Upon further addition of the $CuSO_4.5H_2O$ solution the color becomes yellowish brown and then clear yellow finally to light green which out louds the completion of the reaction.

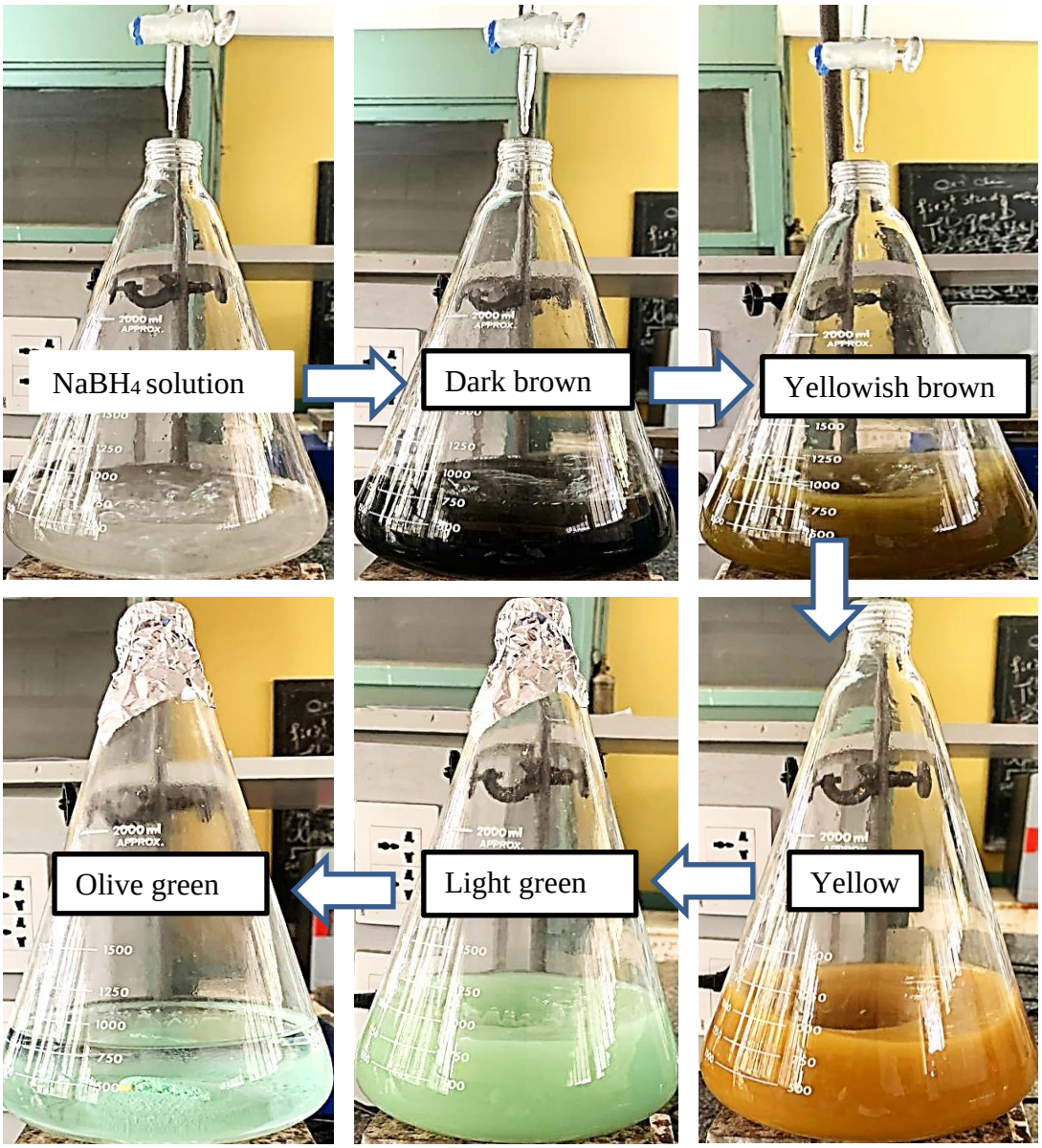

Figure 4-1 Color change scheme of the nano particle preparation process

4.2. Nanoparticle characterization result

Besides the color change, the spectrum of absorption band of Cu nanoparticles was recorded immediately after the completion of the reaction using PerkinElmer Lambda 35

UV-visible spectrometer with in the spectrum range of 500-750nm. As shown in the Fig 4.2, Surface Plasmon Resonance (SPR) peaks at 560nm which was in the general range of copper nanoparticle absorption spectrum (350-800nm) ensuring formation copper nanoparticles.

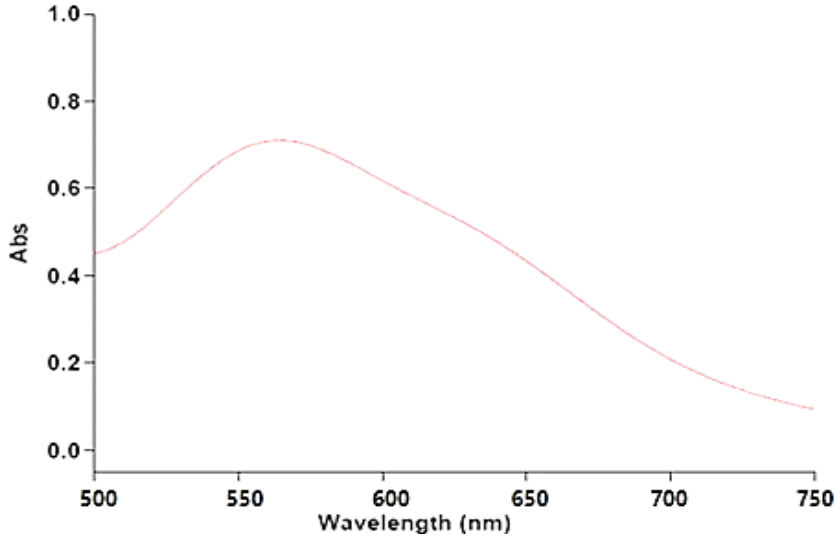

Figure 4-2 UV-visible spectrum of copper nanoparticles

4.2.1. Particle size measurement using dynamic light scattering (DLS)

The average hydrodynamic diameter of the prepared copper nanoparticle was measured by using a DLS instrument (Malvern, Nano-ZS). As shown from the size distribution assessment in the Fig 4.3, the average diameter of the nanoparticles was 23.65nm with a polydispersity index of 0.745, which met the criteria for quality sample preparation.

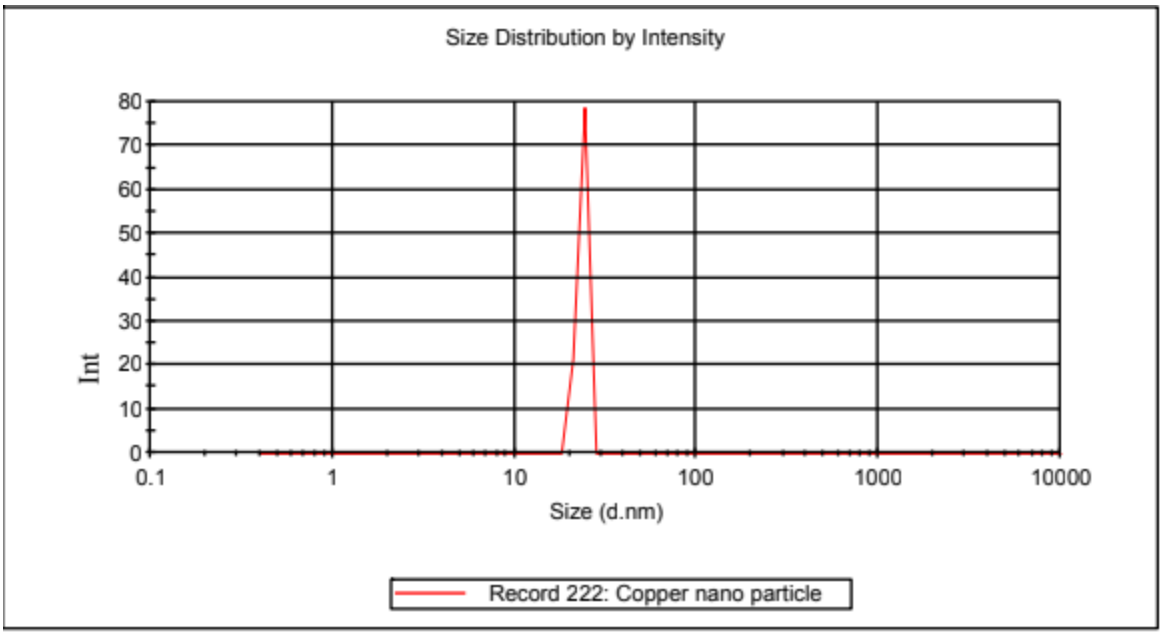

Figure 4-3 Size distribution analysis using DLS

4.3. Experimental results

In this subchapter the recorded temperature values and pressure drop readings of the recalibrated set up were used to calculate Nusselt number and friction factor which then plotted with respect to inlet temperature, particle concentration and Reynolds number.

4.3.1. Calibration of the test set up

In order to verify the accuracy and the reliability of this experimental system, the pressure drop and the local heat transfer coefficient are experimentally measured using pure ethylene glycol a head of the nanofluid preparation. The result was compared with the legendary Gnielinski and Fanning equations. As shown in the Fig 4.4 the Nusselt number of pure ethylene glycol flow at 298.15K of the present study closely agrees with the Gnielinski equation with maximum and average deviation of 7.4% and 3.9% respectively.

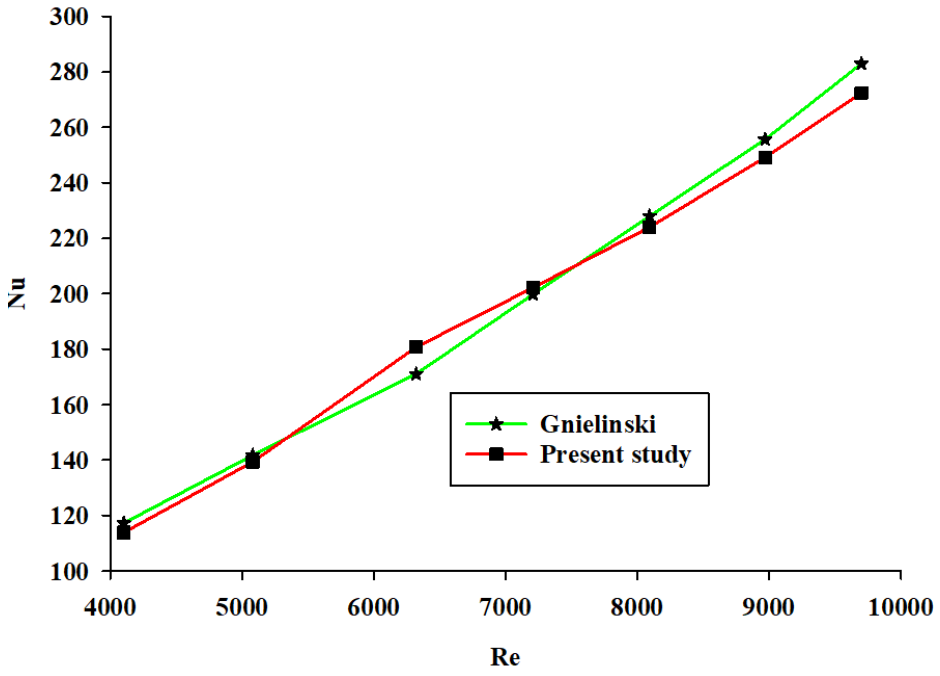

Figure 4-4 Calibration of the experimental set up with Gnielinski equation

Blasius correlation was used for friction factor comparison in the turbulent regime. The experimental friction factor achieved a closer agreement (with maximum and average deviation of ±5.9% and ±2.3% respectively) with the replotted Darcy friction factor from Blasius equation as shown in the Fig 4.5.

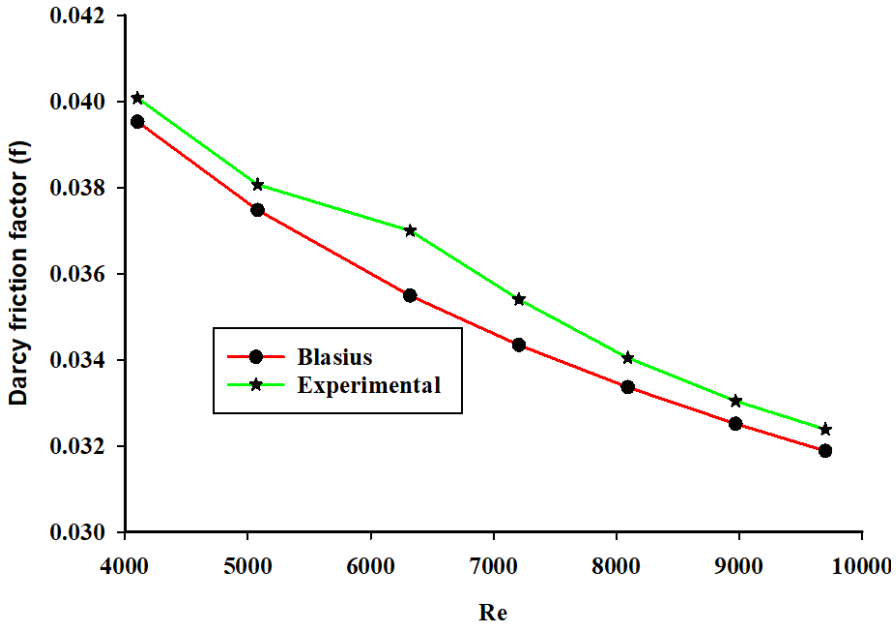

Figure 4-5 Comparison of Darcy friction factor from Blasius equation with experimental friction factor

As witnessed from the surface temperature plot on all axial positions of the thermocouple fixture, surface temperature increases as we go from to inlet to outlet of the test section. This could be mainly because as the fluid goes to the across the test section its temperate increases so the heat it takes from the tube wall decreases.

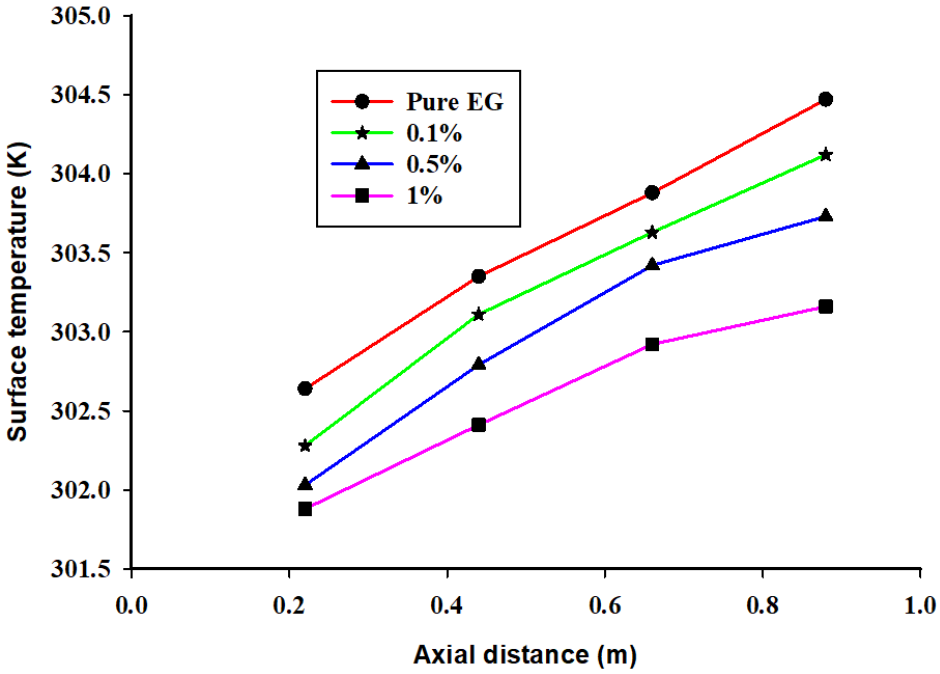

Figure 4-6 surface temperature variation across axial positions

The Nusselt number is increasing with rising Reynolds number, due to the reduction of thickness of the viscous sublayer and the increasing turbulent transport of thermal energy. All studied nanofluid concentrations exhibit higher Nusselt numbers in comparison to those of the base fluid. An increase in Nusselt number occurs with rise in particle concentration. This is mainly caused by the increase in thermal conductivity of the nanofluid which outweighs the impact of increasing dynamic viscosity against Nusselt number. Fig 4.7 a-c shows that Nusselt number increases with inlet temperature, Reynolds number and particle concentrations.

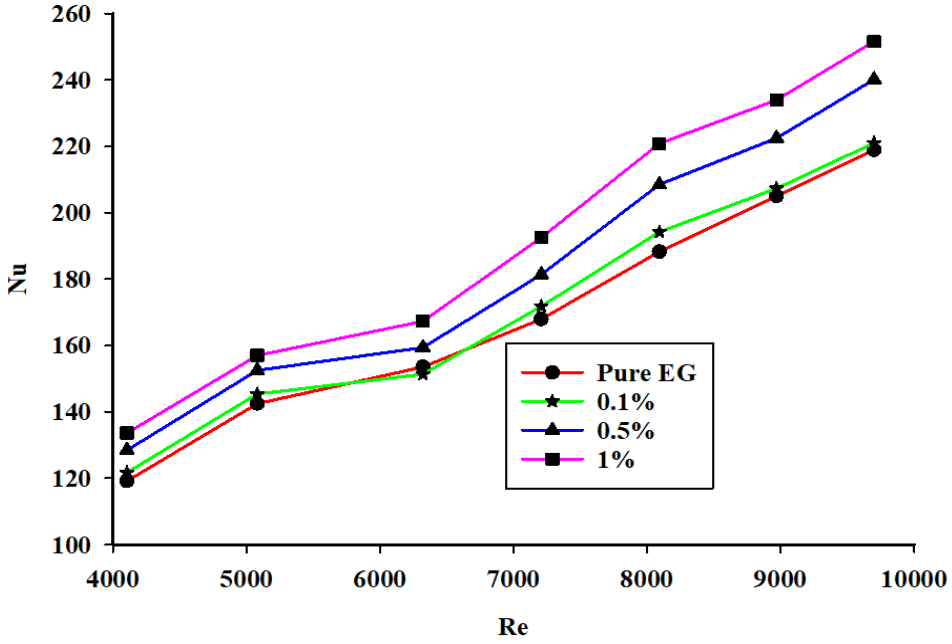
Nu
Re
Pure EG
0.1%
0.5%
1%
100
120
140
160
180
200
220
240
260
4000
5000
6000
7000
8000
9000
10000

a

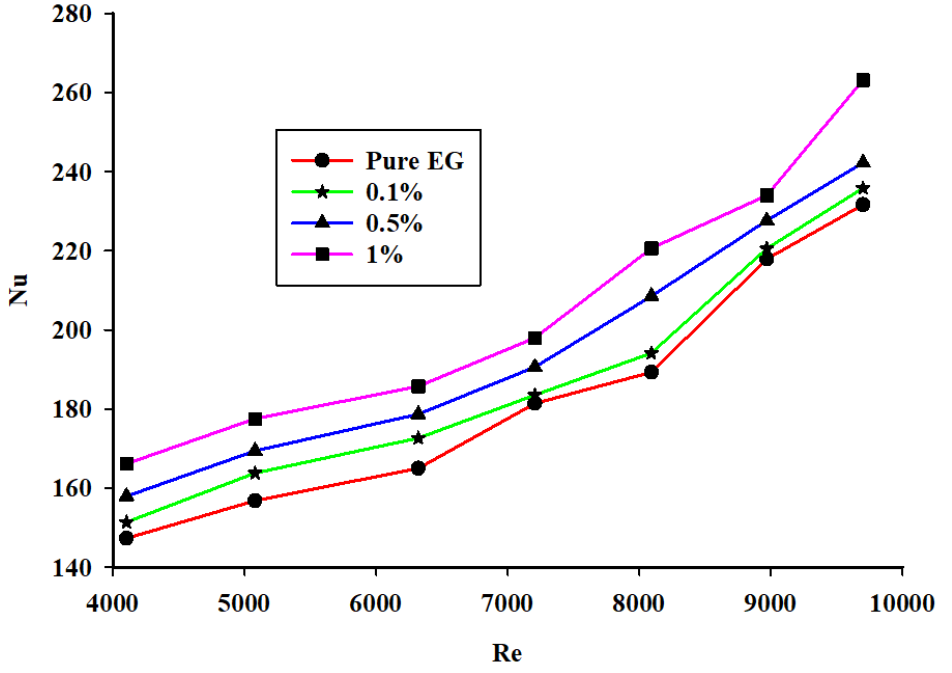
Nu
Re
Pure EG
0.1%
0.5%
1%
140
160
180
200
220
240
260
280
4000
5000
6000
7000
8000
9000
10000

b

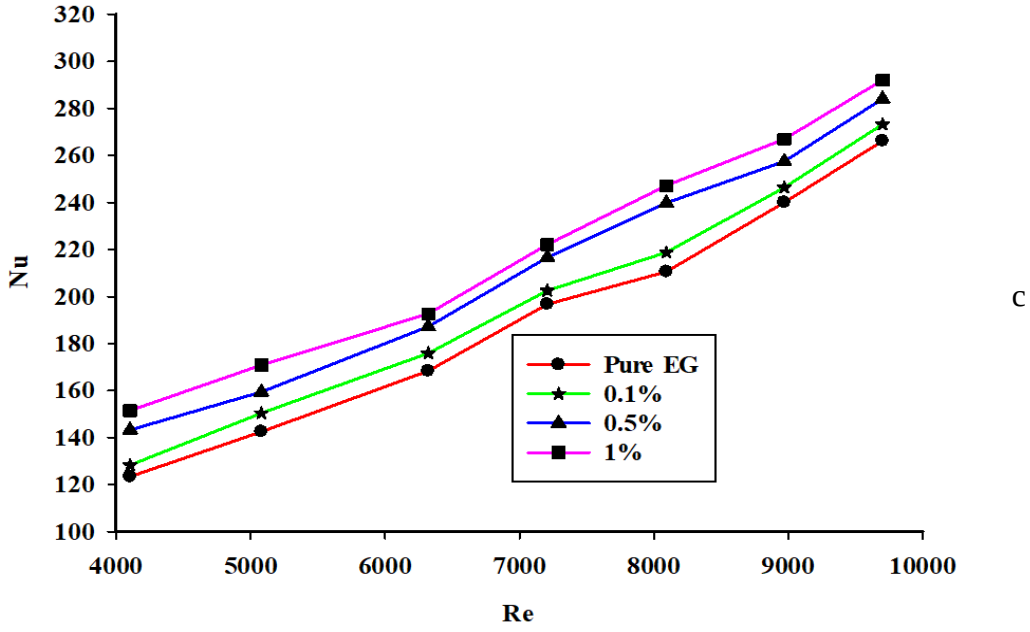

c

Figure 4-7 Nusselt number variation with Reynolds number inlet temperatures of (a) 296.15K, (b) 298.15K and (c) 303.15K

The friction factor increases when the concentration of Cu nanoparticles in EG increases. It is believed that this was caused by the slight increment in dynamic viscosity for nanofluids. Keeping the volume concentration to the lowest with smaller diameter nanoparticles happens to maintain the dynamic viscosity increase to the lowest which thereby limits the increase in friction factor, It was also worth deducing that the fluid velocity plays a vital role in enhancing the pressure loss in the test section as shown in the slightly widening variation of friction factor increase towards increasing Reynolds number.

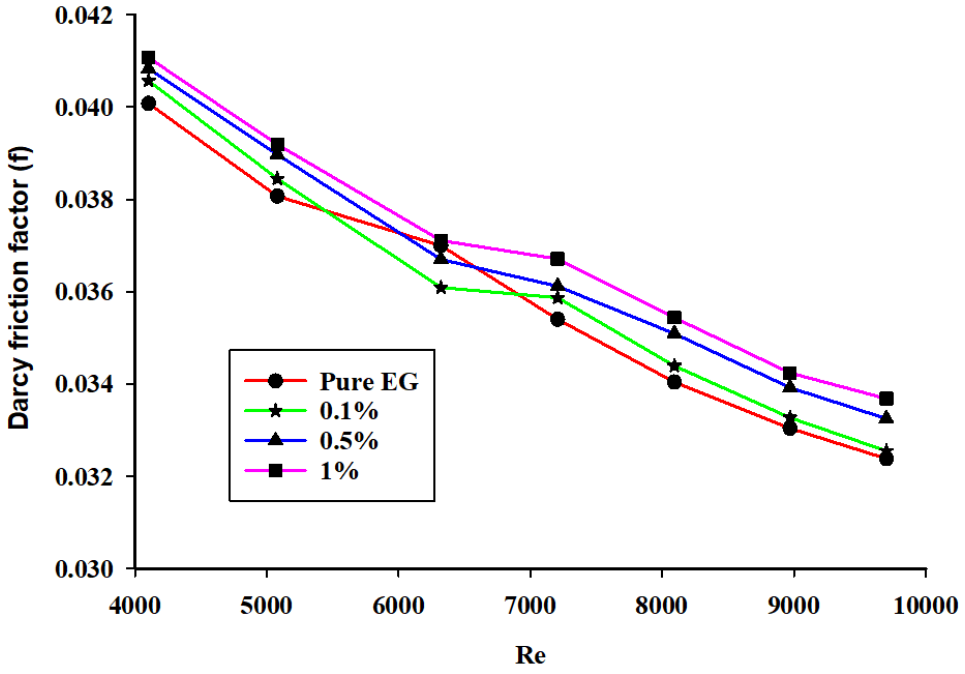

Figure 4-8 Friction factor of the base fluid and nanofluids of different particle loading with respect to Reynolds number

4.4. Numerical results

The system of governing equations subjected to their appropriate boundary conditions, has been successfully solved by using the numerical method that is essentially based on the Finite control volume approach.

4.4.1. Solution convergence

A convergence indicator was essentially set based on the residuals that result from the integration of the conservation over finite control-volumes. During the iterative calculation process, these residuals were constantly monitored and carefully scrutinized. For all of the simulations performed in this study, converged solutions were achieved with residuals as low as 10^{-6} for all the governing equations where plot of the truncation error with respect to the iterations reached a minimum plateau as shown in the Fig 4.9. In addition, the linear appearance of the residual plots after some initial iterations was another way of witnessing the convergence of the solution.

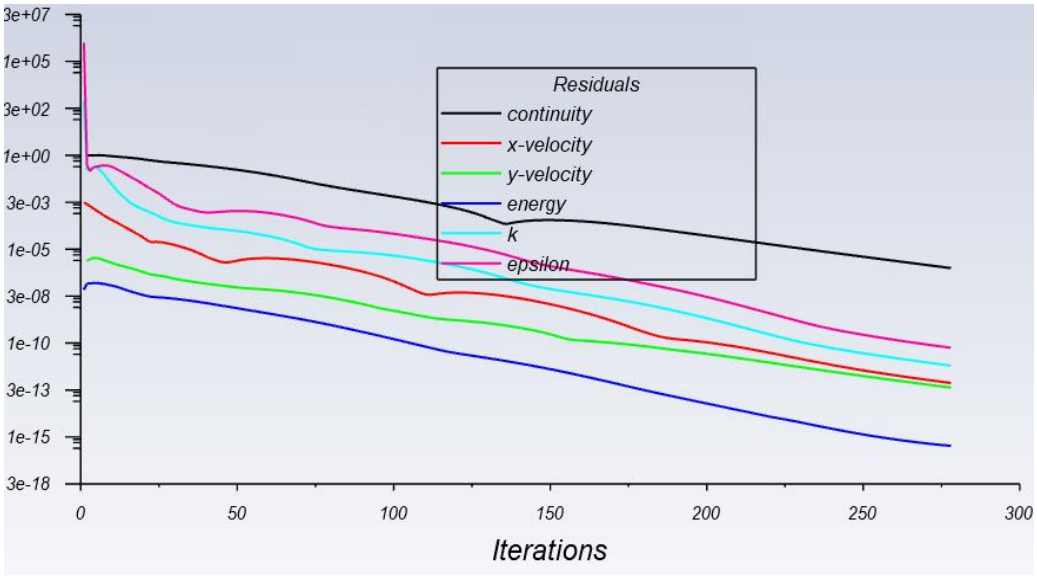

Figure 4-9 Residuals under the convergence criteria

Surface monitors of temperature, velocity and pressure based on area weighted average of respective variables over the surfaces of the inlet, outlet, axis, wall and fluid zone were used to validate that after some iterations the aforementioned variables remains constant which signals the convergence of the calculation as clearly depicted in the Fig 4.10 a-c. As a further examination, the fact that the wall temperature is larger than all the fluid temperatures and amongst them outlet temperature is higher than fluid zone and inlet temperature was used as evidence to ensure that direct negligence and other biased personal simulation errors were avoided. The same analogy was applied to other variables.

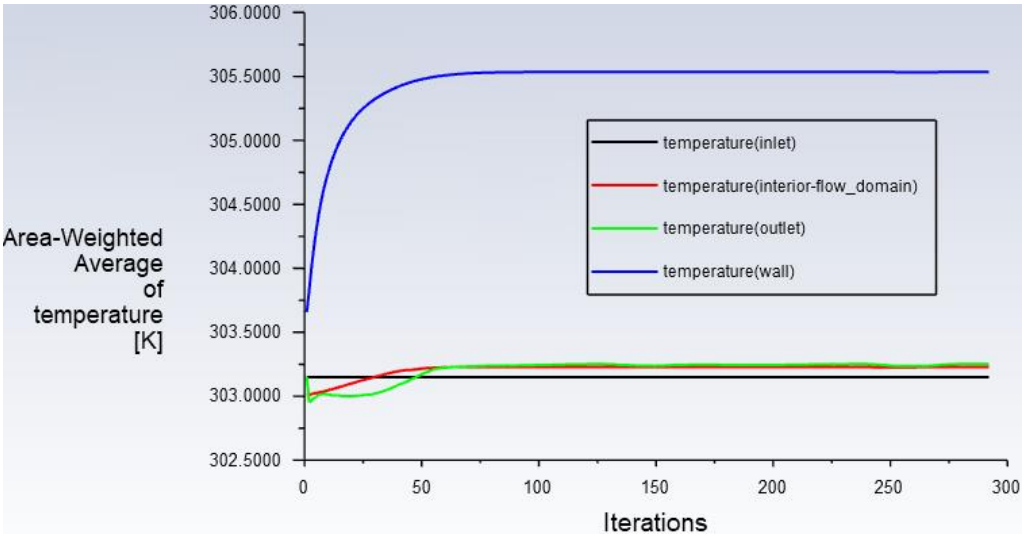

a

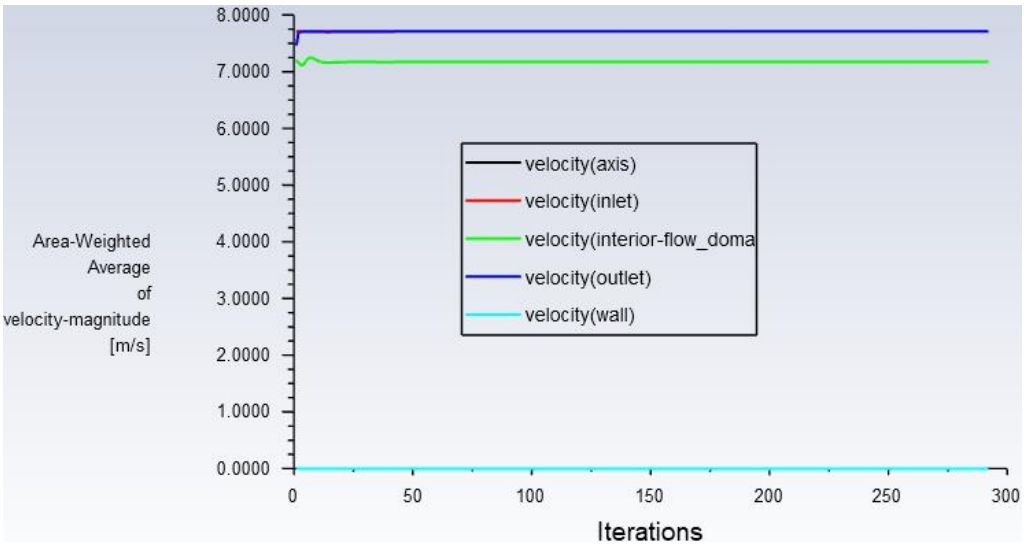

b

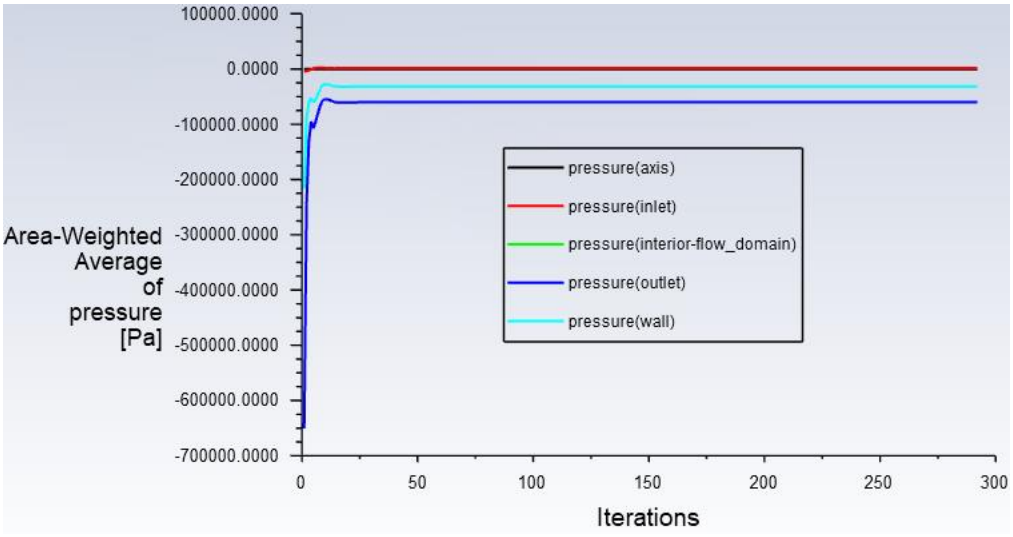

c

Figure 4-10 Surface monitors of (a), temperature (b), velocity and (c), pressure

4.4.2. Grid independence results

In order to ensure that the calculated results are grid independent, nine different radial and axial grid distributions were tested for their performance in predict the Nusselt number Pure ethylene glycol at 298.15K inlet temperature and 10000 Reynolds number as displayed in the Fig 4.11. It was observed that the Nusselt number for EG slightly fluctuated about some average value and finally becomes constant beyond a certain number of cell volumes. Beyond this, any further increase in the number of cell volumes only increased the computational time, without any significant improvement in the Nusselt number. Similar trend was also observed with the nanofluids. So, this “optimum” mesh size was selected for further study with both EG and the nanofluids. As shown in the Fig 4.12, the Nusselt number did not remarkably change for the grid numbers more than 200×500. Therefore, 200×500 was accepted as the optimal grid size.

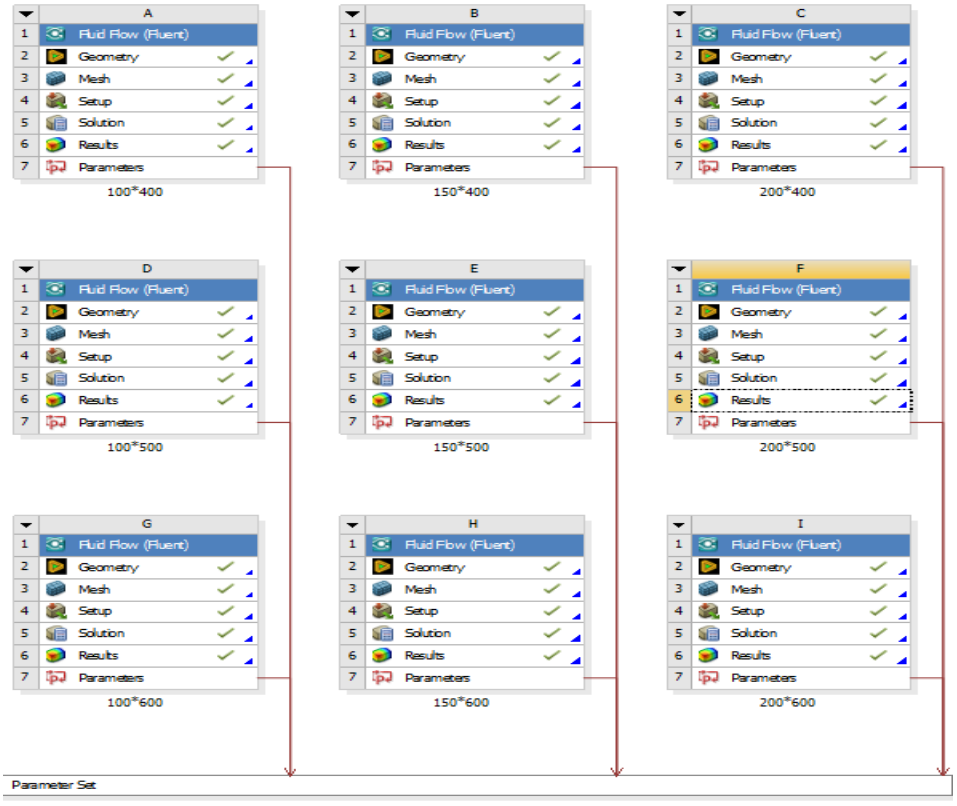

Figure 4-11 Radial and axial grid distributions tested for grid independence test

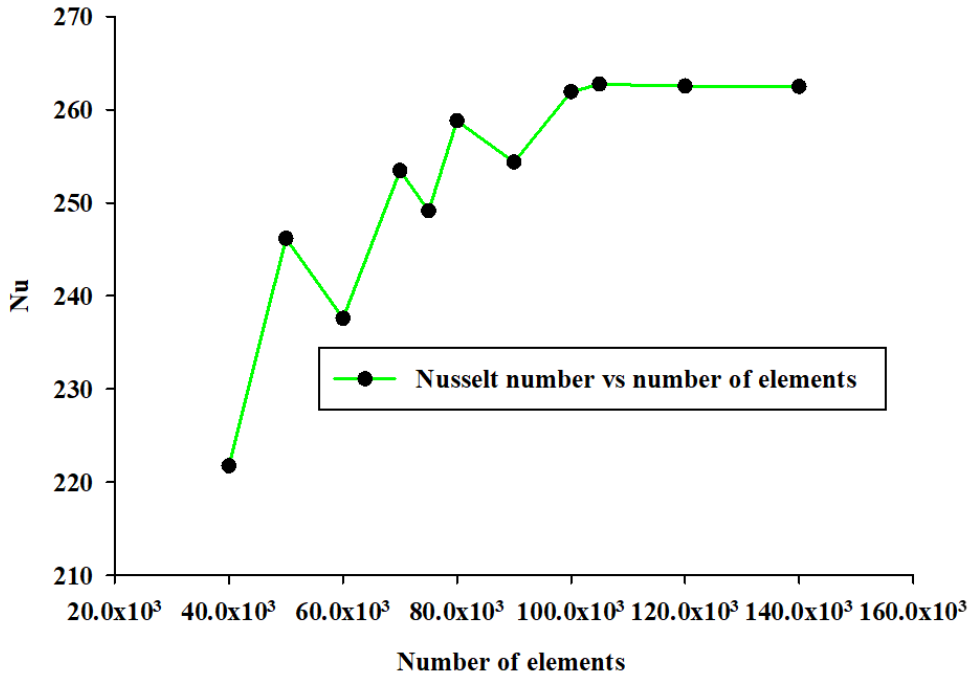

Figure 4-12 Optimum grid size

4.4.3. Calibration of the numerical set up

To ascertain if the numerical methodology is valid and suitable for generating accurate simulation results, the numerical model was calibrated with the literature using pure ethylene glycol as a fluid domain. Fig 4.13 shows the comparison of the present simulation with the Gnielinski's correlation for ethylene glycol to demonstrate the robustness of the numerical set up. A closer agreement with $\pm$7.3% average deviation between simulated results and Gnielinski's equation was found and it was confirmed that the single-phase model with the prescribed boundary conditions and the selected numerical procedure used to solve the problem satisfactorily predicted the Nusselt number of the nano fluids over the range of Reynolds numbers from 4000 to 10000 which falls in the turbulent regime. A desired accuracy was achieved ($< \pm 10\%$) to use the numerical set up for further investigation of heat transfer enhancement by monitoring the fluid properties based on the volume fraction and inlet boundary conditions based on the Reynolds number.

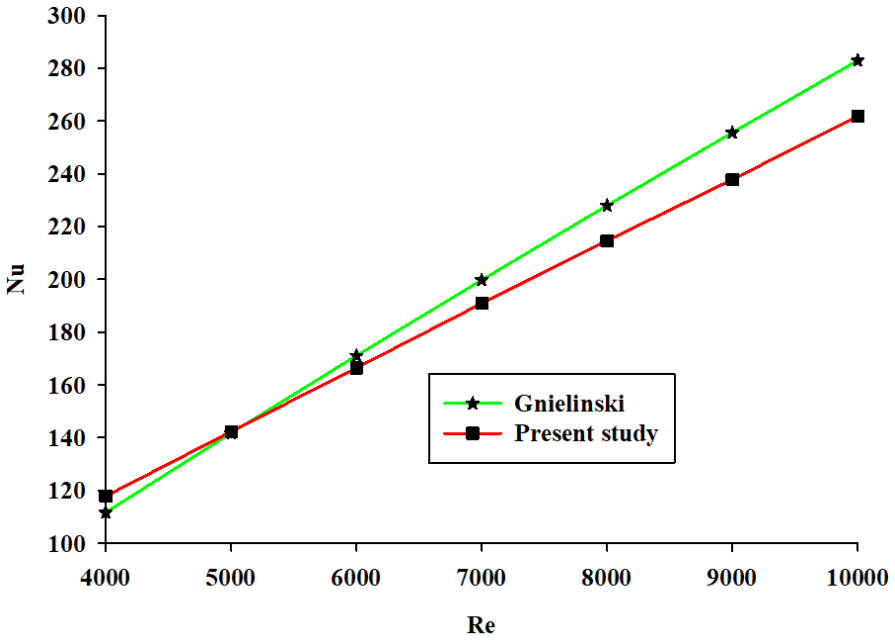

Figure 4-13 Validation of the analysis setup with Gnielinski correlation

Also, the numerical set up was calibrated for friction factor with Blasius equation as shown in the Fig 4.14 and proved to perform well with an average deviation of ±1.9%.

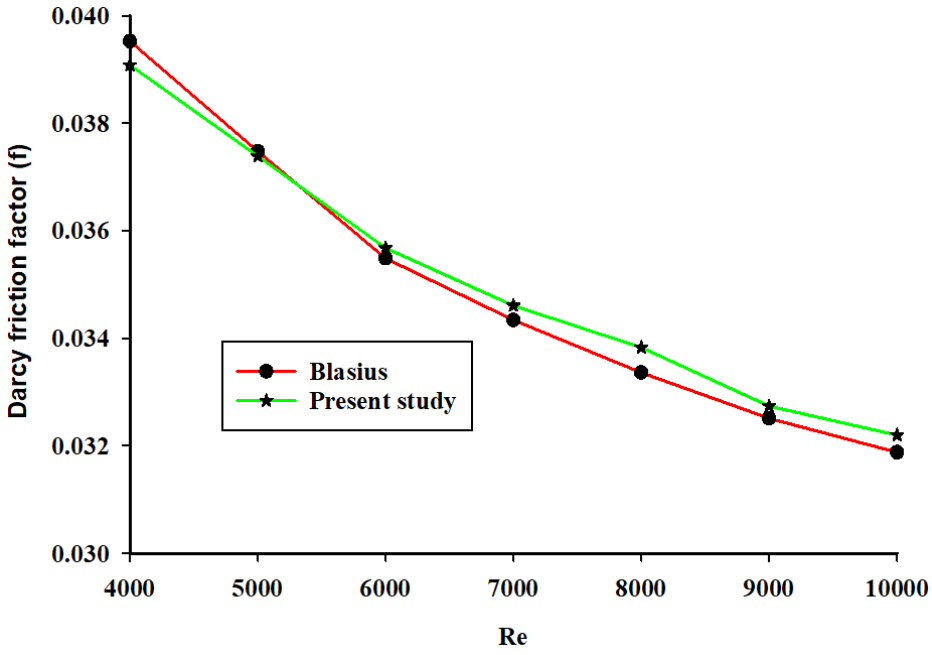

Figure 4-14 Validation of numerical set up with Blasius equation

4.4.4. Temperature contour

From Fig 4.15 it was found that the wall temperature decreases when the nanofluids were used instead of the base fluid. This temperature reduction is evidence of enhanced the heat transfer when nanofluids are used instead of the base fluid. The main reason for this wall temperature drop is the thermal conductivity of the nanofluid is higher than the base fluid which in turn is the result of increased heat transfer area of the nanoparticle surfaces. The temperature drop shows an increasing pattern with the increase of nanoparticle concentration in the base fluid and with higher Reynolds number[55]. This demonstrates that convective heat transfer is enhanced by nanofluids which is carrying more heat from the wall surface than the base fluid as witnessed from Fig 4.15.

Another observation that was witnessed from the temperature contours was entry length reduces as the nanoparticle concentration increases at a given Reynolds number (10,000) and inlet temperature (303.15K) mainly because of the radial migration of nano particles[78].

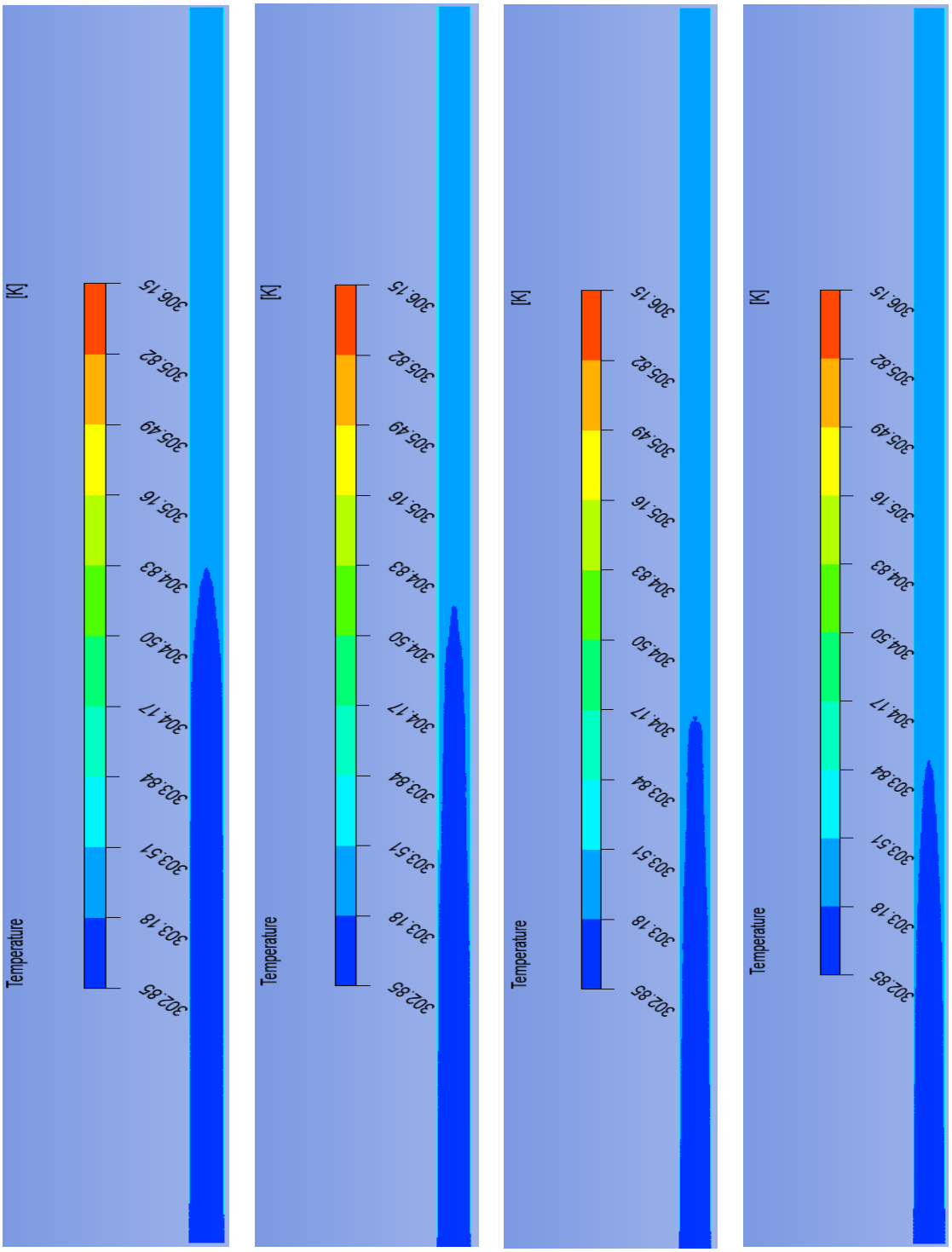

a b c d

Figure 4-15 Temperature contour for the (a) base fluid and the nanofluids of (b) 0.1%, (c) 0.5% and (d) 1% volume concentrations

From the Fig 4.16 it was observed that after the entry point the wall temperature rises enormously and gets to its peak at the axial distance of nearly 0.2m then it became constant for the region of 0.2m to 0.9m where the change in wall and bulk temperature are parallel mainly because the boundary layer becomes slightly thicker. Further increase in axial distance to 1.0 m, it was found that slightly decrease in the wall temperature due to the boundary layer interruption at the exit of the pipe[79].

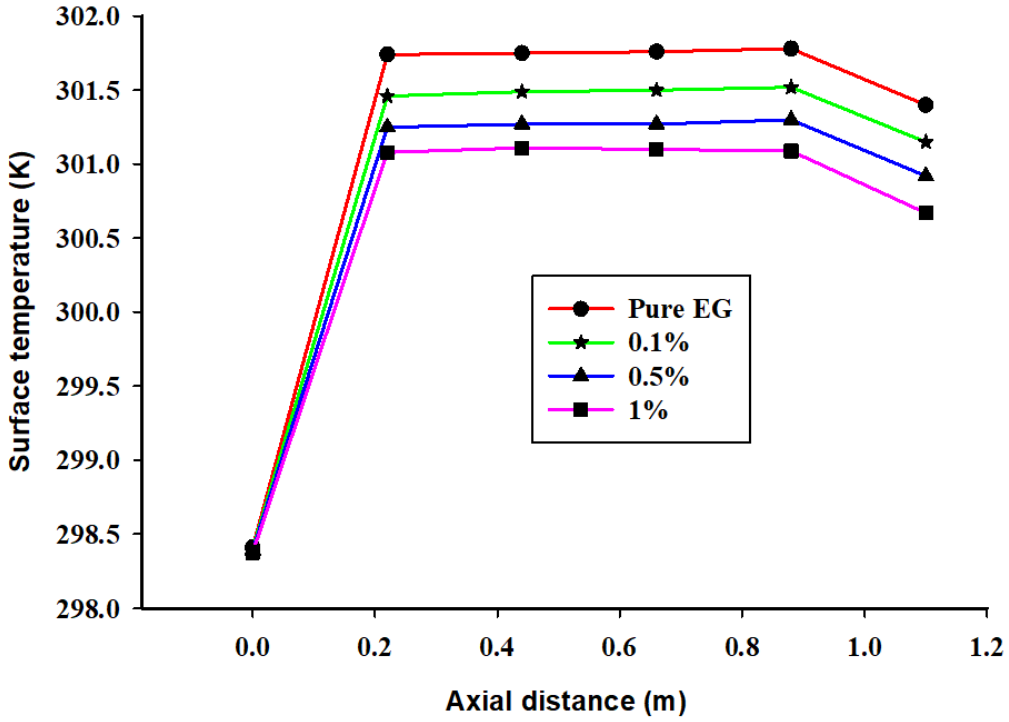

Figure 4-16 Wall temperature distribution for the pure ethylene glycol and Nanofluid with different concentrations along the axial positions of the pipe

The result was also supported by the heat transfer coefficient variation along the axial direction as shown in the Fig 4.17. For 10000 Reynolds number and 298.15K and inlet temperature the heat transfer coefficient was anomalously higher at the entry length for the base fluid and nanofluids because of the flow disturbance and the low temperature of the inlet fluid. But it immediately starts to decrease to nearly constant value all along the rest of the tube length as the flow grows to a fully developed turbulent flow. A slight increase of heat transfer coefficient has occurred at the exit again due to the flow disturbance there.

Those two observations were closely linked all over the volume concentrations and Reynolds number. This shows the heat transfer rate is higher when nanofluid is used as a cooling medium. For the same Reynold's number 10000, it was found that the wall temperatures were decreased to 301.3K, 301.1K and 300.9K when the Cu nanoparticle concentration in the base fluid EG were increased to 0.1%, 0.5% and 1% respectively. The temperature fall was substantially higher with the presence of volume fraction of nanoparticle which clearly indicates that heat transfer is enhanced with increment of volume fractions of Cu nanoparticles du to increase of contact surface area between the EG and Cu nanoparticles[50].

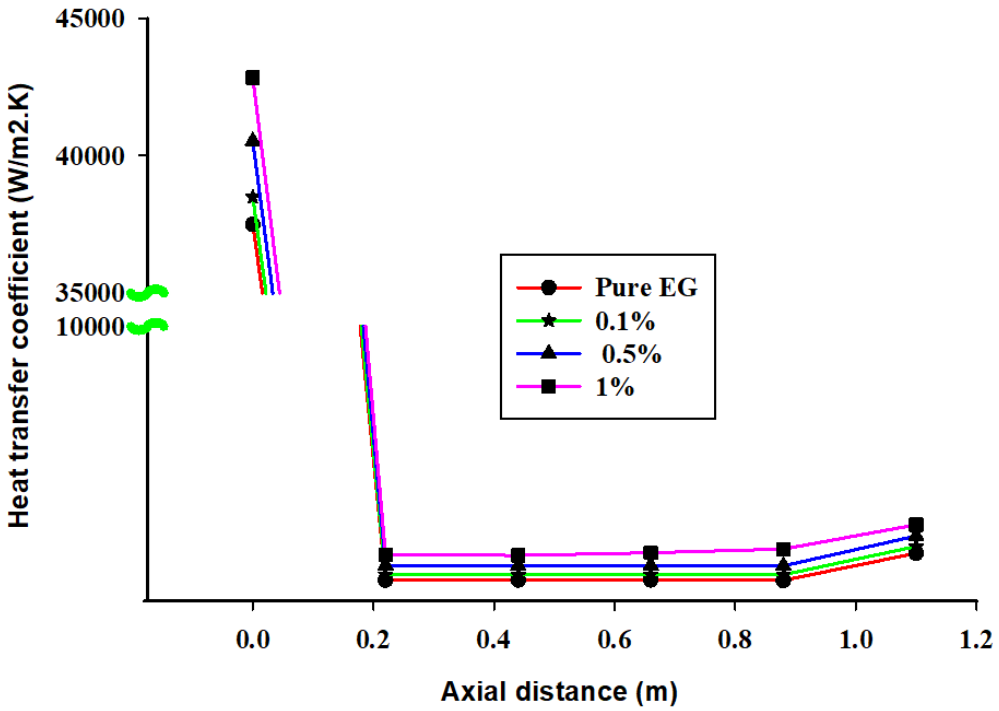

Figure 4-17 Heat transfer coefficient variation for the pure ethylene glycol and Nanofluids with different concentrations along the axial positions of the pipe

It is interesting to note from Fig 4.18 that film temperature of the fluid increases through the tube length and appears more important toward the exit. On the other hand, it was clearly evident that bulk temperatures are also appreciably higher in the presence of nano particle loading. The increase in inside tube wall temperature shows a slight decrease as the particle concentration increase even though the drop wall temperature manly because

the product of specific heat and density also increases which shows that more energy is required to increase the bulk temperature[50].

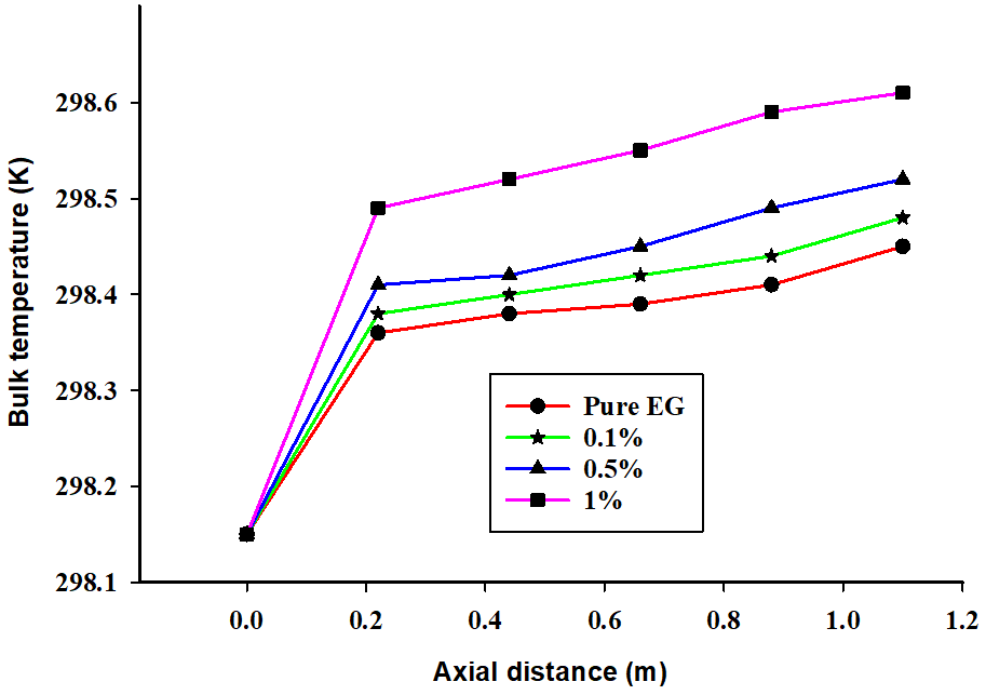

Figure 4-18 Film temperature for pure EG and nanofluids of different particle concentration at 10000 Reynolds number and 298.15K inlet temperature

In addition to the volume fraction of nanoparticles that enhances heat transfer, the inlet temperature has a vital influence on heat transfer. Three inlet temperatures (296.15K, 298.15K, 303.15K) were examined for the same volume fraction of 0.1 % Cu nano particles. The Fig 4.19 showed that the Nusselt number is higher with higher temperature because higher temperature increases particle interaction and migration and thermal conductivity of particle and base fluid, which in turn provides a more efficient radial transport/mixing of heat mainly due to the diffusive nature of the turbulent flow[80]. Consequently, improved turbulent mixing increases temperature gradients near the solid surface. As a result, heat transfer from the solid surface to the fluid is enhanced.

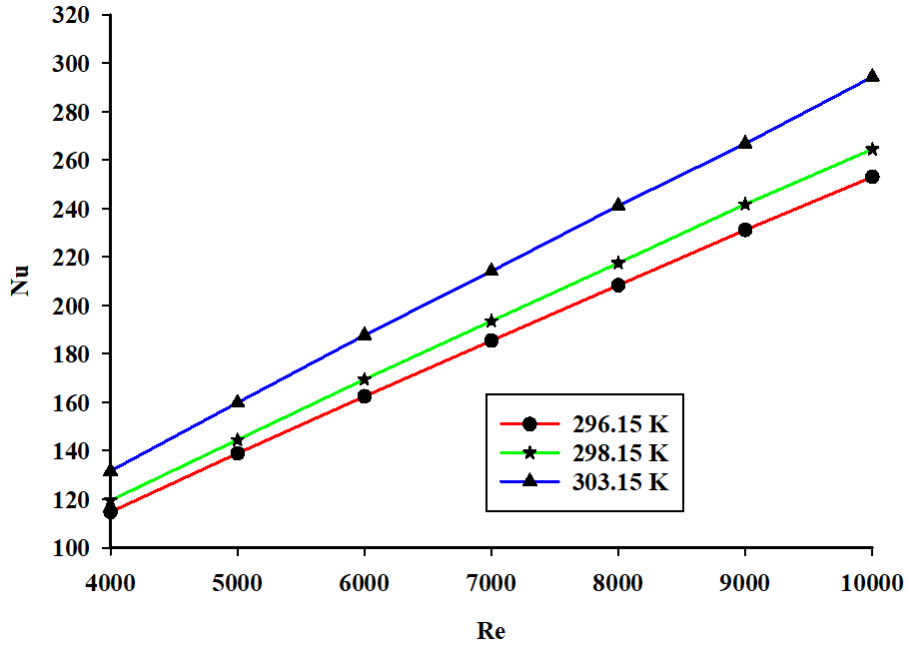

Figure 4-19 Nusselt number variation with inlet temperature at 0.1% volume concentration

3.3. Effect of nanoparticle concentration on the Nusselt number

Fig 4.20 a-c depicted the influence of Cu nanoparticle concentration and Reynolds number on the Nusselt number at inlet temperatures of 296.15K, 298.15K and 303.15K. The Nusselt number has increased by 6.1%, 8.41% and 9.74% for 296.15K, 298.15K and 303.15K inlet temperatures respectively at 10000 Reynolds number and 1% particle loading. On further illustration, the increase in the Nusselt number was on average 1.1 times with 1% volume concentration of Cu nanoparticles over the base fluid EG at Reynolds number of ten thousand. This is mainly due to the increase in Prandtl number at higher volume concentrations and temperature[50]. Reynolds number also appeared to be the main factor for turbulent heat transfer enhancement as shown in the Fig 4.20. Compared to 4000, 7000 and 10000 Reynolds number shows 6.21%, 15.4% and 29.5% higher Nusselt number for 1% particle loading. Since nanofluid heat transfer is significantly dependent on particle motion which in turn is dependent on how fast the fluid moves through the pipe, then a higher Nusselt number was witnessed at higher Reynolds number as shown in the Fig 4.20[56].

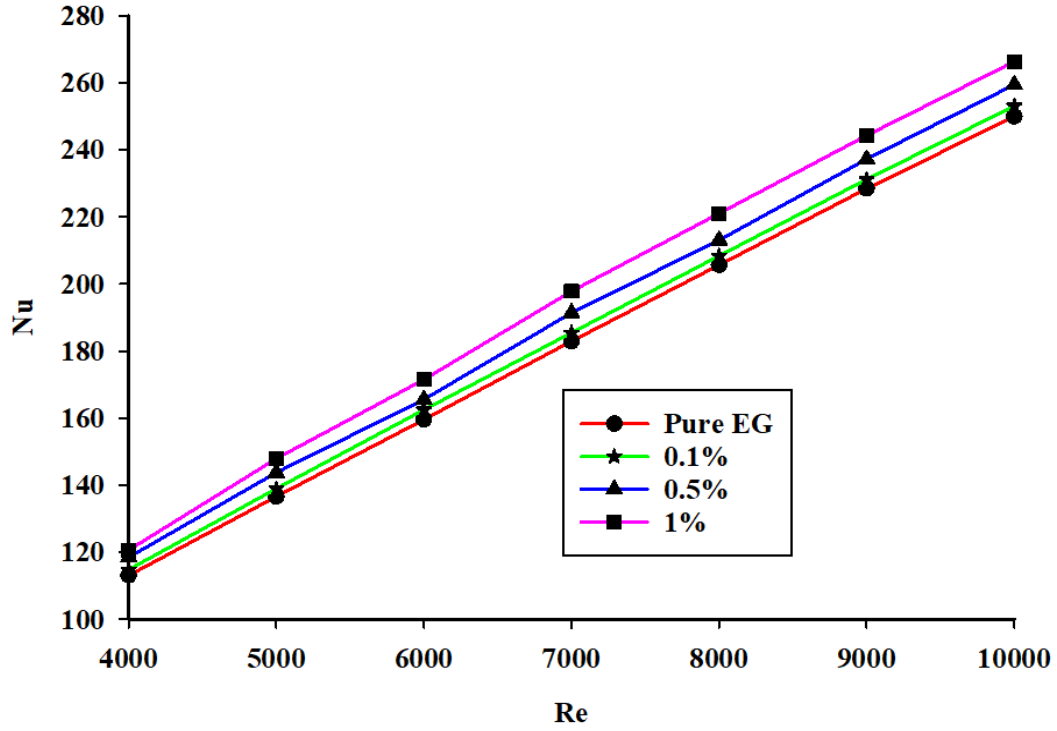
Nu
Re
Pure EG
0.1%
0.5%
1%
100
120
140
160
180
200
220
240
260
280
4000
5000
6000
7000
8000
9000
10000

a

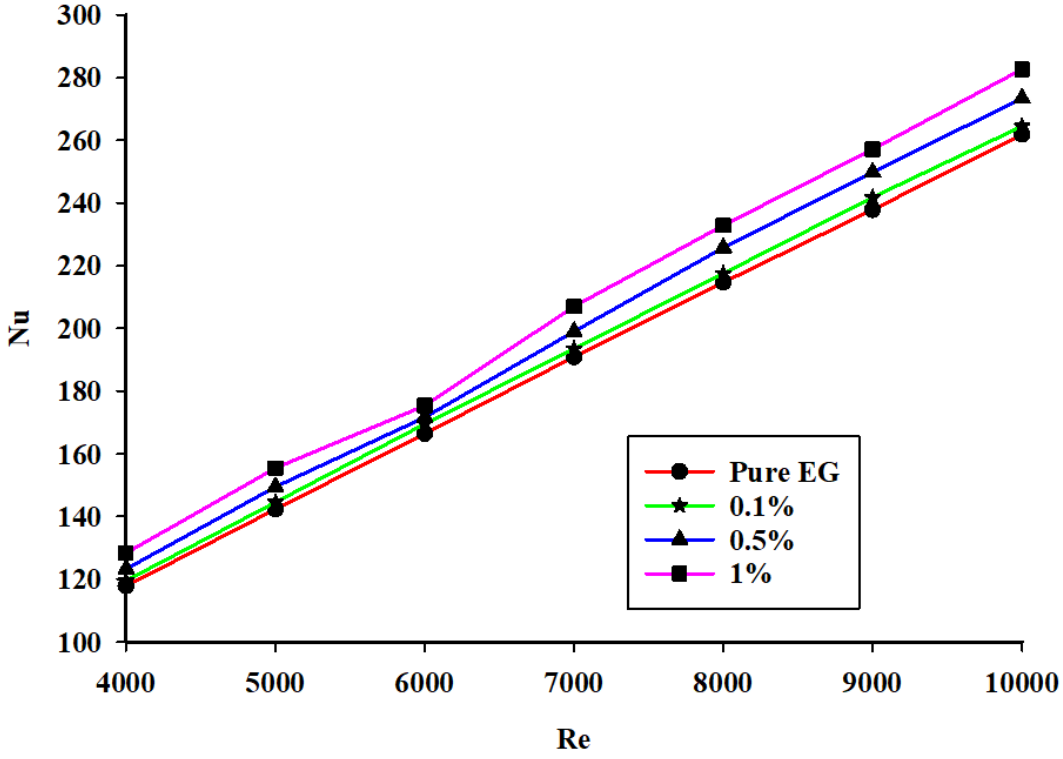
Nu
Re
Pure EG
0.1%
0.5%
1%
100
120
140
160
180
200
220
240
260
280
300
4000
5000
6000
7000
8000
9000
10000

b

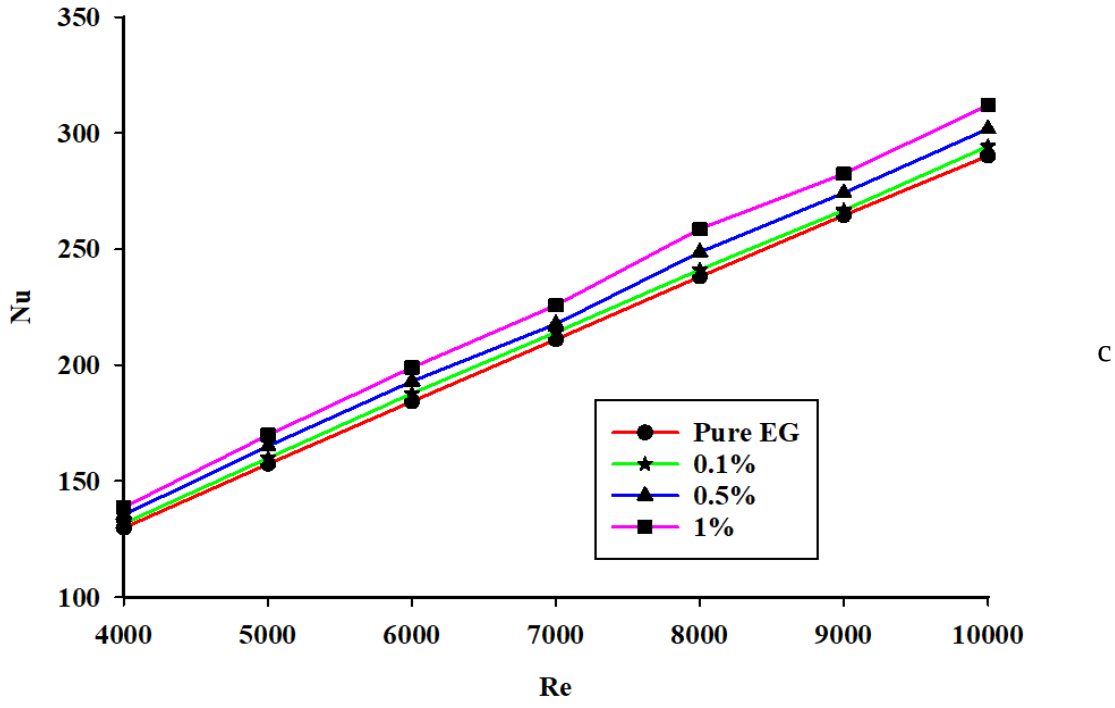

c

Figure 4-20 Nusselt number variation with Reynolds number inlet temperatures of (a) 296.15K, (b) 298.15K and (c) 303.15K

From this numerical study every result showed the meaningful contribution to the heat transfer enhancement by providing nanoparticles to the base fluid, EG. This behavior can be partially explained by the improved thermo physical properties of mixture of nanoparticles with base fluid. Thus, a nanofluid possesses a higher thermal conductivity and more surface area of contact that agrees to increase the heat transfer rates. This enhancement is observed to increase with volume fraction because higher volume fraction means large number of nanoparticles which will make a contact with the neighboring fluid over a greater surface area. It will help in increasing the effective thermal conductivity of the nanofluid and there by the Nusselt number[51].

Moreover, the heat capacity also increases with increase of volume fraction, and hence more heat is transferred by increasing the bulk mean temperature with respect to the base fluid. In addition, given the turbulent diffusion is way more effective to transport heat than molecular diffusion, nano particles laminar sublayer thickness reducing effect is also the other attribute for heat transfer enhancement.

The higher the volume fraction the higher the turbulent dissipation due to higher effective viscosity which in effect will offset the contribution of higher effective thermal conductivity for Nusselt number increase at higher Reynolds number. This fact was demonstrated with the turbulent intensity contours as shown in the Fig 4.21.

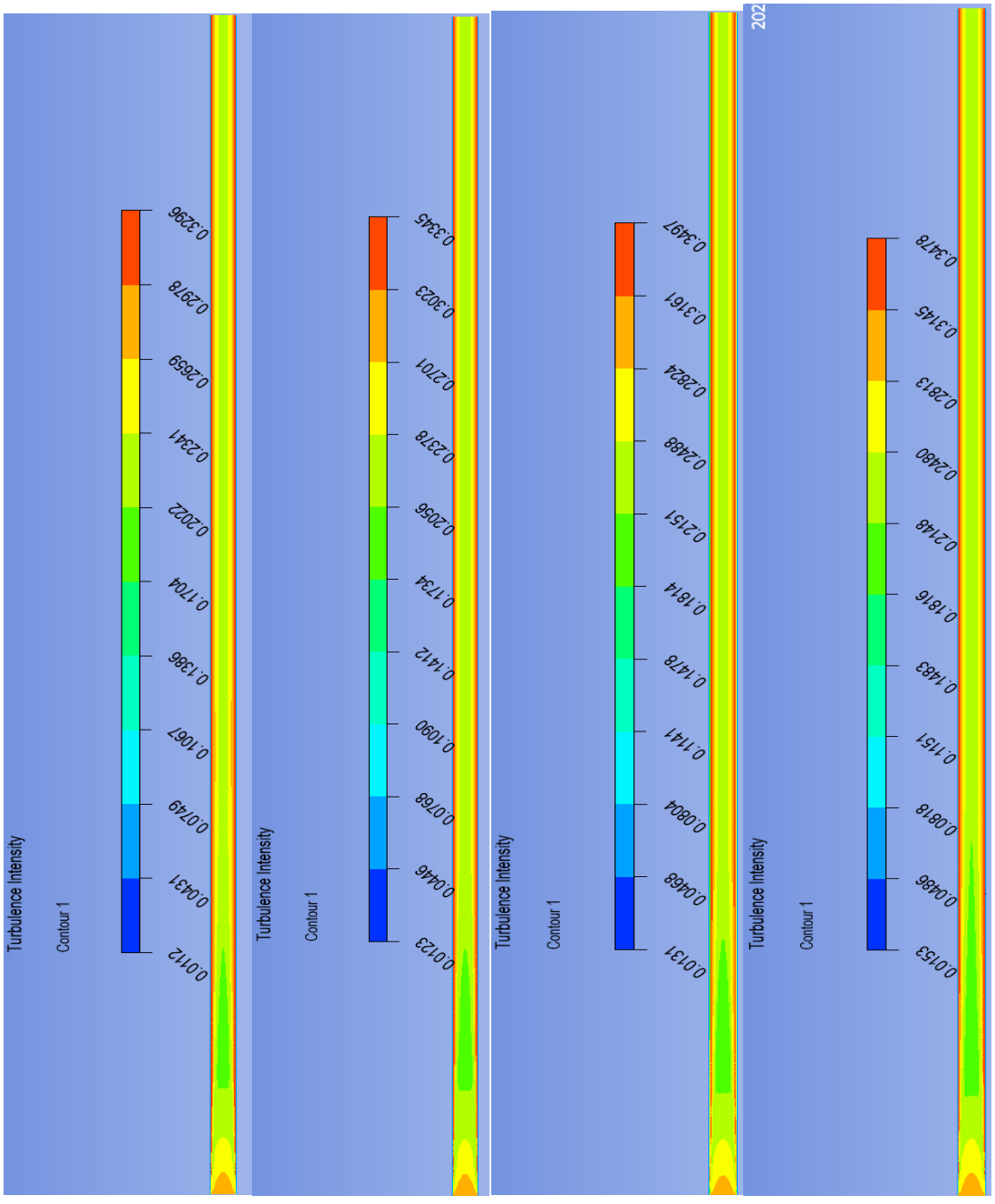

Figure 4-21 Turbulent intensity contour with increasing Reynolds number and volume fraction respectively

As shown in the Fig 4.22 the nanofluid friction factors deviated from the base fluid friction factor and the deviation was increasing with higher particle volume concentrations. This could be explained by a relative movement between fluid and nanoparticles which may lead to an additional momentum transport and increase the friction factor. In other words, the increase in nanofluid viscosity with particle concentration was responsible for the increase in Darcy friction factor.

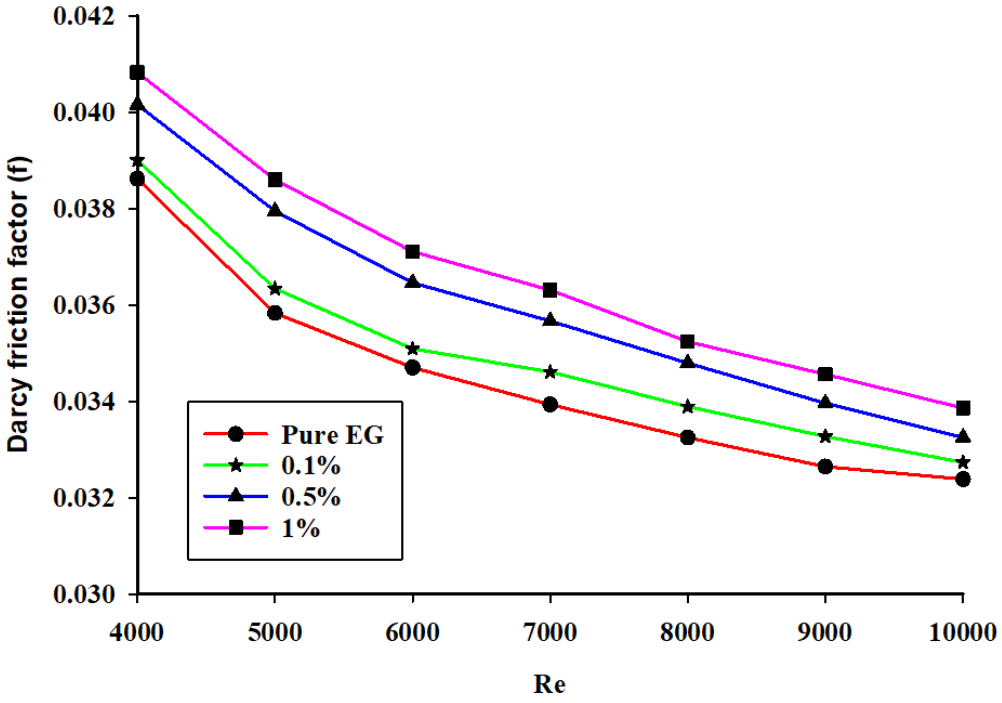

Figure 4-22 Friction factor of the base fluid and nanofluids of different particle loading with respect to Reynolds number

4.5. Validation of experimental and numerical results

A comparison of Nusselt number of nanofluids at 1% volume fraction a 296.15K inlet temperature have been done to indicate the experimental and simulated results validity. A closer agreement of maximum and average deviation of ±9.2% and ±5.7 % respectively was achieved which was still inside the allowable range of deviation (±10%).

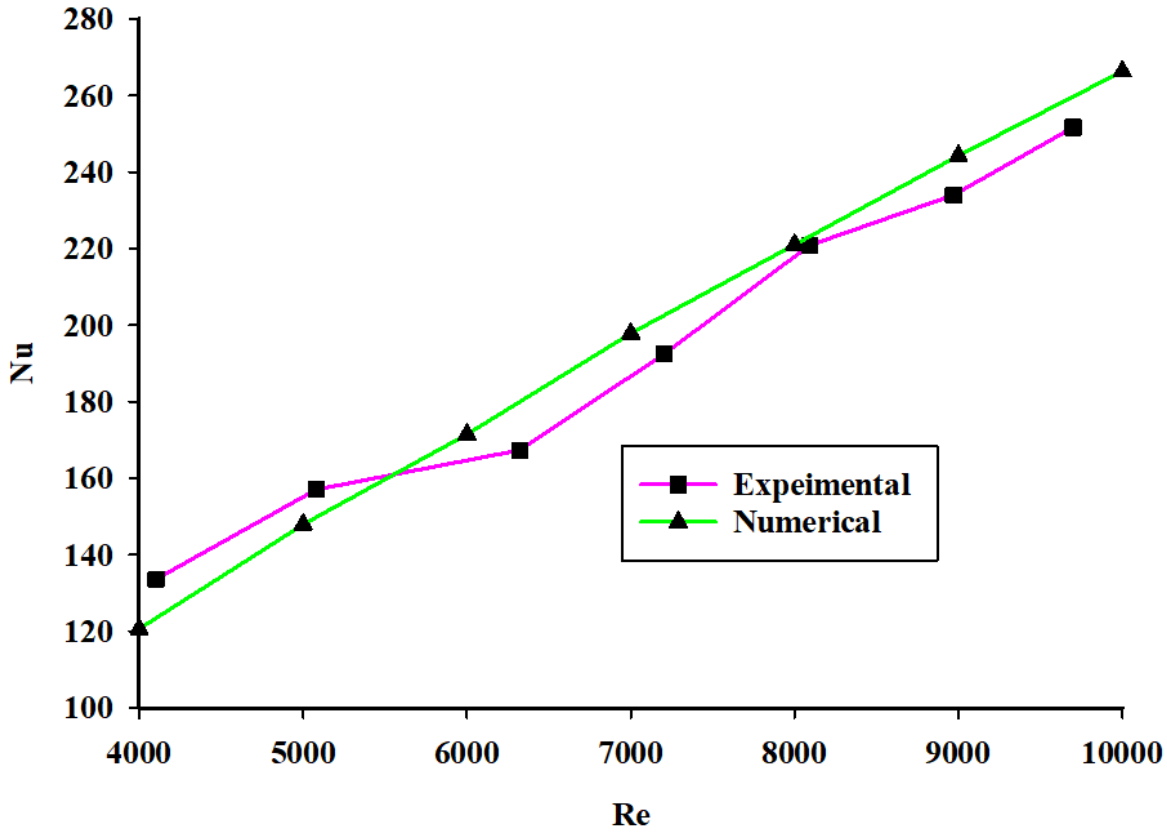

Figure 4-23 Comparison of experimental and numerical Nusselt number at 296.15K inlet temperature and 1% volume fraction

The simulated Nusselt number curve has the same behavior as that experimental one and they are close to each other. At lower flowrates the numerical model under predicted the empirical value but as the Reynolds number increases the numerical Nusselt number got larger than the experimental one. This could be mainly because as the Reynolds number increases, the locally fabricated nature of the test set up gets in the way which goes in line with the fact that as flow gets more turbulent, its sensitivity to flow geometry and surface imperfection increases[81].

Besides Darcy friction factor values of both experimental and numerical analyses agreed closely each other with maximum and average deviations of $\pm 4.3\%$ and $\pm 1.95\%$ respectively.

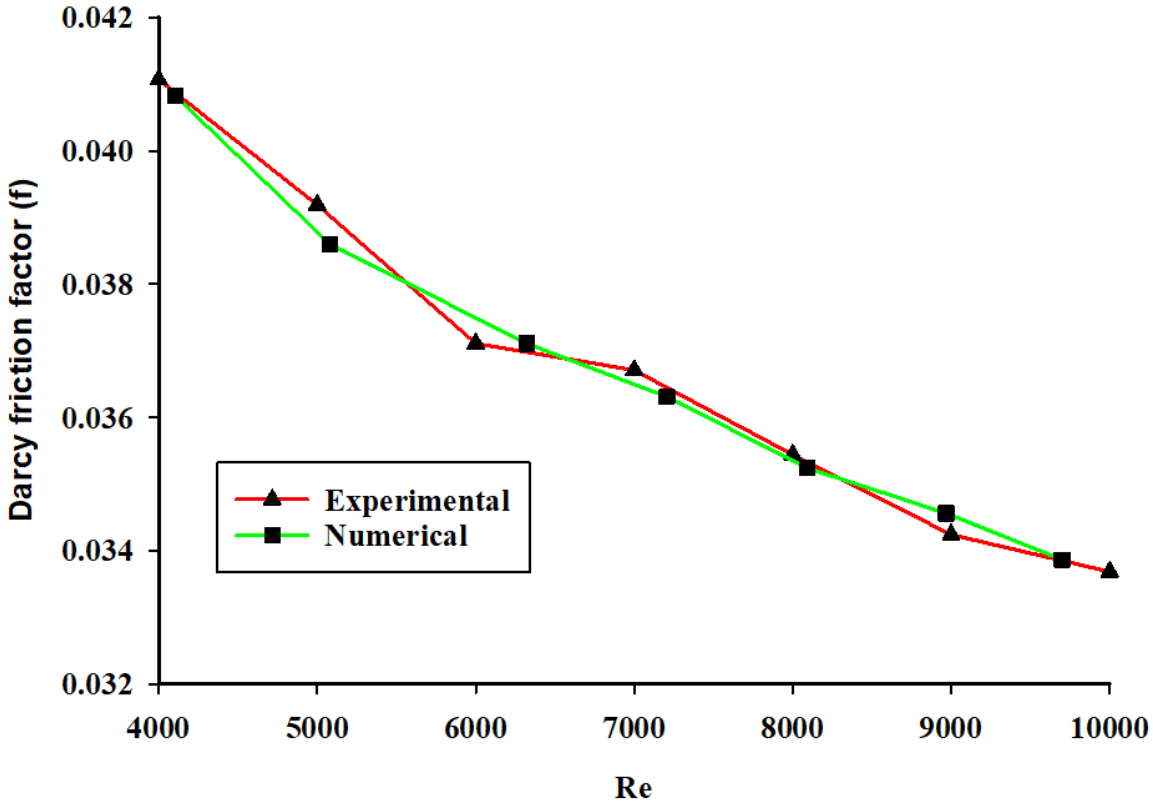

Based on the deviations between the numerical and experimental results for both the Nusselt number and friction factor, the results were indeed encouraging. For the range or of the Reynolds number and particle concentrations used in this study the CFD model was reliable enough to measure the hydrodynamic and heat transfer properties Cu-EG nanofluids.

CHAPTER FIVE

5. CONCLUSIONS AND RECOMMENDATIONS

In this chapter, some of the observations from the result of this thesis work were outlined. Ultimately, some final conclusions and recommendations for future research efforts in this line were made.

5.1. Conclusions

A fully-developed turbulent flow and convective heat transfer characteristics of ethylene glycol-based copper (Cu-EG) nanofluids flowing in a circular tube of 20 mm inner diameter and 1.1m length under a uniform heat flux boundary condition was investigated both numerically and experimentally in this study. Single phase models with temperature dependent thermo physical properties and realizable k-ε turbulent model was considered. From the experimental and numerical analysis, the following list of conclusions are drawn

- The nanofluid causes a heat transfer enhancement as observed by Nusselt number increase compared with the base fluid. The enhancement increases with volume fraction, inlet temperature and Reynolds number. Nusselt number for Cu/EG nanofluid with 1% nanoparticle volume fraction is approximately 1.1 times higher than base fluid at 10000 Reynolds number and 303.15K inlet temperature.
- The heat transfer enhancement is steeper for all volume fraction nanofluids which illustrates that heat transfer augmentation is more significant as the Reynolds number increases.
- The wall temperature is lower (by a maximum of 2.3K for nanofluids and which is noticeable as the particle loading increases but the fluid temperature is higher (a maximum of 0.34K) 7000 Reynolds number and 298.15K inlet temperature. This indicates the reduction of wall temperature for Nano fluids is compensated by rise of fluid temperature than the pure ethylene glycol.
- Friction factor increases with increasing volume fraction and inlet temperature for both the numerical and experimental analyses.

- A good concurrence with average deviation 5.7% and 1.95% for Nusselt number and friction factor respectively was obtained between numerical simulation and experimental results in various ranges of Reynolds number.

5.2. Recommendations

1. The small rating of the pump used to supply pressure limits the experiment to low Reynolds number turbulent flow. Hence, it is necessary to secure a pump of higher ratings which is capable of generating turbulent flow in the test sections for the nanofluid in order to adequately study the friction factor and heat transfer behavior in the turbulent region.
2. Due to the sensitivity of thermophysical properties, some errors might have affected the recorded data owing to disturbances produced by vibration and sound from the surrounding. If these disturbances can be eliminated or at least minimized, a better result should be achieved.
3. Due to high cost of thermocouples used, wall temperature was only measured at four axial positions across the test section. Using many thermocouples closer to each other could provide a more accurate result.
4. Inaccessibility to high computational power computers limits the numerical simulation only to 2D axisymmetric geometry. A 3D analysis considering circumferential migration of nanoparticles could give a more descriptive picture.
5. Having studied the conflicting effect of each parameter on the heat transfer enhancement capability of nanofluids, optimization of those contradicting parameters to achieve the best out of the blessing of the nanofluids is in demand. To be specific the impact of particle size and particle concentration on the thermal conductivity and viscosity and thereby on the friction factor and heat transfer coefficient is to be sorted

REFERENCES

[1] V. Bianco, O. Manca, and S. Nardini, “Numerical investigation of transient single phase forced convection of nanofluids in circular tubes,” vol. 61, pp. 3–12, doi: 10.2495/HT080011.

[2] L. G. Asirvatham, N. Vishal, S. K. Gangatharan, and D. M. Lal, “Experimental study on forced convective heat transfer with low volume fraction of CuO/Water nanofluid,” *Energies*, vol. 2, no. 1, pp. 97–119, 2009, doi: 10.3390/en20100097.

[3] J. Thammanna and A. Srivastav, “Thermal Management in Electronic Equipment,” *Hcl*, no. 1, pp. 2–20, 2010.

[4] A. Dewan, P. Mahanta, K. S. Raju, and P. Suresh Kumar, “Review of passive heat transfer augmentation techniques,” *Proc. Inst. Mech. Eng. Part A J. Power Energy*, vol. 218, no. 7, pp. 509–527, 2004, doi: 10.1243/0957650042456953.

[5] A. A. Minea, “Simulation of Nanofluids Turbulent Forced Convection at High Reynolds Number : A Comparison Study of Thermophysical Properties Influence,” no. 63, 2014, doi: 10.1007/s10494-014-9590-0.

[6] J. C. Maxwell, *A treatise on electricity and magnetism*. 1873.

[7] W. Williams, J. Buongiorno, and L.-W. Hu, “Experimental Investigation of Turbulent Convective Heat Transfer and Pressure Loss of Alumina/Water and Zirconia/Water Nanoparticle Colloids (Nanofluids) in Horizontal Tubes,” *J. Heat Transfer*, vol. 130, no. 4, p. 042412, 2008, doi: 10.1115/1.2818775.

[8] V. Bianco, O. Manca, S. Nardini, and K. Vafai, *Heat Transfer Enhancement with Nanofluids*, no. May. 2015.

[9] H. D. Koca, S. Doganay, A. Turgut, I. H. Tavman, R. Saidur, and I. M. Mahbubul, “Effect of particle size on the viscosity of nanofluids: A review,” *Renew. Sustain. Energy Rev.*, vol. 82, no. February 2017, pp. 1664–1674, 2018, doi: 10.1016/j.rser.2017.07.016.

[10] A. Umer, S. Naveed, N. Ramzan, and M. S. Rafique, “SELECTION OF A SUITABLE METHOD FOR THE SYNTHESIS OF COPPER NANOPARTICLES,” vol. 7, no. 5, 2012, doi: 10.1142/S1793292012300058.

[11] U. T. Khatoon, K. V. Rao, J. V. R. Rao, and Y. Aparna, “Synthesis and

characterization of silver nanoparticles by chemical reduction method," *Int. Conf. Nanosci. Eng. Technol.*, vol. 9, pp. 97–99, 2011, doi: 10.1109/ICONSET.2011.6167920.

[12] T. M. D. Dang, T. T. T. Le, E. Fribourg-Blanc, and M. C. Dang, "Synthesis and optical properties of copper nanoparticles prepared by a chemical reduction method," *Adv. Nat. Sci. Nanosci. Nanotechnol.*, vol. 2, no. 1, 2011, doi: 10.1088/2043-6262/2/1/015009.

[13] J. Adrian Bejan and Peter A. Pfister, "EVALUATION OF HEAT TRANSFER AUGMENTATION TECHNIQUES BASED ON THEIR IMPACT ON ENTROPY GENERATION," *Lett. HEATASDMASS Transf.*, vol. 7, no. c, pp. 97–106, 1980.

[14] _T._Prad [Sarit_K._Das, _Stephen_U._Choi, _Wenhua_Yu, *Nano fluid Science and Technology*. A JOHN WILEY & SONS, INC, 2008.

[15] J. Garg *et al.*, "Enhanced thermal conductivity and viscosity of copper nanoparticles in ethylene glycol nanofluid," *J. Appl. Phys.*, vol. 103, no. 7, 2008, doi: 10.1063/1.2902483.

[16] S. Chandra, A. Kumar, and P. K. Tomar, "Synthesis and characterization of copper nanoparticles by reducing agent," *J. Saudi Chem. Soc.*, vol. 18, no. 2, pp. 149–153, 2014, doi: 10.1016/j.jscs.2011.06.009.

[17] A. Khan, A. Rashid, R. Younas, and R. Chong, "A chemical reduction approach to the synthesis of copper nanoparticles," *Int. Nano Lett.*, vol. 6, no. 1, pp. 21–26, 2016, doi: 10.1007/s40089-015-0163-6.

[18] A. A. Velasco, O. Perales-Perez, and G. Gutiérrez, "Synthesis of Cu Nanoparticles for Preparation of Nanofluids," *Nanotechonoly*, vol. 1, no. Ii, pp. 424–427, 2008.

[19] H. T. Zhu, C. Y. Zhang, and Y. S. Yin, "Rapid synthesis of copper nanoparticles by sodium hypophosphite reduction in ethylene glycol under microwave irradiation," *J. Cryst. Growth*, vol. 270, no. 3–4, pp. 722–728, 2004, doi: 10.1016/j.jcrysgro.2004.07.008.

[20] M. S. Liu, M. C. C. Lin, C. Y. Tsai, and C. C. Wang, "Enhancement of thermal conductivity with Cu for nanofluids using chemical reduction method," *Int. J.*

Heat Mass Transf., vol. 49, no. 17–18, pp. 3028–3033, 2006, doi: 10.1016/j.ijheatmasstransfer.2006.02.012.

[21] W. Yu, H. Xie, L. Chen, and Y. Li, "Investigation on the thermal transport properties of ethylene glycol-based nano fl uids containing copper nanoparticles," *Powder Technol.*, vol. 197, no. 3, pp. 218–221, 2010, doi: 10.1016/j.powtec.2009.09.016.

[22] B. Kavlicoglu, O. Graeve, Y. Liu, M. Saterlie, and H. Sahin, "Particle size effects in the thermal conductivity enhancement of copper-based nanofluids," *Nanoscale Res. Lett.*, vol. 6, no. 1, p. 217, 2011, doi: 10.1186/1556-276x-6-217.

[23] J. A. Eastman, S. U. S. Choi, S. Li, W. Yu, and L. J. Thompson, "Anomalously increased effective thermal conductivities of ethylene glycol-based nanofluids containing copper nanoparticles," *Appl. Phys. Lett.*, vol. 78, no. 6, pp. 718–720, 2001, doi: 10.1063/1.1341218.

[24] M. H. Pirahmadian and A. Ebrahimi, "Theoretical Investigation Heat Transfer Mechanisms in Nanofluids and the Effects of Clustering on Thermal Conductivity," vol. 2, no. 2, 2012.

[25] X. Q. Wang and A. S. Mujumdar, "Heat transfer characteristics of nanofluids: a review," *International Journal of Thermal Sciences*, vol. 46, no. 1. pp. 1–19, 2007, doi: 10.1016/j.ijthermalsci.2006.06.010.

[26] K. S. Hwang, S. P. Jang, and S. U. S. Choi, "Flow and convective heat transfer characteristics of water-based Al2O3nanofluids in fully developed laminar flow regime," *Int. J. Heat Mass Transf.*, vol. 52, no. 1–2, pp. 193–199, 2009, doi: 10.1016/j.ijheatmasstransfer.2008.06.032.

[27] D. Kim *et al.*, "Convective heat transfer characteristics of nanofluids under laminar and turbulent flow conditions," *Curr. Appl. Phys.*, vol. 9, no. 2 SUPPL., pp. e119–e123, 2009, doi: 10.1016/j.cap.2008.12.047.

[28] C. K. Mangrulkar, V. M. Kriplani, and A. S. Dhoble, "Experimental investigation of convective heat transfer enhancement using alumina/water and copper oxide/water nanofluids," *Therm. Sci.*, vol. 2015, no. 5, pp. 1–12, 2015, doi: 10.2298/TSCI141225077M.

[29] B. Sahin, E. Manay, and E. F. Akyurek, "An Experimental Study on Heat

Transfer and Pressure Drop of CuO-Water Nanofluid," vol. 2015, 2015.

[30] S. M. Fotukian and M. N. Esfahany, "Experimental study of turbulent convective heat transfer and pressure drop of dilute CuO / water nano fl uid inside a circular tube ☆," *Int. Commun. Heat Mass Transf.*, vol. 37, no. 2, pp. 214–219, 2010, doi: 10.1016/j.icheatmasstransfer.2009.10.003.

[31] L. I. Qiang and X. Yimin, "Convective heat transfer and flow characteristics of Cu-water nanofluid," vol. 45, no. 4, 2002.

[32] A. Zamzamian, S. Nasseri, A. Doosthoseini, and A. Joneidi, "Experimental investigation of forced convective heat transfer coefficient in nanofluids of Al 2 O 3 / EG and CuO / EG in a double pipe and plate heat exchangers under turbulent flow," *Exp. Therm. Fluid Sci.*, vol. 35, no. 3, pp. 495–502, 2011, doi: 10.1016/j.expthermflusci.2010.11.013.

[33] S. M. Fotukian and M. Nasr Esfahany, "Experimental investigation of turbulent convective heat transfer of dilute γ-Al2O3/water nanofluid inside a circular tube," *Int. J. Heat Fluid Flow*, vol. 31, no. 4, pp. 606–612, 2010, doi: 10.1016/j.ijheatfluidflow.2010.02.020.

[34] M. Chandrasekar, S. Suresh, and T. Senthilkumar, "Mechanisms proposed through experimental investigations on thermophysical properties and forced convective heat transfer characteristics of various nanofluids - A review," *Renew. Sustain. Energy Rev.*, vol. 16, no. 6, pp. 3917–3938, 2012, doi: 10.1016/j.rser.2012.03.013.

[35] M. H. Buschmann *et al.*, "Correct interpretation of nanofluid convective heat transfer," *Int. J. Therm. Sci.*, vol. 129, no. April, pp. 504–531, 2018, doi: 10.1016/j.ijthermalsci.2017.11.003.

[36] J. J. Vadasz, S. Govender, and P. Vadasz, "Heat transfer enhancement in nano-fluids suspensions: Possible mechanisms and explanations," *Int. J. Heat Mass Transf.*, vol. 48, no. 13, pp. 2673–2683, 2005, doi: 10.1016/j.ijheatmasstransfer.2005.01.023.

[37] C. Nie, W. H. Marlow, and Y. A. Hassan, "Discussion of proposed mechanisms of thermal conductivity enhancement in nanofluids," vol. 51, pp. 1342–1348, 2008, doi: 10.1016/j.ijheatmasstransfer.2007.11.034.

[38] S. Z. Heris, S. G. Etemad, and M. N. Esfahany, “Convective Heat Transfer of a Cu / Water Nanofluid Flowing Through a Circular Tube,” vol. 6152, 2009, doi: 10.1080/08916150902950145.

[39] Y. Jung *et al.*, “Temperature Dependence of Convective Heat Transfer with Al₂O₃ Nanofluids in the Turbulent Flow Region,” *J. Nanosci. Nanotechnol.*, vol. 13, no. 12, pp. 7902–7905, 2013, doi: 10.1166/jnn.2013.8109.

[40] S. Torii, “Turbulent heat transfer behavior of nanofluid in a circular tube heated under constant heat flux,” *Adv. Mech. Eng.*, vol. 2010, 2010, doi: 10.1155/2010/917612.

[41] E. B. Haghighi *et al.*, “Experimental Study on Convective Heat Transfer of Nanofluids in Turbulent Flow: Methods of Comparison of Their Performance,” *Exp. Therm. FLUID Sci.*, 2014, doi: 10.1016/j.expthermflusci.2014.05.019.

[42] S. El B, C. Tam, N. Galanis, and G. Roy, “Heat transfer behaviours of nanofluids in a uniformly heated tube,” vol. 35, pp. 543–557, 2004, doi: 10.1016/j.spmi.2003.09.012.

[43] D. Wen and Y. Ding, “Experimental investigation into convective heat transfer of nanofluids at the entrance region under laminar flow conditions,” vol. 47, pp. 5181–5188, 2004, doi: 10.1016/j.ijheatmasstransfer.2004.07.012.

[44] V. Bianco, O. Manca, and S. Nardini, “Numerical investigation on nanofluids turbulent convection heat transfer inside a circular tube,” *Int. J. Therm. Sci.*, vol. 50, no. 3, pp. 341–349, 2011, doi: 10.1016/j.ijthermalsci.2010.03.008.

[45] S. El Bécaye Maïga, S. J. Palm, C. T. Nguyen, G. Roy, and N. Galanis, “Heat transfer enhancement by using nanofluids in forced convection flows,” *Int. J. Heat Fluid Flow*, vol. 26, no. 4 SPEC. ISS., pp. 530–546, 2005, doi: 10.1016/j.ijheatfluidflow.2005.02.004.

[46] Q. Li and Y. Xuan, “Convective heat transfer and flow characteristics of Cu-water nanofluid,” *Sci. China (Series E)*, vol. 45, no. 4, 2002.

[47] A. M, S. M., Z. N, and A. P, “EXPERMENTAL INVESTIGATION OF CONVECTIVE HEAT TRANSFER OF NANOFLUIDS,” in *7th International Conference on Heat Transfer, FluidMechanics and Thermodynamics*, 2010, no.

July, pp. 1459–1464.

[48] Y. Xuan and Q. Li, “Investigation on Convective Heat Transfer and Flow Features of Nanofluids,” *J. Heat Transfer*, vol. 125, no. 1, p. 151, 2003, doi: 10.1115/1.1532008.

[49] B. C. Pak and Y. I. Cho, “Hydrodynamic and heat transfer study of dispersed fluids with submicron metallic oxide particles,” *Exp. Heat Transf.*, vol. 11, no. 2, pp. 151–170, 1998, doi: 10.1080/08916159808946559.

[50] P. K. Namburu, D. K. Das, K. M. Tanguturi, and R. S. Vajjha, “Numerical study of turbulent flow and heat transfer characteristics of nanofluids considering variable properties,” *Int. J. Therm. Sci.*, vol. 48, no. 2, pp. 290–302, 2009, doi: 10.1016/j.ijthermalsci.2008.01.001.

[51] G. Saha and M. C. Paul, “Numerical analysis of the heat transfer behaviour of water based Al2O3and TiO2nanofluids in a circular pipe under the turbulent flow condition,” *Int. Commun. Heat Mass Transf.*, vol. 56, pp. 96–108, 2014, doi: 10.1016/j.icheatmasstransfer.2014.06.008.

[52] M. K. Moraveji and A. R. Beheshti, “CFD Study of the Turbulent Forced Convective Heat Transfer of Non-Newtonian Nanofluid,” vol. 11, no. 2, pp. 92–102, 2014.

[53] B. Gambang and R. City, “Simulation Study of Turbulent Convective Heat Transfer,” vol. c, no. July, pp. 1–3, 2013.

[54] J. Bayat and A. H. Nikseresht, “Thermal performance and pressure drop analysis of nanofluids in turbulent forced convective flows,” *Int. J. Therm. Sci.*, vol. 60, pp. 236–243, 2012, doi: 10.1016/j.ijthermalsci.2012.04.012.

[55] P. Kumar and R. Ganesan, “A CFD Study of Turbulent Convective Heat Transfer Enhancement in Circular Pipeflow,” *Eng. Technol.*, vol. 6, no. 8, pp. 695–702, 2012.

[56] M. Ahmadi and G. Willing, “International Journal of Heat and Mass Transfer Heat transfer measurment in water based nanofluids,” *Int. J. Heat Mass Transf.*, vol. 118, pp. 40–47, 2018, doi: 10.1016/j.ijheatmasstransfer.2017.10.090.

[57] M. Esfandiary, A. Habibzadeh, and H. Sayehvand, “Numerical Study of Single Phase/Two-Phase Models for Nanofluid Forced Convection and Pressure Drop in

a Turbulence Pipe Flow," *Trans. Phenom. Nano Micro Scales*, vol. 4, no. 1, pp. 11–18, 2016, doi: 10.7508/tpnms.2016.01.002.

[58] E. S. Akbay, B. Dereli, and O. Turgut, "The Effect of Turbulence Model and Nanofluid on Fluid Flow and Heat Transfer in a Narrow Rectangular Duct," *J. Polytech.*, vol. 0900, pp. 0–1, 2019, doi: 10.2339/politeknik.589390.

[59] W. Peng, B. Minli, L. Jizu, H. Chengzhi, and W. Yuyan, "NUMERICAL INVESTIGATION ON THE TURBULENT FLOW CHARACTERISTIC OF NANOFLUIDS IN A HORIZONTAL CIRCULAR TUBE," no. 2, pp. 646–668, 2014, doi: 10.1080/10407782.2014.894389.

[60] M. Mahdavi, M. Sharifpur, and J. P. Meyer, "Simulation study of convective and hydrodynamic turbulent nanofluids by turbulence models International Journal of Thermal Sciences Simulation study of convective and hydrodynamic turbulent nano fl uids by turbulence models," *Int. J. Therm. Sci.*, vol. 110, no. December, pp. 36–51, 2016, doi: 10.1016/j.ijthermalsci.2016.05.027.

[61] H. Boertz, A. Baars, J. T. Cieśliński, and S. Smoleń, "Turbulence Model Evaluation for Numerical Modelling of Turbulent Flow and Heat Transfer of Nanofluids," *Appl. Mech. Mater.*, vol. 831, no. April, pp. 165–180, 2016, doi: 10.4028/www.scientific.net/amm.831.165.

[62] M. Corcione, M. Cianfrini, and A. Quintino, "Heat transfer of nanofluids in turbulent pipe flow," *Int. J. Therm. Sci.*, vol. 56, pp. 58–69, 2012, doi: 10.1016/j.ijthermalsci.2012.01.009.

[63] L. Gosselin, A. K. Silva, and A. K. Silva, "Combined ' heat transfer and power dissipation ' optimization of nanofluid flows Combined ' heat transfer and power dissipation ' optimization of nanofluid flows," vol. 4160, no. 2004, pp. 16–19, 2013, doi: 10.1063/1.1813642.

[64] A. Kamyar, R. Saidur, and M. Hasanuzzaman, "International Journal of Heat and Mass Transfer Application of Computational Fluid Dynamics (CFD) for nanofluids," *Int. J. Heat Mass Transf.*, vol. 55, no. 15–16, pp. 4104–4115, 2012, doi: 10.1016/j.ijheatmasstransfer.2012.03.052.

[65] B. Sahin, E. Manay, and E. F. Akyurek, "An Experimental Study on Heat Transfer and Pressure Drop of CuO-Water Nanofluid," vol. 2015, 2015.

[66] A. D. Adrian Bejan; Kraus, *HEATTRANSFER HANDBOOK*. 2003.

[67] D. P. Kulkarni, P. K. Namburu, H. Ed Bargar, and D. K. Das, "Convective heat transfer and fluid dynamic characteristics of SiO 2 - Ethylene glycol/water nanofluid," *Heat Transf. Eng.*, vol. 29, no. 12, pp. 1027–1035, 2008, doi: 10.1080/01457630802243055.

[68] M. Hejazian, M. K. Moraveji, and A. Beheshti, "Comparative study of Euler and mixture models for turbulent flow of Al2O3nanofluid inside a horizontal tube," *Int. Commun. Heat Mass Transf.*, vol. 52, pp. 152–158, 2014, doi: 10.1016/j.icheatmasstransfer.2014.01.022.

[69] F. R. Menter, "Two-equation eddy-viscosity turbulence models for engineering applications," *AIAA J.*, vol. 32, no. 8, pp. 1598–1605, 1994, doi: 10.2514/3.12149.

[70] I. ANSYS, "ANSYS Fluent Theory Guide Release 2020 R1." 2020.

[71] M. S. Chaudhari, D. B. Nalawade, and M. Jagadale, "Heat Transfer Enhancement of Solar Flat Plate Collector by Using V Corrugated Fins and Various Parameters," vol. 5, no. 5, pp. 119–123, 2016.

[72] R. Davarnejad, S. Barati, and M. Kooshki, "Cfd simulation of the effect of particle size on the nanofluids convective heat transfer in the developed region in a circular tube," *Springerplus*, vol. 2, no. 1, pp. 1–6, 2013, doi: 10.1186/2193-1801-2-192.

[73] D. Eyl, S. Ve, and S. Tez, "Numerical investigation into the convective heat transfer of CuO nanofluids flowing through a straight tube with," *Indian J. Sci. Technol.*, vol. 5, no. May 2011, pp. 2455–2458, 2012.

[74] M. Akbari, N. Galanis, and A. Behzadmehr, "Comparative analysis of single and two-phase models for CFD studies of nanofluid heat transfer," *Int. J. Therm. Sci.*, vol. 50, no. 8, pp. 1343–1354, 2011, doi: 10.1016/j.ijthermalsci.2011.03.008.

[75] M. Corcione, "Empirical correlating equations for predicting the effective thermal conductivity and dynamic viscosity of nanofluids," *Energy Convers. Manag.*, vol. 52, no. 1, pp. 789–793, 2011, doi: 10.1016/j.enconman.2010.06.072.

[76] D. Bohne, S. Fischer, and E. Obermeier, "Thermal Conductivity, Density, Viscosity, and Prandtl-Numbers of Ethylene Glycol-Water Mixtures," *Ber.*, vol.

742, pp. 739–742, 1984.

[77] F. P. Incropera, D. P. DeWitt, T. L. Bergman, and A. S. Lavine, “Fundamentals of Heat and Mass Transfer-Incropera.pdf.” p. 997, 2007.

[78] S. Kumar, M. H. Chandra, and A. Arora, “Effect of velocity and rheology of nanofluid on heat transfer of laminar vibrational flow through a pipe under constant heat flux,” *Int. Nano Lett.*, vol. 9, no. 3, pp. 245–256, 2019, doi: 10.1007/s40089-019-0276-4.

[79] M. Esfandiary, A. Habibzadeh, H. Sayehvand, and M. Branch, “Numerical Study of Single Phase / Two-Phase Models for Nanofluid Forced Convection and Pressure Drop in a Turbulence Pipe Flow,” vol. 4, no. 1, pp. 11–18, 2016, doi: 10.7508/tpnms.2016.01.002.

[80] S. S. Thakre and J. B. Joshi, “CFD modeling of heat transfer in turbulent pipe flows,” *AIChE J.*, vol. 46, no. 9, pp. 1798–1812, 2000, doi: 10.1002/aic.690460909.

[81] S. Vijiapurapu and J. Cui, “Performance of turbulence models for flows through rough pipes,” *Appl. Math. Model.*, vol. 34, no. 6, pp. 1458–1466, 2010, doi: 10.1016/j.apm.2009.08.029.

APPENDIX

Appendix 1 Fluent Code

```
/************************************************************

udf for defining nano fluid properties

************************************************************/

#include "udf.h"

#define fi 0.1

#define ro_s 8933

/*#define cp_f 1845*/


DEFINE_PROPERTY(cell_density, cell, thread)

{

real ro_nf;

real ro_f;

real tt= C_T(cell, thread);

ro_f=1000*(1.127776-0.00070548*tt-0.000000065278*tt*tt);

ro_nf=(((1-fi)*(ro_f))+(fi*(ro_s)));

return ro_nf;

}

DEFINE_SPECIFIC_HEAT(cell_specific_heat, T, Tref, h, yi)

{
```

```
real cp;

real cp_f;

real cp_s;

real ro_f;

cp_s= 390;

cp_f=1000*(2.3407+0.0046*tt);

ro_f=1000*(1.127776-0.00070548*tt-0.000000065278*tt*tt);

cp=((1-fi)*(ro_f*(cp_f))+(fi*(ro_s*(cp_s))))/(((1-fi)*ro_f)+fi*ro_s);

*h = cp*(T-Tref);

return cp;

}

DEFINE_PROPERTY(thermal_conductivity, cell, thread)

{

real tt= C_T(cell, thread);

real mu_f;

real ro_f;

real k_eff;

real ks;

real kf;

real Re;

real Pr;
```

```
real cp_f;

cp_f =1000*(2.3407+0.0046*tt);

kf=0.24511+0.0001755*tt-0.000000852*tt*tt;

ks=401;

mu_f=0.0373*exp(-0.0756*tt)+0.0196*exp(-0.0235*tt);

ro_f=1000*(1.127776-0.00070548*tt-0.000000065278*tt*tt);

Re= (2*ro_f*tt*1.3806488e-23)/((22/7)*20e-9*(mu_f*mu_f));

Pr= (mu_f*cp_f)/(kf);

k_eff=kf*(1+(4.4*(pow((Re) ,0.4)))*(pow((Pr) ,0.66))*(pow((tt/260.2) ,10))*(pow((ks/kf)
,0.03))*(pow((fi) ,0.66)));

return k_eff;

}

DEFINE_PROPERTY(viscosity, cell, thread)

{

real mu_f;

real mu_eff;

real tt= C_T(cell, thread);

mu_f=0.0373*exp(-0.0756*tt)+0.0196*exp(-0.0235*tt);

mu_eff =(mu_f)/(1-13.404543*(pow((fi) ,1.03)));

return mu_eff;

}
```

Appendix B DLS result

Size Distribution Report by Intensity

v2.2

Malvern

Sample Details

Sample Name:	Copper nano particle		
SOP Name:	CNC.sop		
General Notes:			
File Name:	Particle size	**Dispersant Name:**	Water
Record Number:	22	**Dispersant RI:**	1.330
Material RI:	1.59	**Viscosity (cP):**	0.8872
Material Absorbtion:	0.010	**Measurement Date and Time:**	Friday, September 17, 2021...

System

Temperature (°C):	25.0	**Duration Used (s):**	290
Count Rate (kcps):	7.8	**Measurement Position (mm):**	0.65
Cell Description:	Disposable sizing cuvette	**Attenuator:**	11

Results

			Size (d.nm):	% Intensity:	St Dev (d.n...
Z-Average (d.nm):	98	**Peak 1:**	23.65	100.0	1.366
PdI:	0.745	**Peak 2:**	0.000	0.0	0.000
Intercept:	0.613	**Peak 3:**	0.000	0.0	0.000

Result quality : Good

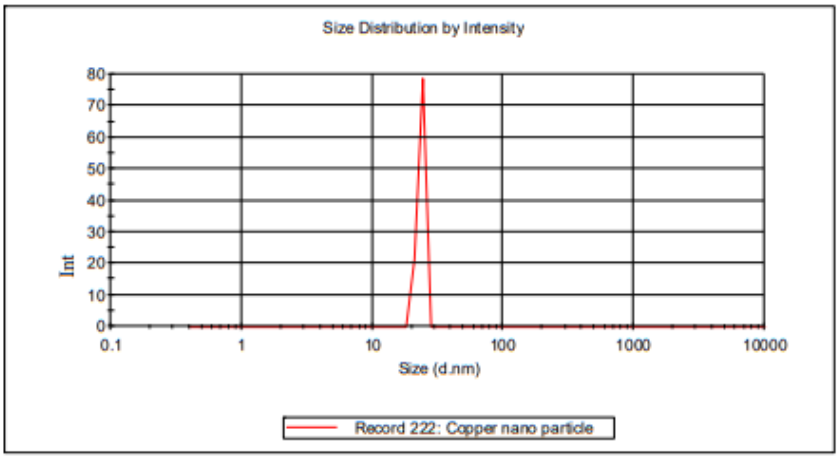

Appendix C Stochiometric calculation for preparation of nanofluid

Mass of Cu

To prepare a nanofluid with a maximum volume fraction of 1% in 10 litters of ethylene glycol, the required amount of copper nanoparticle is calculated

$$\boldsymbol{m_{Cu}} = \left(\frac{\phi}{100-\phi}\right)\left(\frac{\rho_{cu}}{\rho_{eg}}\right)\boldsymbol{m_{eg}}$$

$$\boldsymbol{\rho_{cu}} = 8933 \text{ kg/m}^3$$

$$\boldsymbol{\rho_{eg}} = 1109 \text{ kg/m}^3$$

$$\boldsymbol{m_{eg} = \rho_{eg} \times V_{eg} = 1109 \times 0.01 = 11.09} \text{ kg}$$

So, the mass of copper required

$$\boldsymbol{m_{Cu}} = \left(\frac{1}{100-}\right)\left(\frac{8933}{1109}\right) \times \boldsymbol{11.09 = 0.931} \text{ kg}$$

Balanced equation

$Cu^{2+} + 2BH_4^- + 6H_2O \rightarrow Cu + 2H_3BO_3 + 7H_2$

From the balanced equation, synthesizing 1 mole (63.546 gms) of Cu nanoparticles requires 1 mole (249.68gms) of $CuSO_4 \cdot 5H_2O$. Which means we need 3.642 kg of $CuSO_4 \cdot 5H_2O$ is required.